



**Tomas Bata University in Zlín**  
**Faculty of Technology**

*Doctoral Thesis*

**Solvothermal Synthesis of Advanced Composite  
Materials**

**Solvotermální syntéza pokročilých kompozitních  
materiálů.**

**Shawqi Almajdalawi**

Czech Republic, Zlín 2012

*A Thesis Submitted for Fulfillment of PhD Degree*

*In*

Doctoral study programme: P 2808 Chemistry and Materials Technology  
2808V006 Technology of Macromolecular  
Compounds

Supervisor: Assoc. Prof. Vladimír Pavlínek

Consultant: Assoc. Prof. Ivo Kuřitka

## ACKNOWLEDGMENT

I express extreme gratitude to my supervisor *Associate Professor Vladimir Pavlinek* and *Associate Professor Ivo Kuritka*, Polymer Centre, Faculty of Technology, Tomas Bata University in Zlin, Czech Republic, for allowing me to join their research group and also for their effective guidance, support, encouragement, inspiration and for academic freedom that they allowed me during the entire period of my research work.

I would like to thank *Professor Petr Saha* for his support during my work especially at the first time I started my study here.

In addition, I want to thank Mr. Miroslav Mrlik, Mr. Michal Sedlacik and Mr. Martin Stenicka for their help and friendship through last three years.

My thanks go to Mr. Michal Machovsky for Scanning Electron Microscopy photos.

I would like to thank Dr. Qilin Cheng for Transmission Electron Microscopy and his help and support.

I am grateful to the Ministry of Education, Youth and Sports of the Czech Republic for providing financial support to carry out this research and to the Ministry of Education in Hashemite Kingdom of Jordan for taking care of my family there.

I convey special thanks to my mother for support to take care of the family, to my wife for support, to my children, sisters and brothers.

Finally, to the entire staff of the Polymer Centre and all U12 accommodators are acknowledging.

Last but not least, I am grateful to Allah for his blessings that helped me to complete this work successfully.

# CONTENT

ACKNOWLEDGMENT .....	3
CONTENT.....	4
ABSTRACT.....	7
ABSTRAKT.....	9
CHAPTER 1.....	11
THEORETICAL BACKGROUND.....	11
1. SOLVOTHERMAL SYNTHESIS.....	11
1.1 Solvothermal synthesis .....	11
2. SOLVOTHERMAL AND TiO <sub>2</sub> SYNTHESIS.....	12
3. INTELLEGINT FLIUDS .....	15
4. RHEOLOGICAL PROPERTIES OF ER FLUIDS.....	16
4.1 Shear stress.....	16
4.2 Yield stress.....	16
4.3 Viscoelastic measurements.....	17
5. PARAMETERS INFLUENCING ER EFFECT .....	17
5.1 Electric field strength.....	17
5.2 Volume fraction, particle size and shape .....	18
5.3 Dielectric properties.....	19
5.4 Temperature.....	19
6. MATERIALS USED FOR ER SYSTEM .....	20
6.1. Organic materials.....	20
6.2. Inorganic materials .....	20
6.3. Organic/ inorganic composites.....	21
6.4. TiO <sub>2</sub> ER effect.....	22
6.5. Polypyrrole synthesis .....	22
6.5.1 Chemical synthesis .....	22
6.5.2 Electrochemical synthesis.....	23
7. ER MECHANISM .....	24
7.1 Polarization model .....	24
7.2 Conduction model .....	25
7.3 Dielectric loss model.....	26
8. AIMS OF THE THESIS.....	28

<b>CHAPTER 2</b> .....	<b>29</b>
<b>CHEMICALS AND METHODOLOGY</b> .....	<b>29</b>
<b>2.1 Synthesis of TiO<sub>2</sub> nanorods with nanocavities</b> .....	<b>29</b>
2.1.1 Materials .....	29
2.1.2 Synthesis of Titanium oxide nanorodes.....	29
2.1.3 Morphology and structure characterization .....	30
2.1.4 Dielectric properties.....	30
2.1.5 Preparation and ER measurements of TiO <sub>2</sub> nanorods suspensions .....	30
<b>2.2 Synthesis of polypyrrole ribbon-like particles</b> .....	<b>31</b>
2.2.1 Materials .....	31
2.2.2 Synthesis of PPy ribbon-like structure.....	31
2.2.3 Morphology characteristic .....	31
2.2.4 Dielectric properties.....	31
2.2.5 Preparation and ER measurements of PPy suspensions .....	31
<b>2.3 Morphology effect on ER behavior of TiO<sub>2</sub></b> .....	<b>32</b>
2.3.1 Materials .....	32
2.3.2 Synthesis.....	32
2.3.3 Morphology characterization.....	32
2.3.4 Dielectric properties.....	33
2.3.5 ER measurements .....	33
<b>CHAPTER 3</b> .....	<b>34</b>
<b>RESULTS AND DISCUSSION</b> .....	<b>34</b>
<b>3.1 TiO<sub>2</sub> nanorods</b> .....	<b>34</b>
3.1.1 Morphology characterization and composition.....	35
3.1.2 Rheological properties .....	40
3.1.3 Conclusions.....	52
<b>3.2 Polypyrrole results</b> .....	<b>53</b>
3.2.1 Morphology and structure .....	53
3.2.2 Rheological properties and conductivity.....	54
3.2.3 Conclusions.....	60
<b>3.3 TiO<sub>2</sub> with different morphology and its ER effect</b> .....	<b>61</b>
3.3.1 Morphology characterization.....	61
3.3.2 ER properties .....	68

3.3.3	Conclusions.....	74
<b>CHAPTER 4.....</b>		<b>75</b>
<b>CLOSING REMARKS.....</b>		<b>75</b>
4.1	General conclusions .....	75
4.2	Contribution to science and practice.....	76
4.3	Future works .....	76
<b>REFERENCES.....</b>		<b>77</b>
<b>LIST OF FIGURES AND TABLES.....</b>		<b>86</b>
<b>NOMENCLATURE AND SYMBOLS.....</b>		<b>90</b>
<b>CURRICULUM VITAE.....</b>		<b>93</b>

## ABSTRACT

The Solvo-thermal technique is a chemical synthesis method used for the preparation of compounds with different morphologies. It has gained a lot of attention in recent years, and has been developed into an important solid-state synthetic method employing molecular solvents at intermediate temperatures (100-400)° C. The solvo-thermal technique uses organic solvents like ethanol, acetone, ethylene glycol, etc. to synthesize some powders. The morphology of the powder depends on the solvent used, reactants' concentration, temperature and the solution's pH. However, when the solvent used is water, the name used is hydrothermal synthesis - which is mostly used in literature. It was used to synthesize a well-crystallized, fine oxide powder, with uniform shape and narrow particle size distribution, without using a very high post-treatment temperature.

Intelligent materials are materials whose feature characteristics can change under external stimuli, such as electric and magnetic fields. Among these, electro-rheological (ER) and magneto-rheological (MR) fluids which are composed of small particles dispersed in non-conducting liquids, are fascinating materials whose structure and rheological properties are dramatically altered by external electric-magnetic fields. They change from a liquid-like state to a solid-like state within a millisecond under the application of electric or magnetic fields. This property gives them the ability for stress transfer applications.

The electronic control of stress transfer has applications in devices such as active shock absorbers, engine mounts, clutches and brakes, etc.

Many ER fluids have been studied, and some of them have shown high yield stresses in kPa, and these are called giant ER fluids. However, there are still many problems needing to be solved for the suitable ER fluid like wide- range temperature performance, stability against sedimentation, and non-abrasive and environmentally friendly.

Various materials were studied for this work:

- Titanium oxide (TiO<sub>2</sub>) nanorods with nanocavities doped with different percentages of Chromium (Cr) as a novel material for ER fluids using the solvothermal route and using water as a solvent. Morphology and structure analyses were performed by different techniques. ER properties were measured for their suspensions in silicone oil. The effect of conductivity of doping on ER behavior was also investigated.
- Polypyrrole (PPy) ribbon-like particles prepared by oxidative polymerization using ammonium persulfate as an oxidizing agent and also, as a novel material for ER fluids. Two different samples of PPy with different conductivities were prepared. The effect of conductivity on ER behavior was investigated.

- Solvothermal synthesis of different TiO<sub>2</sub> morphologies by changing the concentration and heating time to study the effect of morphology on the ER properties.

Key words:

Solvothermal synthesis, electro-rheological effect, magneto-rheological fluid, titanium oxide, nanorods, polypyrrole, conductivity, morphology.



## ABSTRAKT

Solvotermální technika je metoda chemické syntézy používaná pro přípravu sloučenin s různými morfologiemi. V současnosti získala pozornost a rozvinula se v důležitou metodu přípravy tuhých látek pomocí molekulárních rozpouštědel používaných při středních teplotách (100-400)°C. Solvotermální technika používá pro přípravu práškových materiálů organická rozpouštědla jako ethanol, aceton, ethylen glykol apod. Morfologie připravených prášků závisí na použitém rozpouštědle, koncentraci reaktantů, teplotě a pH roztoku. Nicméně, v případě že je jako rozpouštědlo použita voda používá se název hydrotermální syntéza. Tato metoda byla použita pro přípravu vysoce krystalického jemného oxidového prášku s uniformním tvarem a úzkou distribucí velikosti částic bez nutnosti použít velmi vysokých teplot po provedené syntéze.

Inteligentní materiály jsou materiály, jejichž charakteristické znaky mohou být měněny pod vlivem externího stimulu jako je elektrické nebo magnetické pole. Mezi takové materiály lze řadit electoreologické (ER) a magnetoreologické (MR) kapaliny, které jsou složeny z malých částic dispergovaných v nevodivých kapalinách, kdy se jejich struktura a reologické vlastnosti dramaticky mění za účinků elektrického či magnetického pole. Při aplikování pole mohou měnit svůj stav z kapalného na tuhý v rozmezí několika milisekund. Tato vlastnost jim dává schopnost v aplikacích umožňujících přenos napětí.

Elektronické ovládání přenosu napětí má použití v zařízeních jako aktivní napěťové absorbery, u motorů, spojek a brzd.

V minulosti byla již zkoumána široká paleta ER systémů, některé vykazovaly vysoká prahová napětí až v kPa. Tyto systémy jsou nazývány „Giant ER Fluids“, tj. kapaliny s „obřím“ ER efektem. Nicméně, stále existuje řada problémů, které je potřeba vyřešit jako jsou široká teplotní použitelnost, sedimentační stabilita, abrazivita ER systémů a jejich nezávadnost vůči životnímu prostředí předtím, než se jejich využívání dále rozšíří.

V této práci byly studovány různé materiály:

- Nanotyčinky oxidu titaničitého  $\text{TiO}_2$  s nanodutinami dopované různým množstvím Chromu (Cr) jako nového materiálu pro ER kapaliny připravené pomocí solvotermální cesty za použití vody jako rozpouštědla. Studium morfologie a analýzy struktury bylo provedeno pomocí různých technik. ER vlastnosti byly měřeny na suspenzích v silikonovém oleji. Byl také zkoumán vliv vodivosti různě dopovaných materiálů na ER chování.
- Páskovité částice polypyrolu připravené pomocí oxidační polymerace při použití peroxidisíranu amoného jako oxidačního činidla byly také použity jako nový materiál pro ER kapaliny. Byly připraveny dva různé vzorky

polypyrolu o různých vodivostech a byl zkoumán vliv jejich vodivosti na ER chování.

- Částice  $\text{TiO}_2$  byly připraveny pomocí solvotermální syntézy, kdy jejich různé morfologie bylo získáno změnou koncentrace a doby zahřívání a tyto byly zkoumány za účelem zjištění vlivu morfologie na ER vlastnosti.

Klíčové slova:

Solvotermální syntéza, elektoreologický efekt, elektoreologická kapalina, oxid titaničitý, nanotyčinky, polypyrol, vodivost, morfologie.

# CHAPTER 1

## THEORETICAL BACKGROUND

### 1. SOLVOTHERMAL SYNTHESIS

#### 1.1 Solvothermal synthesis

The Solvothermal synthesis is a soft chemical synthesis method with important advantages due to low crystallization temperatures enabling the direct production of nanocrystalline powders without any firing step [1]. This method allows controlling the morphology of the materials produced under temperature ranged from (100 – 400)°C [2]. Three different routes are possible in this method:

- The solvothermal precipitation of the solid phase when the reactants are soluble in the solvent.
- The solvothermal decomposition of the precursor's insoluble in the solvent.
- The solvothermal recrystallization of the finely divided amorphous starting material with the same composition as the final microcrystallites [3].

One of the solvothermal methods is hydrothermal synthesis, where the solvent used is water. It has attracted a great deal of attention since particles with the desired characteristics can be prepared with this technique by controlling the solution pH, reaction temperature, reaction time, solute concentration and the type of solvent depending on the particular application [4]. The difference in structure, size and other properties affect ER behavior. So, the hydrothermal technique is becoming one of the most important tools for advanced materials processing, particularly owing to its advantages in the processing of nanostructure materials for a wide variety of technological applications such as electronics, optoelectronics, catalysis, ceramics, magnetic data storage, biomedical, biophotonics and ER fluids [5]. This method was used to synthesize a well-crystallized, fine oxide powder, with uniform shape and particle size distribution, without using a very high post-treatment temperature [6]. Solvothermal process has been reported to synthesize the transition family particles. The preparation of CuInSe<sub>2</sub> powders via the solvothermal route using ethylenediamine as a solvent produce a one-dimensional microstructures [7].



*Fig. 1. Images of autoclaves used for solvothermal synthesis.*

## **2. SOLVOTHERMAL AND TiO<sub>2</sub> SYNTHESIS**

Solvothermal was considered as one of the methods for preparation of different material morphologies. Among these materials, TiO<sub>2</sub> nanoparticles have gained a lot of attention because of their many potential applications. TiO<sub>2</sub> microspheres were prepared by hydrothermal synthesis route using autoclaves as shown in figure 1. It was approved by scanning electron microscopy that the first growth was in form of nanorods followed by microspheres structure depending on reaction temperature, time, concentration of titanium (III) chloride TiCl<sub>3</sub> [8]. The anatase TiO<sub>2</sub> morphology was controlled by introducing variable hydrophobicity by dodecanediamine (DDA). It was successful to prepare different morphology such as nanoparticles, nanorods, nanotubes, and flower-like shape in the same system by controlling the reaction conditions [9].

The different morphologies of TiO<sub>2</sub> shown in figure 2 were obtained by changing the reaction conditions like concentration, temperature and reaction time.

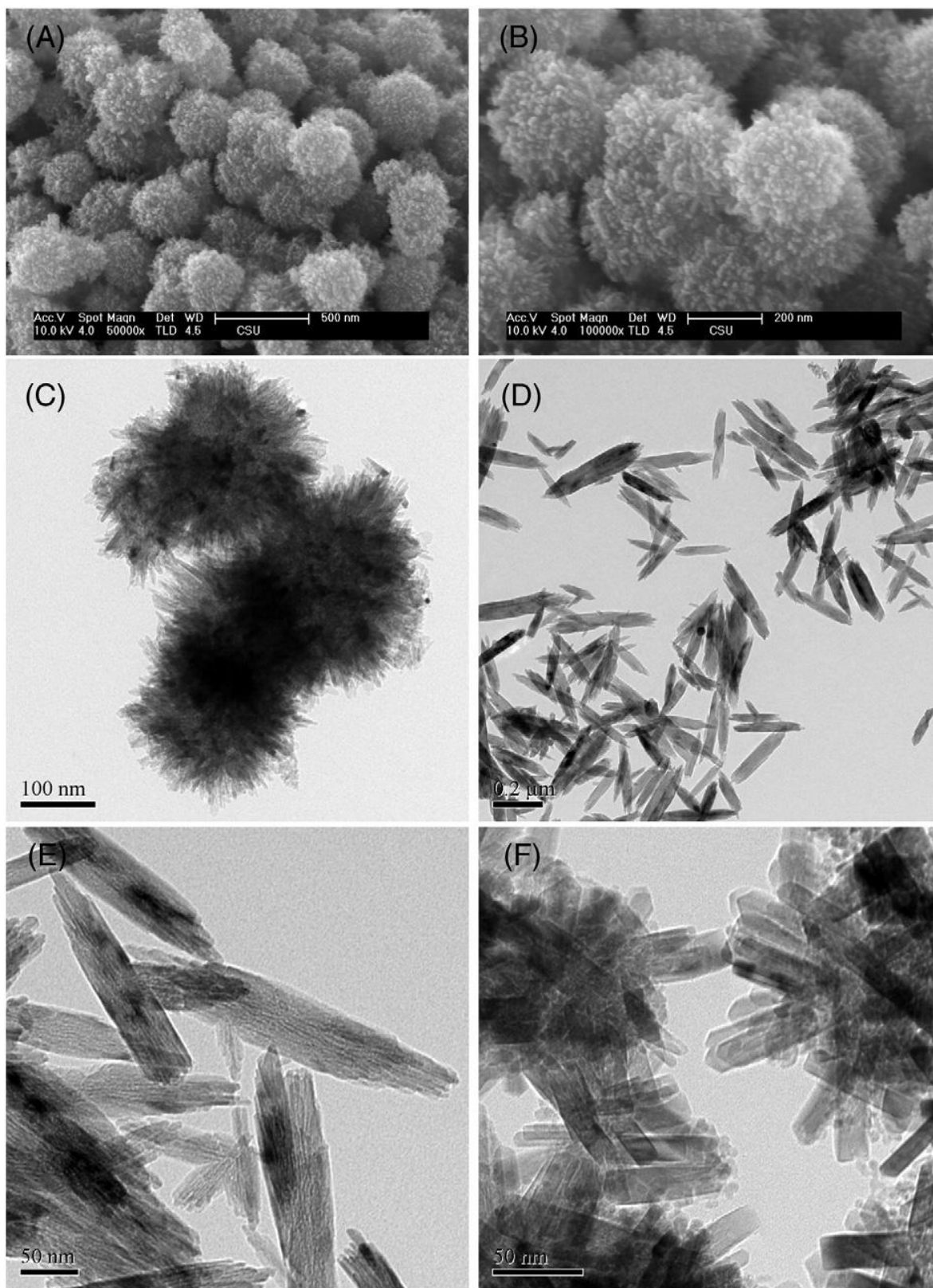


*Fig. 2. Scanning electron microscopy (SEM) and Transmission electron microscopy (TEM) images for TiO<sub>2</sub> nanoparticles [10].*

The effect of inorganic/organic ions on the morphology of  $\text{TiO}_2$  prepared by hydrothermal synthesis was reported [11, 12]. The mechanism of crystals growth was investigated and showed the effect of reaction temperature on the growth mechanism and final shape of  $\text{TiO}_2$  nanoparticles [13, 14]. The acid washing treatment after hydrothermal synthesis of  $\text{TiO}_2$  was shown to have a role in the crystal morphology [15]. The suggested mechanism was the dissolution–growth mechanism which starts as anatase nanoparticles  $\text{K}_2\text{Ti}_6\text{O}_{13}$  then grows gradually to nanofibres along certain crystalline axis [16].

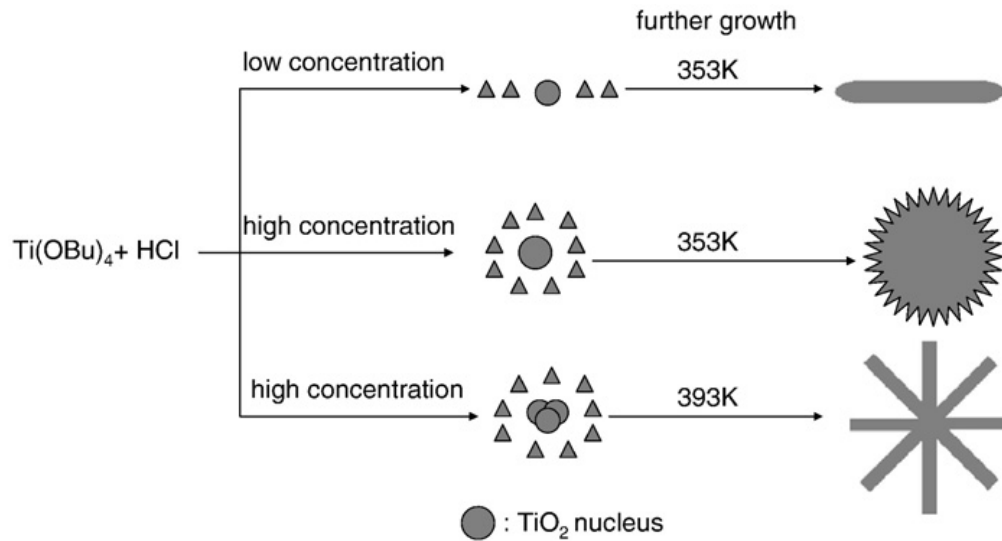


*Fig.3. Growth mechanism of  $\text{TiO}_2$  nanoparticles crystal [10].*

Solvothermal synthesis of different nanostructures  $\text{TiO}_2$  morphology for ER application has been synthesized. Titanate nano-whiskers were prepared by hydrothermal synthesis with large length-diameter ratio and layered tube-like structure as an ER fluid [17]. Also,  $\text{TiO}_2$  particles with different microstructures in crystal type, surface area, pore size, pore volume and grains size were synthesized by hydrothermal treatment of titanium tetrachloride ( $\text{TiCl}_4$ ) [18].

### 3. INTELLEGINT FLUIDS

The name “intelligent materials” encloses a wide group of materials whose properties can be controlled to a certain extent by external stimuli. ER and MR fluids belong to this group. ER and MR fluids exhibit a remarkable property in their rheological properties are dramatically altered by applying external electric field or magnetic fields, respectively. As originally described by Winslow [19] and Rabinow [20], these materials have a variety of potential applications in stress transfer and damping devices such as active shock absorbers, engine mounts, clutches and brakes [21]. ER and MR fluids share some common features. Both are typically composed of small particles suspended in liquids. Their field-induced steady-shear rheological properties are often modeled by the Bingham equation:

$$\begin{aligned} \tau(E, H, \dot{\gamma}) &= \tau_0(E, H, \dot{\gamma}) + \eta_{pl} * \dot{\gamma}, & \text{for } |\tau| \geq |\tau_0| \\ \dot{\gamma} &= 0 & \text{for } |\tau| < |\tau_0| \end{aligned} \quad (1)$$

Where  $\tau(\dot{\gamma}, E, H)$  is the shear stress,  $\tau_0(E, H)$  is the dynamic yield stress which is an increasing function of the electric ( $E$ ) or magnetic ( $H$ ) field strength,  $\eta_{pl}$  is the plastic viscosity, and  $\dot{\gamma}$  is the shear rate. Apparent suspension viscosities can increase, by several orders of magnitude for field strength of 1 kV/mm and 100 kA/m, for ER and MR fluids, respectively. ER and MR suspensions also display dramatic microstructural changes when the fields are applied, with columnar structures forming rapidly in the applied field direction [22].

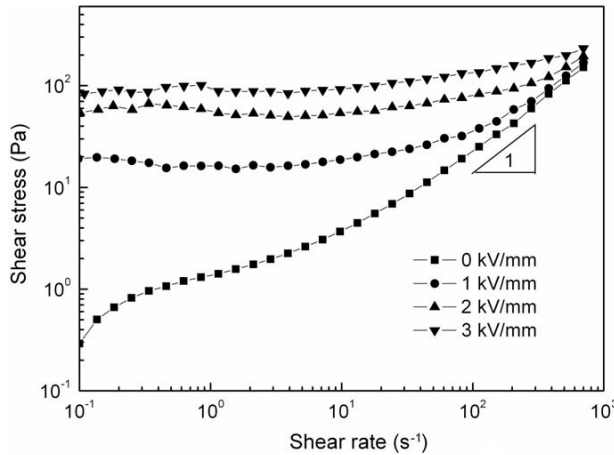


Fig. 4. Shear stress versus shear rate curves for 10 wt. % PPy/MCM-41 particles in silicone oil at different electric field strengths [23].

## 4. RHEOLOGICAL PROPERTIES OF ER FLUIDS

### 4.1 Shear stress

For most ER fluids, the typical steady-shear behavior under an external electric field is most often characterized as a Bingham- like solid given by eq. (1). The Bingham fluid model consists of two flow regions: a rigid pre-yield behavior for shear stress less than yield stress and Newtonian or non-Newtonian flow response beyond the yield stress (post-yield region) [24]. However, deviations from the Bingham fluid model have been observed for several ER systems, especially the semiconducting polymer based ER fluids since it cannot predict or explain the behavior with shear rate. Many models were proposed to describe the behavior of ER fluids such as the three parameters De Kee-Turcotte model and others [25]

$$\tau = \tau_0 + \eta_1 \cdot \dot{\gamma} \cdot e^{-t_1 \dot{\gamma}} \quad (2)$$

Choi *et.al* model [26]

$$\tau = \frac{\tau_y}{1+(t_2 \dot{\gamma})^\alpha} + \eta_\infty \left(1 + \frac{1}{(t_3 \dot{\gamma})^\beta}\right) \dot{\gamma} \quad (3)$$

and Herschel-Bulkley model [22]

$$\tau = \tau_0 + m\dot{\gamma}^n \quad (4)$$

### 4.2 Yield stress

The yield stress  $\tau_0$  ranks among the rheological parameters usually used for characterization of ER efficiency. There are known two different values of the yield stresses- the dynamic yield stress produced in control shear rate (CSR) and the static yield stress from control shear stress (CSS) mode, respectively.

In contrast to CSR mode, in which a shear rate is applied to the ER fluid and then the resulting shear stress is measured giving a dynamic yield stress, in CSS the ER fluid is stressed until the particle chain structure is perfectly broken and the flow occurs. The stress at this point is known as the static yield stress [27]. The yield stress determined from CSR method typically deviated from that obtained via the CSS method [28].



### 4.3 Viscoelastic measurements

In addition to rheological behavior in steady shear mode, the knowledge of the viscoelastic behavior of ER suspensions is important, especially from the real application point of view. The frequency,  $f$  or more frequently angular frequency,  $\omega$  dependence of storage (elastic)  $G'$ , and loss  $G''$  (viscous) moduli or complex viscosity  $\eta^*$  are usually chosen for characterization of viscoelastic behavior. However, the stability of ER structures is reduced to the limiting value of deformation  $\gamma$ . After its overcoming, the hydrodynamic forces dominate over the electrostatic ones. Therefore, the finding of linear viscoelastic range (LVE) should be always addressed before the frequency sweep is performed [29].

## 5. PARAMETERS INFLUENCING ER EFFECT

### 5.1 Electric field strength

Usually, the electrostatic forces between the polarized particles increase upon electric field  $E$  application and cause the formation of the chain network which is reflected by increase in the yield stress. Only when  $E$  exceeds a certain electric field value  $E_c$ , make the ER fluid show a detectable ER effect. The yield stress is proportional to the electric field strength  $E^n$ , where  $n$  differs depending on the used model [30, 31]. The shear stress of cellulose phosphate ester suspensions exhibited a dependence on the electric field. The results show that the shear stress is proportional to 1.41 power of the electric field [32]. Both alternative current (AC) and direct (DC) electric fields can be used to generate ER effect. However, the frequency of the AC electric field affects the ER characteristics [33]. It reported that a decrease in the shear stress with an increasing shear rate occurs under DC electric fields [34]. The effect of electric field on yield stress is shown in figure 5.

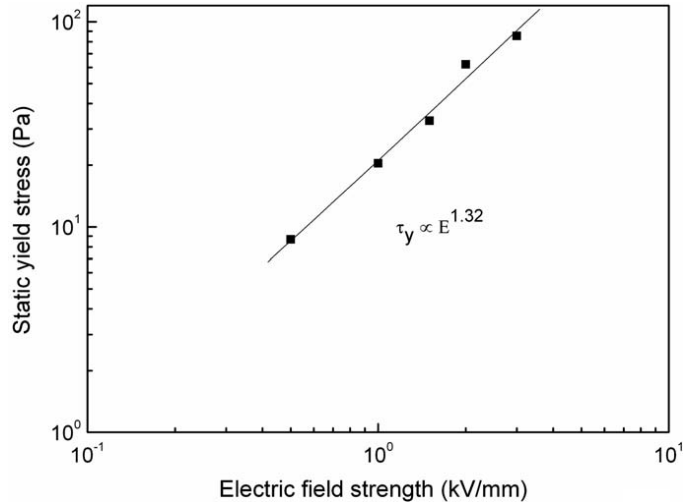


Fig. 5. Static yield stress versus electric field strength for PPy-SBA-15 based ER fluids [23].

## 5.2 Volume fraction, particle size and shape

A detectable ER effect also mostly depends on concentration of the dispersed phase. There is no change in shear stress and shear viscosity when particle volume fraction is below critical concentration. The effect of volume percent of PPy-silica-methylcellulose nanocomposite suspensions was investigated and showed an increase in the shear stress with increasing volume percent [35]. The viscosity of polyindole/polyethylene composite suspensions increased with increasing of volume fraction [36]. The shear stress of cellulose phosphate ester suspension showed a linear dependence on the volume fraction of particles [31]. The increase of urea treated silica suspension weight fraction from 20 wt. % to 25 wt. % lead to double increase in the shear stress of the suspension [37].

The shape, size and the thickness of the deposited layer in composite materials of the particles in suspension either increase or decrease ER effect. If the particles are too small, ER effect could be very weak due to Brownian motion competing with particle fibrillation; whereas ER fluids with big particles also show weak ER activity due to sedimentation. The effect of shape and size of different inorganic powder on ER properties were studied and it was showed an increase in ER effect with irregularity of the particles [38]. The effect of polyaniline coated silica particles and aluminum hydroxide on electric properties were investigated [39, 40]. The shear stress increase steeply with coating thickness and after specific thickness it became constant or slightly increases in shear stress. The influence of particle size on shear behavior of amine-group-immobilized polyacrylonitrile dispersed suspension showed that the fine particles suspension showed stable shear stress under a DC electric field compared to the rough one [41]. The ER effect of various

lengths of aliphatic spacer of polymethacrylate liquid crystalline polymers showed increasing trend with increasing the length of the spacer [42]. The effect of polyaniline layer deposited on silica particles on ER properties was showed that the ER effect is limited to optimum coating thickness [43]. The layer thickness of PPy coated polyethylene showed yield stress enhancement [44].

### **5.3 Dielectric properties**

Since the ER effect is induced by an applied electric field, the polarization is believed to play a key role, and the particle dielectric properties should be dominant in the ER effect. The ER fluid should have a dielectric  $\epsilon''$  relaxation peak in the range  $10^2$ - $10^5$ Hz and should have a large difference in relative permittivity  $\epsilon'$  at  $10^2$  and  $10^5$  Hz [45]. The increase of  $\Delta\epsilon'$  of PPy coated polyethylene particles reflected as increase in the yield stress [46]. Shear stress of Na- titanate nanotube was higher than H-titanate nanotube as measured under rheometer and the dielectric loss factor showed a peak at 600 Hz for Na-titanate nanotube while there was no peak in the expected region for H-titanate nanotubes [47].

### **5.4 Temperature**

Increasing temperature significantly changes polarizability of ER fluids as well as the particle conductivity, dielectric properties or current density. For industrial applications of ER fluids, sustained ER activity over a wide range of temperature is required. Increasing temperature leads to higher thermal motion which destroys the chain network for ER fluids and decreases properties such as viscosity and yield stress. However, freezing ER fluid cause also decrease in ER properties [48]. The shear stress of polyindole (PIN)/polyethylene (PE) composite suspensions showed a decrease with increasing temperature and the difference in shear stress depends on polyethylene content [36]. The shear stress of Na-titanate nanotube ER fluid increased with temperature. However, H-titanate ER fluid showed nearly stable shear stress with temperature increasing [47].

## 6. MATERIALS USED FOR ER SYSTEM

A typical ER fluid usually consisting of two parts: liquid phase which is mostly mineral oil [49], silicone oil [50, 51] with different viscosities, and the dispersed phase having many varieties of organic, inorganic or combined materials [52, 55, 58].

### 6.1. Organic materials

Many organic material suspensions were investigated as ER fluids to overcome the sedimentation and abrasion of devices. Among these, the effect of temperature on rheological properties of nitrogen- enriched carbonaceous nanotubes were reported and showed a decrease in yield stress with increasing sample treatment temperature as well as the zero-field viscosity [52]. The effect of base form of polyphenylenediamine suspension was higher than the protonated one [53]. The effect of oxidant and surfactant amount on ER properties of prepared PPy was studied. It showed an increase in ER properties until a maximum, and then decrease with amount of both oxidant and surfactant [49]. The ER effect in suspension of urea modified by poly[(glycidyl methacrylate)-co-(ethylene dimethacrylate)] particles showed slight enhancement compared to uncoated one [54]. The ER behavior of aniline/pyrrole copolymer showed a critical shear rate and the critical shear rate is larger at high electric field strengths than that at low field strengths [55]. PPy-polycaprolactone composites were synthesized by emulsion polymerization and rheological characteristics of their suspensions were investigated. The ER properties increased with increasing amount of polycaprolactone in the composite and the rheological behavior can be explained by conduction model [56]. Polyaniline coated poly(methyl methacrylate) microspheres were prepared by graft polymerization and showed a yield stress around 100 Pa at 3 kV/mm [57]. ER of suspensions of poly(ethylene glycol(PEG))/poly(vinyl alcohol(PVA)) blend particles were studied and showed that PEG/PVA blends with 10- 20 wt. % suspension shows higher yield stress than the neat PEG suspension [58].

### 6.2. Inorganic materials

Also, many inorganic material suspensions were investigated as ER fluids mostly because of their high dielectric constant. Some of these materials showed a giant ER effect like  $\text{TiO}_2$ , section 4. ER properties of elongated goethite ( $\beta\text{-FeOOH}$ ) and hematite ( $\alpha\text{-Fe}_2\text{O}_3$ ) anisotropic particles suspensions were reported [59]. The ER effect was only noticeable for sufficiently high electric field strength and particle concentrations, typically  $> 1\text{kV/mm}$  and  $> 4\%$  in volume fraction. The

ER behavior of hematite in silicone oil enhanced by water until a maximum followed by a decrease [60].  $\text{SnO}_2$  and  $\text{Y}_2\text{O}_3$  nanoparticles and composite suspensions were investigated and showed a weak ER effect [61]. The effect of surface characteristics of silica particles on electrorheological behavior were examined by dehydrating process above and below  $200^\circ\text{C}$ . It was found that there was an appropriate amount of free water for an optimum ER effect. Also, it was showed that the cetanol treated silica particles suspension shows lower ER effect because it has less bound water than untreated silica [62]. The ER behavior of zinc oxide (ZnO) nanowires was tested. In contrast to the usual ER behavior, a decrease in viscosity of the suspensions is observed with increasing in electric field strength. Such behavior results from the migration of ZnO nanowires to the electrodes under a DC electric field. This phenomenon was confirmed by optical microscope observations and the occurrence of electrophoresis is proposed as the origin of the decrease in shear stress [63].

### **6.3. Organic/ inorganic composites**

Different organic/inorganic composites were synthesized as ER materials in trials to combine two different properties; the conductivity of organic materials and the high dielectric constant of inorganic materials. This combination enhanced the ER effect and the dispersed stability. PPy nanocomposite with inorganic oxide was reported, with Tin dioxide ( $\text{SnO}_2$ ) and showed the dependence of ER effect on the amount of  $\text{SnO}_2$  and methylcellulose in the composite [64]. The ER fluids of silica nanoparticles modified by urea and N, N-dimethylformamide were measured and showed higher yield stress compared to both untreated one and the treated only with urea [37]. Carbon nanotube (MWCN)/polystyrene (PS) composite prepared by layer-by-layer assembly showed different ER behavior according to the number of coating layers characterized by  $\xi$ -potential. With increases in the number of layers on the surface of PS particles, the shear stress increased at the same shear rate [65]. PS/MWCN composites were investigated and showed a weak ER effect [66]. PPy composites with silica nanoparticles (MCM-41) were prepared and their ER properties were measured. Conducting PPy with swollen MCM-41 nanocomposites showed a typical weak ER effect [67]. Mesoporous PPy/MCM-41 composite was prepared and showed 100 Pa yield stress at 3 kV/mm [68]. A pore-expanded mesoporous silica (MCM-41-E) having particles of conducting PPy was prepared and their ER characteristics were investigated. The composite performed excellent ER behavior compared with that of the pure MCM-41-E [69]. Polyaniline fibres and silica nanoparticle decorated polyaniline were obtained through interfacial polymerization as a dispersed phase of an ER fluid. The shear stress was higher for pure polyaniline than that for polyaniline/silica composite [70].

## 6.4. TiO<sub>2</sub> ER effect

TiO<sub>2</sub> has gained a lot of attention because of its high dielectric constant. The ER effect for TiO<sub>2</sub> showed a giant ER effect for many suspensions. Surface modified TiO<sub>2</sub> nanoparticles using sodium dodecyl sulfate showed giant ER effect and the yield stress reached 130 kPa at 4 kV/mm DC electric field when the volume fraction was 56 vol.% [71]. Sea urchin-like TiO<sub>2</sub> hollow spheres were synthesized, its ER characteristics were studied and showed higher ER effect than pure TiO<sub>2</sub> [72]. Sea-urchin-like hierarchical Cr-doped titania particles were synthesized using solvothermal route. The ER behavior of hierarchical particles was better than that of smooth one and the yield stress reached 1500 Pa at 4kV/mm [73]. TiO<sub>2</sub> particles doped with Lanthanum (La) and Cerium (Ce) were tested as ER fluids and showed giant ER effect [74] and the ER effect depends on the doping ratio and showed giant ER effect [75]. TiO<sub>2</sub> with different morphologies were synthesized as a composite with different materials. ER effect of hollow globular TiO<sub>2</sub>/PPy particles suspension were investigated showing 0.7 kPa yield stress at 3 kV/mm and the sedimentation stability was improved [76]. PPy doped with mesoporous TiO<sub>2</sub> were synthesized and characterized. The ER efficiency increased with increasing doping degree until a maximum followed by a decrease [77]. Conducting polyaniline (PANI)/titanium oxide (TiO<sub>2</sub>) hybrid particles were synthesized and their ER characteristics were examined. It expected that the fast relaxation time of PANI/TiO<sub>2</sub> hybrid enhanced electrostatic force over shear force under a shear flow, showing the improved ER performance [78].

## 6.5. Polypyrrole synthesis

Among other conductive polymers, PPy and its derivatives are of particular interest, owing to their high conductivity, stability in the oxidized state and interesting redox properties. The simplicity of the synthetic procedures and availability of the initial monomers are also attractive features of PPy.

### 6.5.1 Chemical synthesis

PPy was synthesized through chemical redox reaction using the suitable oxidizing radical initiator agent such as Iron (III) chloride (FeCl<sub>3</sub>) and ammonium persulfate ((NH<sub>4</sub>)<sub>2</sub>S<sub>2</sub>O<sub>8</sub>) [79]. The main important step is forming the first radical to initiate the polymerization process. The radical formed by ammonium persulfate to initiate the reaction is sulfate radical ion (SO<sub>4</sub><sup>•-</sup>).

The reaction of chemical polymerization is shown in figure 6. The polymer produced by this method is more conductive than that prepared by electrochemical

polymerization due to the doping of the reduced part of the oxidizing agent in the polymer chain such as  $\text{SO}_4^{2-}$ . The conductivity of the produced polymer can be changed by washing and treatment with suitable reagent such as ammonium hydroxide ( $\text{NH}_4\text{OH}$ ).

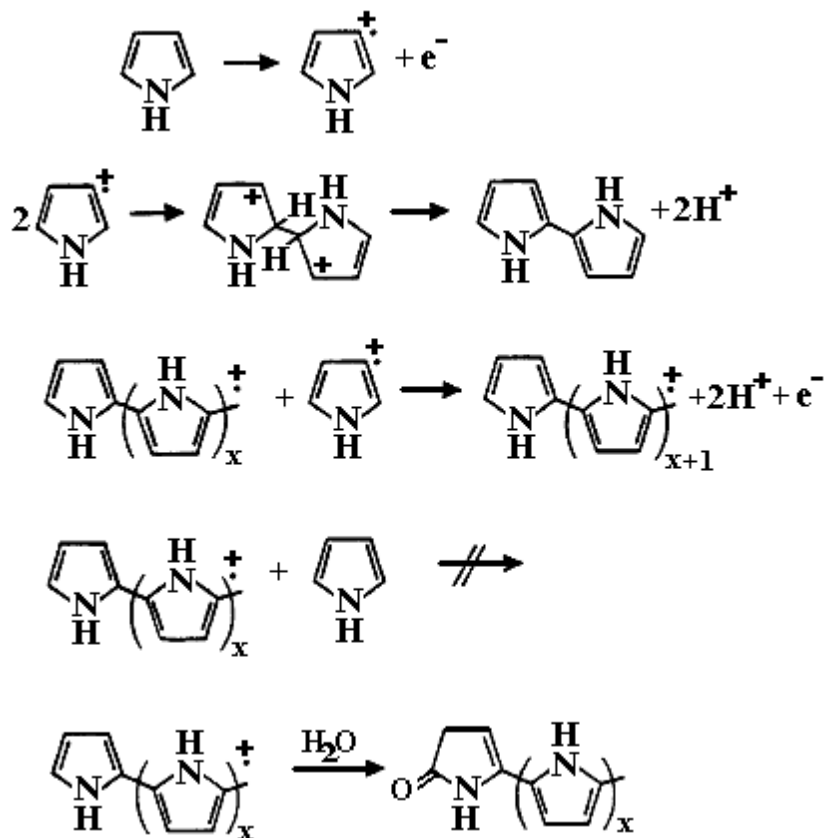


Fig. 6. Mechanism of chemical polymerization of pyrrole [80].

### 6.5.2 Electrochemical synthesis

The main difference between electrochemical polymerization and chemical polymerization is the use of the current electrons as starting initiator. PPy film was synthesized using electrochemical synthesis of pyrrole at different voltages. The voltages used ranged from 0.4- 0.8 V [81].

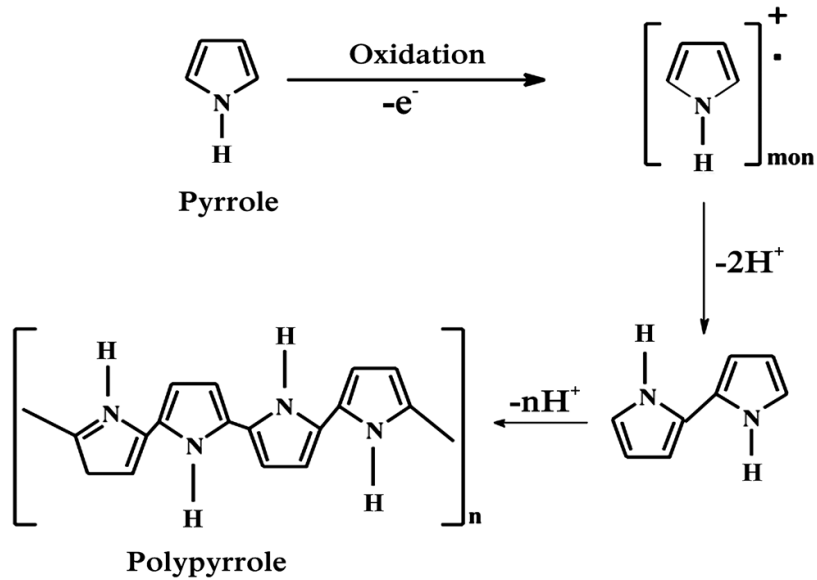


Fig. 7. The reaction mechanism of electropolymerization of pyrrole [82].

## 7. ER MECHANISM

Since the discovery of ER effect by Winslow, many models were proposed to explain the ER effect. However, none of proposed mechanism can predict sufficiently behavior of all materials. The most important models are described below

### 7.1 Polarization model

System that possesses high dielectric constant particles would lead to higher polarization. The static yield stress is proportional to the energy density  $-P \cdot E$  where  $P$  is the polarization density. Higher dielectric constant leads to higher polarization density which means higher yield stress. Saturation polarization mechanism was suggested to explain the ER effect of urea-doped  $\text{TiO}_2$  nanoparticles [83].

$$\tau \propto P \cdot E \quad (5)$$



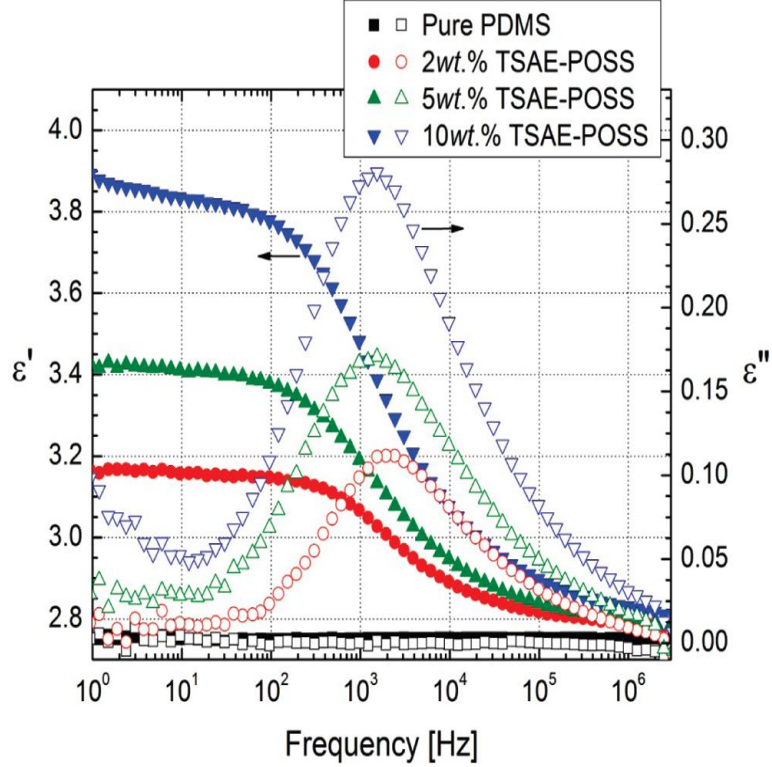


Fig. 8. Frequency dependencies of the relative permittivity and dielectric loss factor on the left and right respectively [84].

Kinetics of structure formation in ER suspensions using electrostatic polarization model showed the effect of shape, size and concentration of the particles on polarization time and hence ER effect. It was found that for hydrated glass spheres longer time needed to form the chain structure at small concentration. However, this time decrease to 10 ms at large concentrations with 2kV/mm [85]. The mechanism of saturation polarization was proposed to explain the higher ER effect for ER fluids [86].

## 7.2 Conduction model

Another model to explain ER behavior of the ER materials is the conduction model. This mechanism was expected to explain the ER effect of cellulose phosphate ester suspension. There are two predicted conduction models used to calculate yield stress for ER fluids. These models are Tang et al. and Wu and Conrad as shown in Equations 6, 7 respectively [31].

$$\tau_E = A_s K_f \tau_0 \phi E_0^2 \quad (6)$$

Where  $A_s$  is a structure factor pertaining to the alignment of the particles,

$K_f$  is the dielectric constant,  $\phi$  is the volume fraction,  $\gamma$  is the shear strain,  $F_\gamma$  is the force at specific shear strain and  $E$  is the electric field strength.

$$\tau_E = \frac{3}{2} A_S K_f \tau_0 \phi E_0^2 F_\gamma / (1 + \gamma)^{1/2} \quad (7)$$

Figure 9 shows the comparison between shear stress calculated by Wu and Conrad equations and experimental shear stress for cellulose phosphate ester suspension at different electric field strengths. The predicted values of Tang et al. of two conduction models are in agreement with the experimental values.

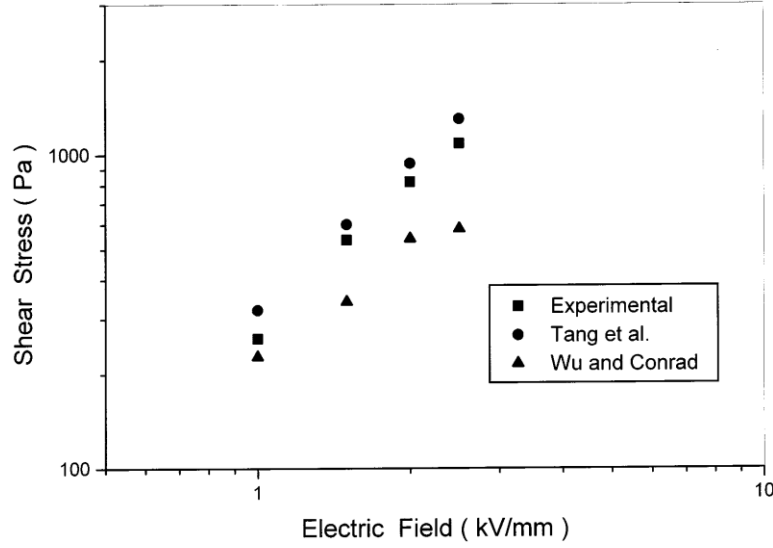


Fig. 9. Comparison of the predicted shear stresses with that measured for cellulose phosphate ester suspension ( $\phi = 0.3$  volume fraction,  $(\dot{\gamma} 10 \text{ s}^{-1})$  [31]).

Choi et al. proposed hybrid model from polarization and conduction models with critical electric field strength,  $E_c$  to describe the deviation of the yield stress from polarization model. The equation includes a parameter  $\alpha$  which depends on the dielectric constant of the fluid and the volume fraction [87].

$$\tau_y \propto 1/\dot{\gamma}^\alpha \quad (8)$$

### 7.3 Dielectric loss model

Both ER fluids and non-ER fluids can be polarized upon application of the electric field. However, the particle of ER fluids oriented in the direction of the electric field producing the chain network which causes ER effect. To have good

ER effect the suspensions should have suitable dielectric loss, suitable response time and more stable chain structure [88]. A large dielectric loss was thought to be responsible for the particle turning process, while a large dielectric constant was assumed to contribute to thermal stability and mechanical strength of fibrillated chains [89].

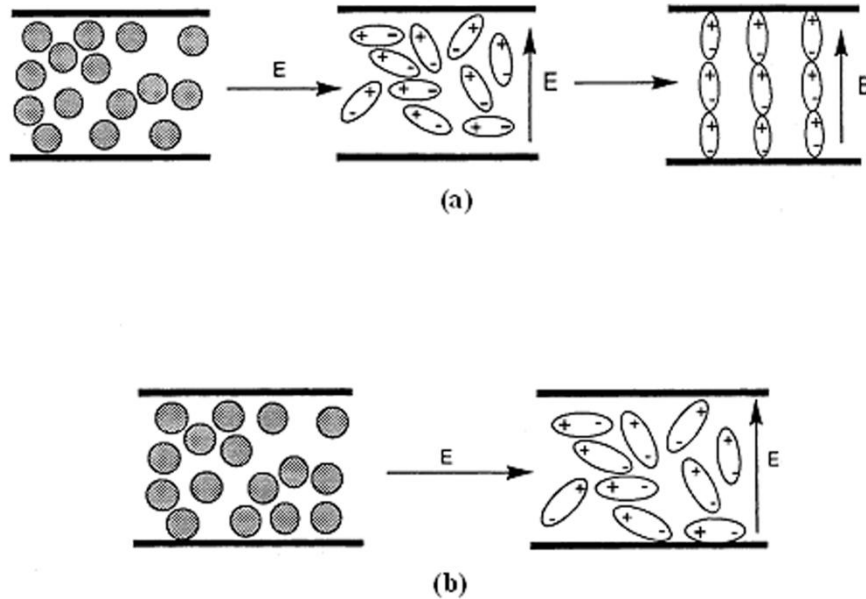


*Fig. 10. Schematic illustration of the ER particles (a) and the non-ER particles (b) behavior before and after an external electric field is applied [90].*

Figure 10 shows the effect of electric field on particles. The suitable particles for ER fluids respond to the electric field and aligned in the same direction while the non-ER particles kept a random order.

## 8. AIMS OF THE THESIS

The aim of the present work is to use solvothermal synthesis for the preparation of materials suitable for ER fluids. From the experience that has been gained during the researchers doctoral studies, the literature review, and the current work, it could be claimed that the best properties of suitable ER fluids are the suitable dielectric constant and suitable conductivity. So, the aim of this work is to investigate these factors by the:

- Preparation of PPy ribbon like with different conductivities.
- Preparation of TiO<sub>2</sub> nanorods with nanocavities which has high dielectric constant doped with chromium (Cr) to increase the conductivity.
- Preparation of different TiO<sub>2</sub> morphologies to study the effect of morphology on ER behavior.

## CHAPTER 2

### CHEMICALS AND METHODOLOGY

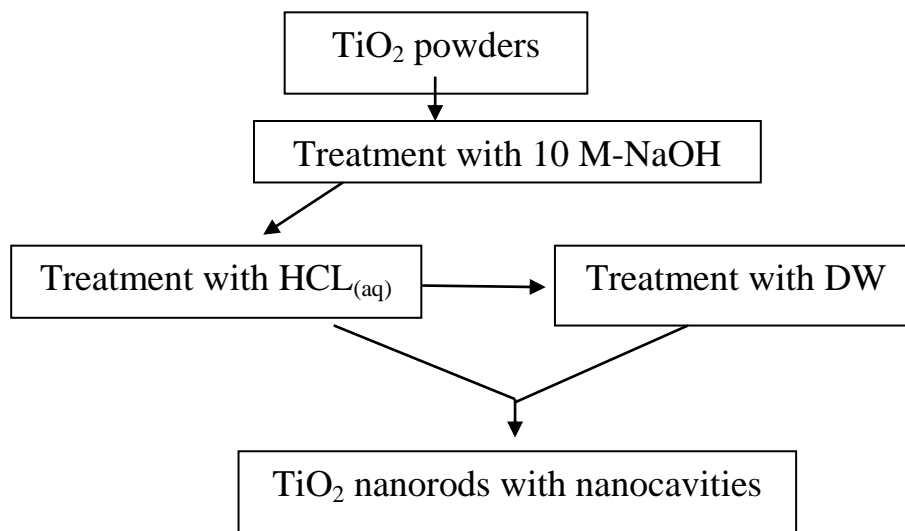
#### 2.1 Synthesis of TiO<sub>2</sub> nanorods with nanocavities

##### 2.1.1 Materials

Commercial titanium oxide nanopowder TiO<sub>2</sub> (p25), hydrochloric acid, sodium hydroxide (NaOH) and Hydrated Chromium hexachloride (CrCl<sub>6</sub>.6H<sub>2</sub>O) were purchased from Sigma-Aldrich Incorporation (St. Lois, USA). All chemicals were used as received.

##### 2.1.2 Synthesis of Titanium oxide nanorodes

TiO<sub>2</sub> nanorods were prepared according to literature [91], with some modifications. TiO<sub>2</sub> (0.75 g) was mixed uniformly with (70 mL) of 10 M NaOH in a 100 mL Teflon-lined autoclave. A specific amount of CrCl<sub>6</sub>.6H<sub>2</sub>O was added to the above solution. The molar ratios of Cr/Ti were 0%, 0.7%, 1.7%, 3.8%, 4.4% and 4.9%, respectively. The autoclave was heated at 180<sup>0</sup>C for 48 h in the oven, subsequently followed by HCl washing. The samples were dried at 80<sup>0</sup>C for 24 h and after that all of them were heated at 650<sup>0</sup>C for one hour. The same procedure was repeated for all six samples with one difference which is washing it with distilled water (DW) after acid treatment.



*Scheme 1. Synthesis method of TiO<sub>2</sub> nanoparticles.*

### **2.1.3 Morphology and structure characterization**

The morphology of the samples was characterized by SEM (Scanning Electron Microscope VEGA II LMU, Tescan, Czech Republic). Elemental analysis was done by EDX (Energy-Dispersive X-ray Spectroscopy VEGA II LMU, Tescan, Czech Republic). TEM (Transition Electron Microscopy) images were done using JEOL 1200.

### **2.1.4 Dielectric properties**

Dielectric properties were measured for 5wt. % suspension using Impedance Material Analyzer Agilent 4294-A, (Agilent, Japan) in frequency range 50 Hz- 1 MHz.

### **2.1.5 Preparation and ER measurements of TiO<sub>2</sub> nanorods suspensions**

The ER properties of 5wt. % of TiO<sub>2</sub> in silicone oil (Fluid 200, Dow Corning, UK; viscosity 100 mPa s, density 0.965 g/cm<sup>3</sup>) ultrasonically dispersed suspensions were carried out using a rotational rheometer (Bohlin Gemini, Malvern Instruments, UK), with coaxial cylinder geometry (length 27.4 mm, inner cylinder of 14 mm in diameter and the outer cylinder separated by a 0.7 mm gap), modified for ER experiments. Different DC electric field strengths generated by a DC high-voltage source TREK (TREK 668B, USA) were used (0.0- 3) kV/mm. All steady-flow measurements in the controlled shear rate (CSR) mode were performed in the shear rate range 0.1- 300 s<sup>-1</sup>.

The oscillatory tests were carried out through dynamic strain sweeps and frequency sweeps. The strain sweeps were performed in the applied strains range of 10<sup>-4</sup> to 1.0 under an electric field in order to get the position of the linear viscoelastic region (LVR). Afterwards, the viscoelastic moduli were obtained from the frequency sweep tests (0.1- 5 Hz) at fixed strain amplitude in the LVR. All the oscillatory measurements were performed in the CSR mode. Before viscoelastic measurements at new electric field strength, the formed internal structure was destroyed by shearing of the sample at 40 s<sup>-1</sup> for 60 s. The temperature in all experiments was kept at 25 ± 0.1 °C.

## **2.2 Synthesis of polypyrrole ribbon-like particles**

### **2.2.1 Materials**

Pyrrole (Py), ammonium persulfate (APS), cetyltrimethylammonium bromide (CTAB) and ammonia hydroxide (NH<sub>4</sub>OH) were used as received except for Py which was distilled under reduced pressure before using.

### **2.2.2 Synthesis of PPy ribbon-like structure**

PPy ribbon like structure was synthesized according to literature [92] with minor modification. PPy was prepared by oxidative polymerization of Py using APS as an oxidant (radical initiator) and CTAB as a surfactant. The resulted material was filtered and washed with NH<sub>4</sub>OH to decrease the conductivity. The sample which was treated twice -lower conductivity- named PPy2 and the sample treated once - higher conductivity- named PPy1.

### **2.2.3 Morphology characteristic**

The morphology of the samples was characterized by SEM (Scanning Electron Microscope VEGA II LMU, Tescan, Czech Republic).

### **2.2.4 Dielectric properties**

Dielectric properties were measured for 5wt. % suspension using Impedance Material Analyzer Agilent 4294-A, (Agilent, Japan) in frequency range 50 Hz– 5 MHz.

### **2.2.5 Preparation and ER measurements of PPy suspensions**

The ER properties of 3 wt. % of PPy1 and PPy2 in silicone oil (M200, Lukosiol Chemical Works Kolin, Czech Republic; viscosity 200 mPa s, density 0.965) ultrasonic dispersed suspensions were carried out using a rotational rheometer (Bohlin Gemini, Malvern Instruments, UK), with parallel plates geometry (40 mm diameter separated by a 0.5 mm gap), modified for ER experiments. Different DC electric field strength generated by a DC high-voltage source TREK (TREK 668B, USA) were used (0.0- 3.0) kV/mm. All steady-flow measurements in the controlled shear rate (CSR) mode were performed in the shear rate range 0.1- 200 s<sup>-1</sup>.

The oscillatory tests were carried out through dynamic strain sweeps and frequency sweeps. The strain sweeps were performed in the applied strains range of 10<sup>-4</sup> to 1.0 under an electric field in order to get the position of the linear

viscoelastic region (LVR). Afterwards, the viscoelastic moduli were obtained from the frequency sweep tests (0.1- 5 Hz) at fixed strain amplitude in the LVR. All the oscillatory measurements were performed in the CSR mode. Before viscoelastic measurements at new electric field strength used, the formed internal structure was destroyed by shearing of the sample at  $20 \text{ s}^{-1}$  for 60 s. The temperature in all experiments was kept at  $25 \pm 0.1^\circ\text{C}$ .

## **2.3 Morphology effect on ER behavior of $\text{TiO}_2$**

### **2.3.1 Materials**

Anatase-type titania nanopowders ( $\text{TiO}_2$ ), sodium hydroxide (NaOH) and absolute ethanol ( $\text{C}_2\text{H}_5\text{OH}$ ) were used without further purification.

### **2.3.2 Synthesis**

Different amount of anatase-type titania nanopowders were mixed with specific amount of 10 M NaOH solution and absolute ethanol with ratio 1:1. The mixture was heated at different temperatures for 24 hours, after cooling naturally to room temperature the product was obtained by filtration and subsequently continuously washed by distilled water to  $\text{pH} \approx 7$  to remove free NaOH adsorbed on the surfaces of the materials. The materials were dried at  $60^\circ\text{C}$  for 24 h.

### **2.3.3 Morphology characterization**

The morphology of the samples was characterized by SEM (Scanning Electron Microscope VEGA II LMU, Tescan, Czech Republic). Elemental analysis was done by EDX (Energy-Dispersive X-ray Spectroscopy VEGA II LMU, Tescan, Czech Republic).

XRD patterns were obtained with a PANalytical X'Pert PRO with theta-theta goniometer,  $\text{CuK}\alpha$  radiation (0.1542 nm) and PIXcel detector. All the measurements were operated at ambient temperature in reflection mode, at 40 kV and 30 mA with automatic slits in the range of angles from  $5$  to  $95^\circ$  ( $2\theta$ ) and step size  $0.0263^\circ$ , counting time 42.84 s per step.



### **2.3.4 Dielectric properties**

Dielectric properties were measured for 5wt. % suspension using Impedance Material Analyzer Agilent 4294-A, (Agilent, Japan) in frequency range 50 Hz- 1 MHz.

### **2.3.5 ER measurements**

The ER properties of 5wt. % of TiO<sub>2</sub> in silicone oil (M200, Lukosiol Chemical Works Kolin, Czech Republic; viscosity 200 mPa s, density 0.965) ultrasonic dispersed suspensions were carried out using a rotational rheometer (Bohlin Gemini, Malvern Instruments, UK), with coaxial cylinder geometry (length 27.4 mm, inner cylinder of 14 mm in diameter and the outer cylinder separated by a 0.7 mm gap), modified for ER experiments. Different DC electric field strength generated by a DC high-voltage source TREK (TREK 668B, USA) were used (0.0-3) kV/mm. All steady-flow measurements in the controlled shear rate (CSR) mode were performed in the shear rate range 0.1- 300 s<sup>-1</sup>.

**CHAPTER 3**  
**RESULTS AND DISCUSSION**  
**3.1 TiO<sub>2</sub> nanorods**

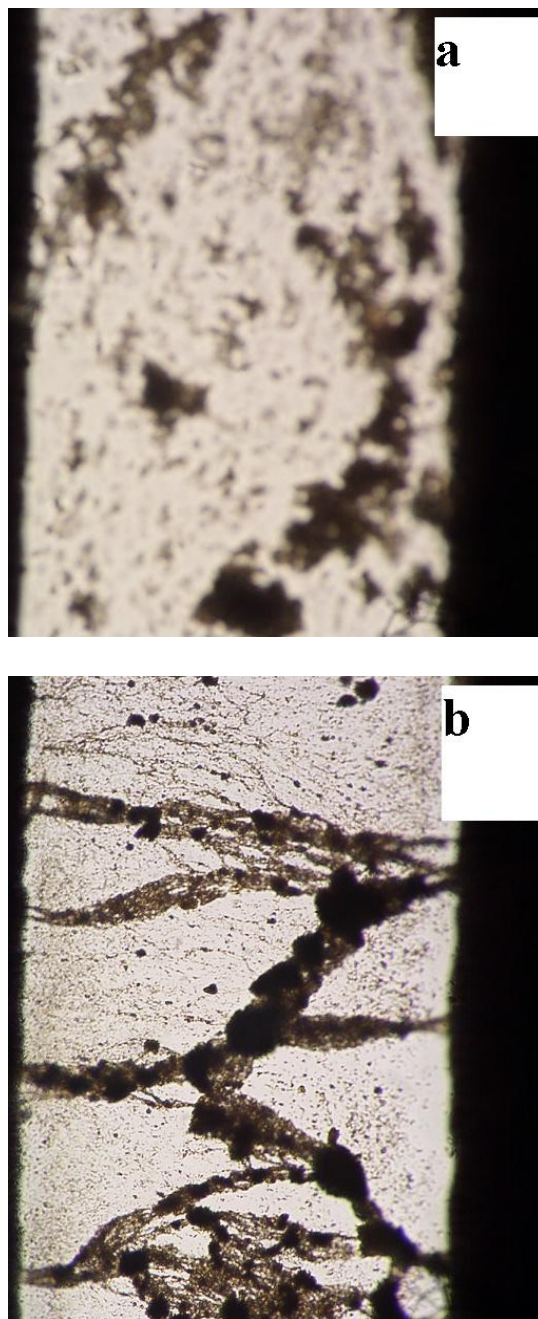


*Fig. 11. Images of TNR particle suspension under optical microscope before (a) and (b) after electric field application. (1 mm- gap)*

The microstructure image of the ER fluid (1 wt. % of TiO<sub>2</sub> nanorods suspension with 1 mm gap between the slides) in figure 11 was obtained using an optical microscope. The random structure of particles suspension in the absence of electric field can be seen in figure 11a. In figure 11b, the formation of a chain structure was demonstrated under an applied electric field of 1.0 kV/mm and the gap between the two electrodes was fixed precisely at 1 mm. As a response to the electric field the particles become polarized and attract each other by electrostatic forces. The formation of this structure is the reason why the high-field state of an ER fluid exhibits increased viscosity and is able to sustain shear in the direction perpendicular to the applied electric field. Therefore, the appearance of microstructure image shown in figure 11b is due to the electrostatic interaction between the conductive particles, which is caused by the mismatch of the dielectric constants between the conductive particles and oil. The Cr doped TiO<sub>2</sub> nanorod composites form chains of particles within seconds after the application of an electric field, and the chain-like structure remained stable as long as the electric field was applied. We also observed the aggregated particles in the chain. It is possible that the induced dipole-dipole interaction made the particles aggregate. Moreover, the fibrillated chain structure might provide a path for the transport of electrons, and thereby contribute to the conducting behavior of the ER fluids [93].

### **3.1.1 Morphology characterization and composition**

Figures 12-15 show the SEM image of TiO<sub>2</sub> doped with Cr at different weight percent (0.0, 0.7, 3.8, and 4.9) % respectively. It can be thought that there are two kinds of shapes in the composites. One is from the TiO<sub>2</sub> particles, and the other is the Chromium oxide which forms mostly on the surface of the rods instead of the nanocavities of the rods. This can be approved by SEM image for 4.9 Cr mol % TiO<sub>2</sub> nanorods which showed the disappearance of the rod-like shape because the chromium oxide covers it completely.

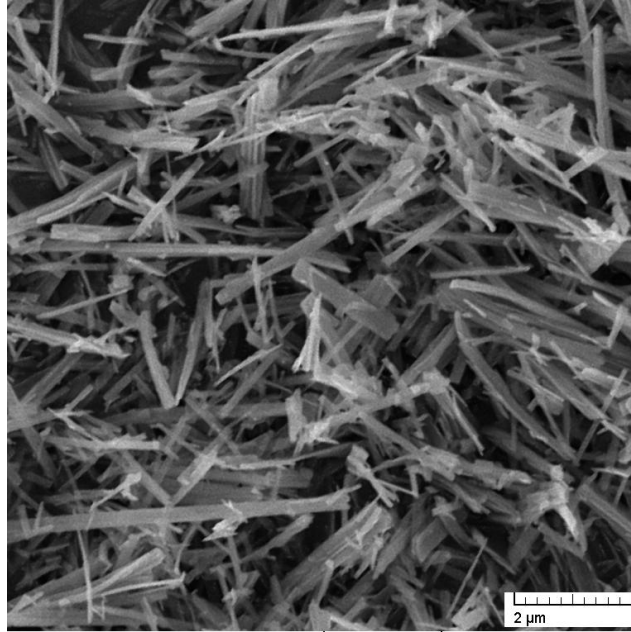


*Fig. 12. SEM image for 0.0 Cr mol % TiO<sub>2</sub> nanorods.*

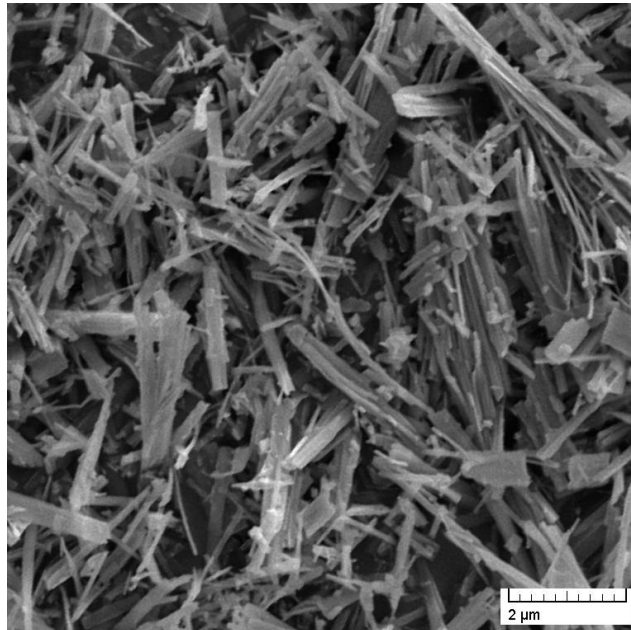


*Fig. 13. SEM image for 0.7 Cr mol % TiO<sub>2</sub> nanorods.*

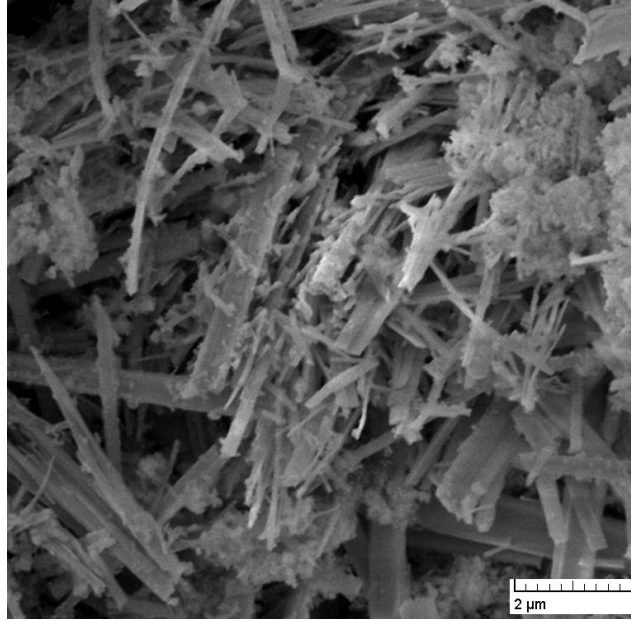


*Fig. 14. SEM image for 3.8 Cr mol % TiO<sub>2</sub> nanorods.*

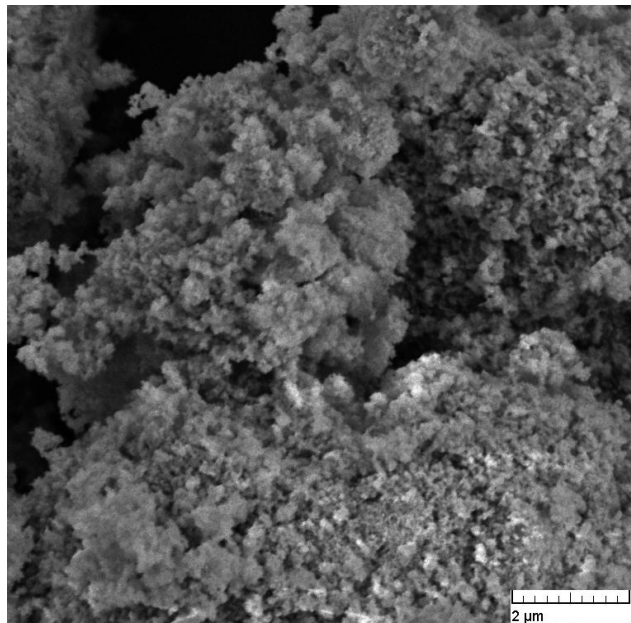


*Fig. 15. SEM image for 4.9 Cr mol % TiO<sub>2</sub> nanorods.*

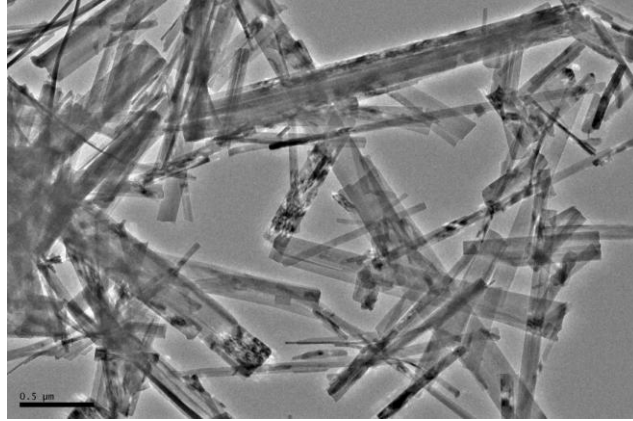


*Fig. 16. TEM image for 0.0 Cr mol % TiO<sub>2</sub> nanorods before heating.*

Figures 16-18 present the TEM images of undoped and 0.7 mol% Cr doped TiO<sub>2</sub> nanorods after heating at 650 °C. There were many nanocavities inside both the undoped and doped TiO<sub>2</sub> nanorod shown in figures 17, 18. The size of the nanocavities shown in the figures are about 10-20 nm in diameter and there are different shapes of these nanocavities, such as circle, hexagon, and rectangle [91]. The surface Cr<sub>2</sub>O<sub>3</sub> can be seen as aggregates on the surface of TiO<sub>2</sub> nanorods.

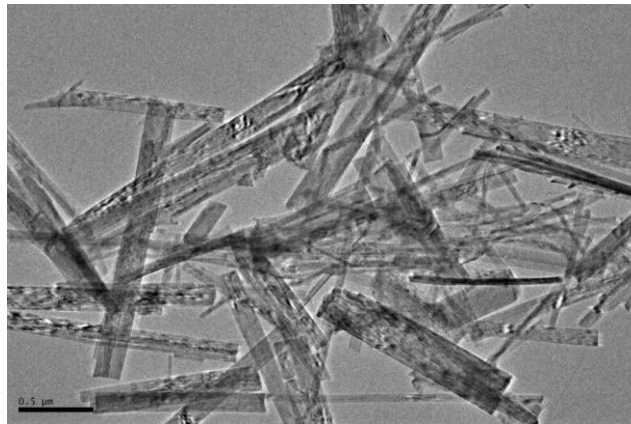


*Fig. 17. TEM image for 0.0 Cr mol % TiO<sub>2</sub> nanorods after heating.*

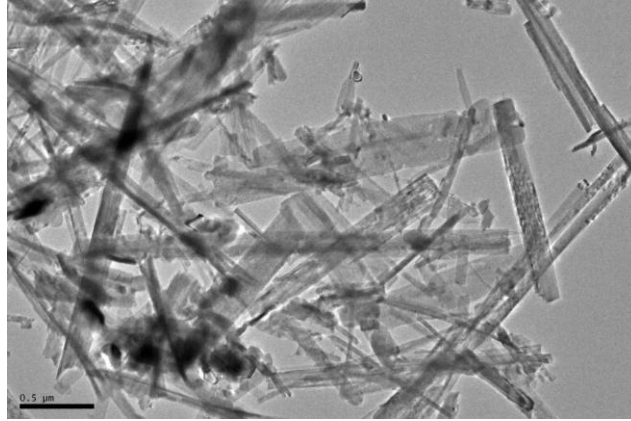


Fig. 18. TEM image for 0.7 Cr mol %  $\text{TiO}_2$  nanorods after heating.

EDX as an analytical technique used for elemental analysis of the sample. The main principle of this characterization method is to use a high-energy beam of electrons to hit the sample being studied. As a result to the collision of energetically electrons with the sample electrons, sample electrons absorb energy and excite to a higher level within the atom. However, the electron now in excited state which is unstable state so, the electron returns to its original ground state emitting the energy representing in spectrum as a peak with specific value of energy measured by electron Volt (eV). Energy value is like a finger-print for individual atoms. Figures 19, 20 show the EDX results of 0.7 Cr mol % doped  $\text{TiO}_2$  water treated and 4.3 mol % Cr-doped  $\text{TiO}_2$  acid treated after heat treatment, which indicate that Cr element exists in the  $\text{TiO}_2$  nanorods. However, there is a difference between the calculated and the real molar ratio of Cr/Ti which indicate that a small quantity ran off in the experimental washing process. Carbon was used as the energy reference material, and its characteristic peak appeared at around 285 eV. Copper (Cu) appears in some spectrum because of the grid used in measurements.

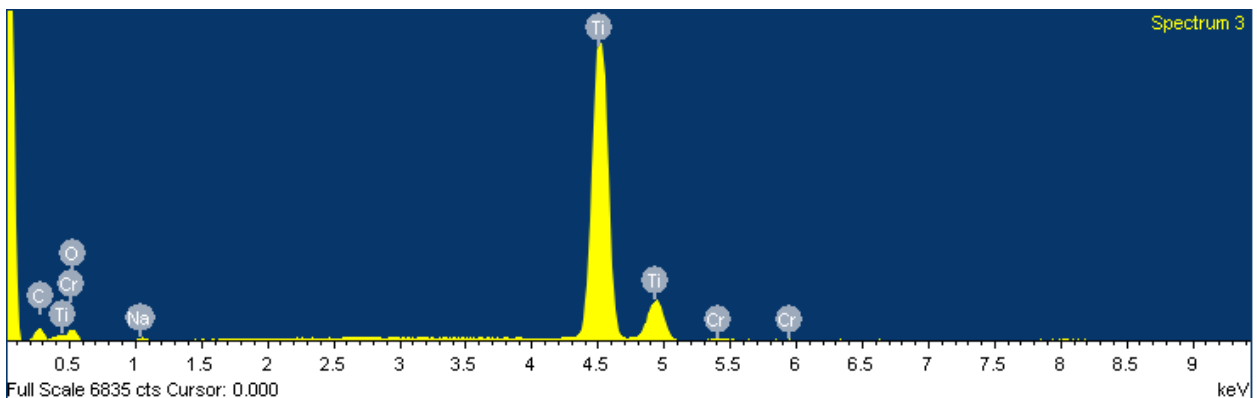


Fig. 19. EDX for 0.7 Cr mol %  $\text{TiO}_2$  nanorods water treated.



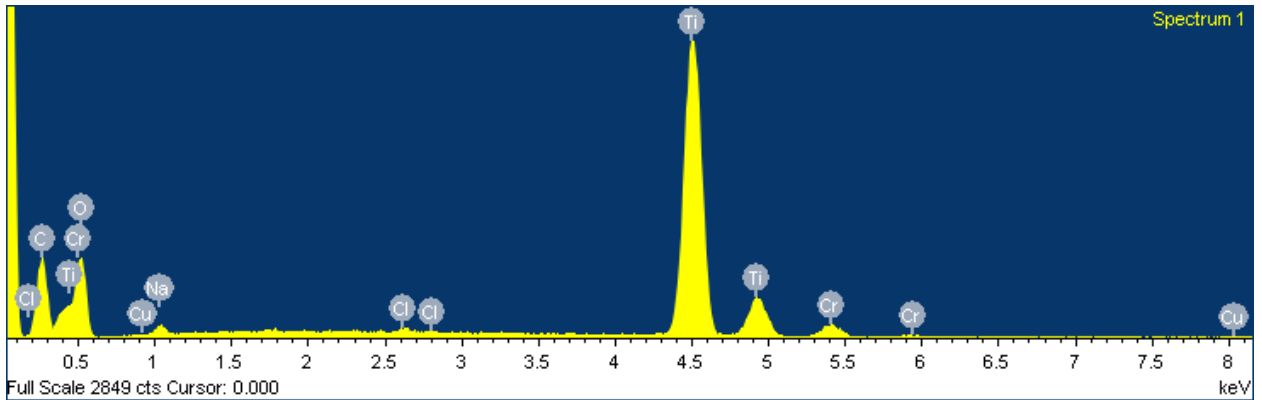


Fig. 20. EDX for 4.3 Cr mol% TiO<sub>2</sub> nanorods hydrochloric acid treated.

### 3.1.2 Rheological properties

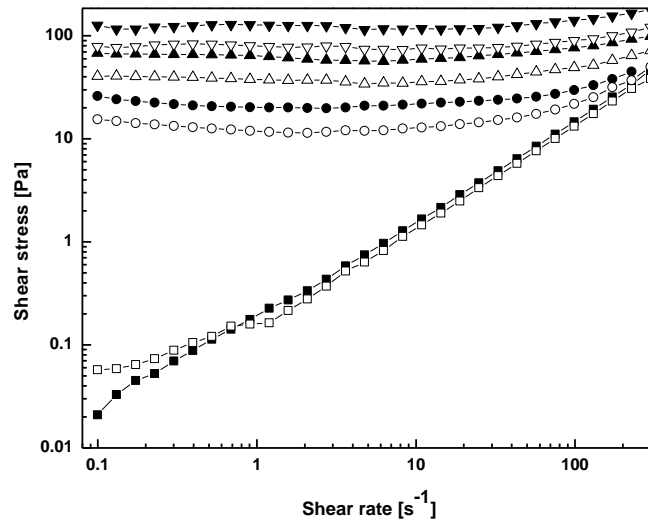


Fig. 21. Shear stress versus shear rate of 5 wt. % suspensions of 0.7 mol % Cr-TiO<sub>2</sub> nanorods particles (solid-water treated) and 0.8 % Cr-TiO<sub>2</sub> nanorods particles (open-HCl treated) in silicone oil at 0,(■), 1,(●), 2,(▲), 3,(▼)kV/mm.

Fig. 21 shows the flow curve of shear stress vs. shear rate measured by CSR mode for suspensions containing 5 wt. % of 0.7 mol % Cr-TiO<sub>2</sub> nanorods water treated and 0.8 Cr mol % TiO<sub>2</sub> nanorods acid treated. In absence of an electric



field, both suspensions show almost a Newtonian behavior. When an electric field is applied, the suspensions exhibit a shear stress and the yield phenomena can be found. The yield stress of water treated suspension was higher than that for acid treated suspension. However, both samples maintain a wide plateau level in the measured shear rate regions. It is known that the ER fluids effect is related to two processes: reorganization and destruction. These structure changes were further dominating by the competition between the electrostatic interaction among particles induced by electric field and the hydrodynamic interactions induced by shearing process. The electrostatic interactions were responsible for the reorganization of ER structure and hindered the flow, while the hydrodynamic interactions tended to destroy ER structures and promoted flow. At low shear rate regions, the hydrodynamic interactions were small and the electrostatic interactions dominated the flow. As the shear rate increases, the hydrodynamic interactions became stronger and gradually overcame the electrostatic interactions, so that the destruction rate of ER structure became faster than the reorganization rate and thus the shear stress decreased. According to fig. 21 the particle organization of ER structure for TiO<sub>2</sub> nanorods water treated is higher than that of acid treated one.

The shear viscosity vs. shear rate curves of 0.7 Cr mol % TiO<sub>2</sub> nanorods-water treated and 0.8 Cr mol % TiO<sub>2</sub> nanorods- acid treated are shown in figures 22, 23. Both suspensions behave mostly as Newtonian fluids i.e. exhibit constant viscosity with change in shear rate with slight deviation for the acid treated TiO<sub>2</sub> particles at low shear rate. However, as the electric field was applied, the viscosity enhanced and increased more than four orders at 3kV/mm and suspensions followed non-Newtonian behavior. The relative viscosity for water treated TiO<sub>2</sub> nanorods suspension was higher than that of acid treated one. At higher shear rate, the hydrodynamic force increased and the effect of electric field on shear viscosity started to diminish and this can be seen by extrapolation of the curves to higher shear rate where all curves will coincide.

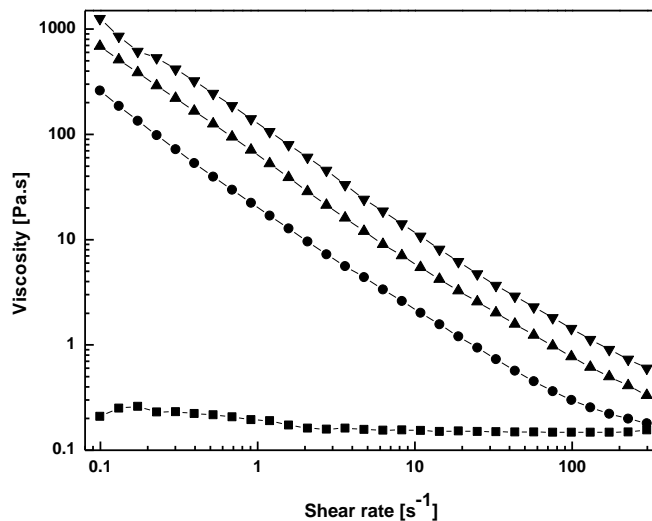


Fig. 22. Shear viscosity versus shear rate of 0.7 mol % Cr-TiO<sub>2</sub> nanorods suspension in silicone oil at different electric field strengths. (water-treated) 0, (■), 1, (●), 2, (▲), 3, (▼) kV/mm.

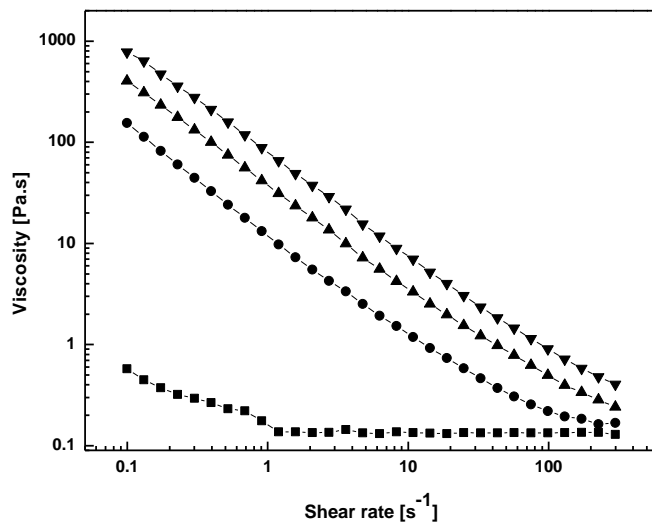


Fig. 23. Shear viscosity versus shear rate of 0.8 mol % Cr-TiO<sub>2</sub> nanorods suspension in silicone oil at different electric field strengths. (Acid treated) 0, (■), 1, (●), 2, (▲), 3, (▼) kV/mm.

Figure 24 shows the dependence of yield stress on the mol percent of doped Cr in TiO<sub>2</sub> nanorods at 3 kV/mm electric field strength. The effect of doping Cr in TiO<sub>2</sub> nanorods increase the yield stress until a maximum followed by a decrease. The highest yield stress was for the 0.7 mol % Cr doped TiO<sub>2</sub> nanorods which reached 130 Pa at 3 kV/mm with 5 wt. % suspensions. On the other hand, the more doping Cr mol % of TiO<sub>2</sub> nanorods leads to increase in conductivity of the particles and relatively more current density pass through suspensions which is relevant to the degradation of the ER properties at high Cr mol % doping TiO<sub>2</sub> nanorods.

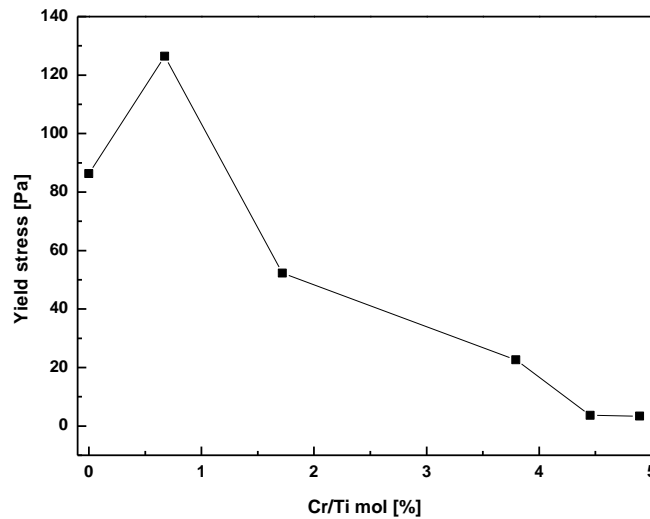
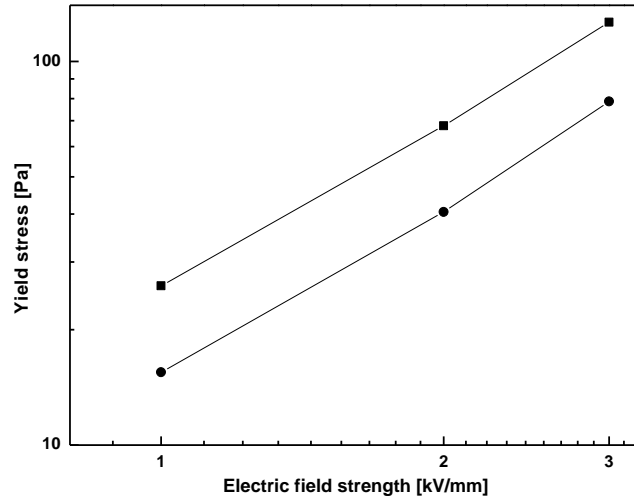


Fig. 24. Yield stresses versus Cr mol % doping for 5 wt. % of TiO<sub>2</sub> nanorods suspensions (water treated) at 3kV/mm.

The strength of the structure created under electric field can be determined from the dependence of static yield stress on the electric field strength. This is presented in figure 25 for the materials of 0.7 Cr mol % TiO<sub>2</sub>- water treated and 0.8 Cr mol % TiO<sub>2</sub> –acid treated particle suspensions; it was obtained in the CSS mode. The correlation of the yield stress  $\tau_y$  to the electric field strength  $E$  is generally expressed as  $\tau_y \propto E^\alpha$  thus, in log scale  $\alpha$  is the slope of the dependence. In fig. 25, it was found that  $\alpha = 1.46$  for TiO<sub>2</sub> particle suspensions which corresponds to theoretical prediction for well developed ER structures ( $\alpha = 1.5$ ) [94].

Also, the dependence of yield stresses on the electric field shows a nearly linear behavior at low electric fields which agree with the surface saturation polarization mechanism proposed by Wen [95]. As a whole the linearity disappear in this relation and  $\alpha$  was calculated to be 1.14, we can say the mechanism of polarization

is a combination of polarization and conduction models. The nonlinear ER behavior usually is related with the increased particle conductivity at higher electric field strengths.



*Fig. 25. Yield stresses values versus electric field strengths for 0.7 Cr mol % TiO<sub>2</sub> nanorods-water treated (■) and 0.8 Cr mol % TiO<sub>2</sub> nanorods-acid treated (●).*

Figures 26, 27 show the viscoelastic properties of 0.7 Cr mol % TiO<sub>2</sub> nanorods-water treated and 0.8 Cr mol% TiO<sub>2</sub> nanorods-acid treated respectively. Without the electric field the elastic modulus was slightly higher than viscous modulus in water treated suspension which means it is more viscous than acid treated one which shows the opposite. This behavior of the suspensions at 0.0 kV/mm reflected on the behavior at 3 kV/mm. The elastic modulus increased more than five orders of magnitude in both suspensions with higher elastic modulus for water treated suspensions mostly because of increasing conductivity. The elastic moduli show almost no dependence on frequency which mean that the structures of these particle suspensions show a stiff and elastic chain structure.

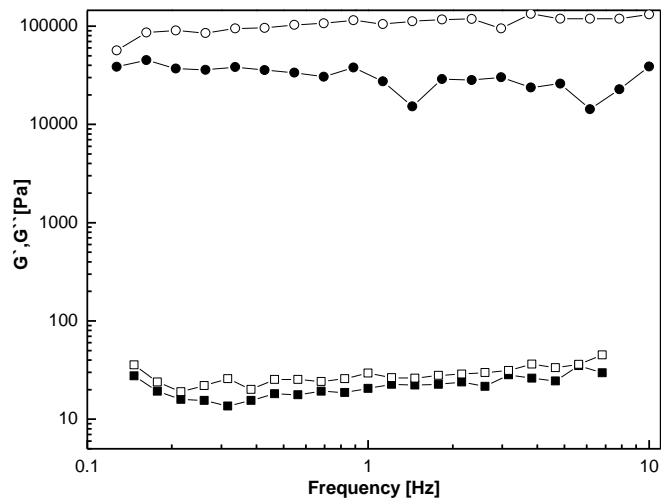


Fig. 26. Viscoelastic moduli  $G'$  and  $G''$  versus frequency for 5 wt. % suspension of 0.7 Cr mol %  $\text{TiO}_2$  nanorods water treated.  $G'$  (open),  $G''$  (solid) at 0kV/mm (■) and 3 kV/mm (●).

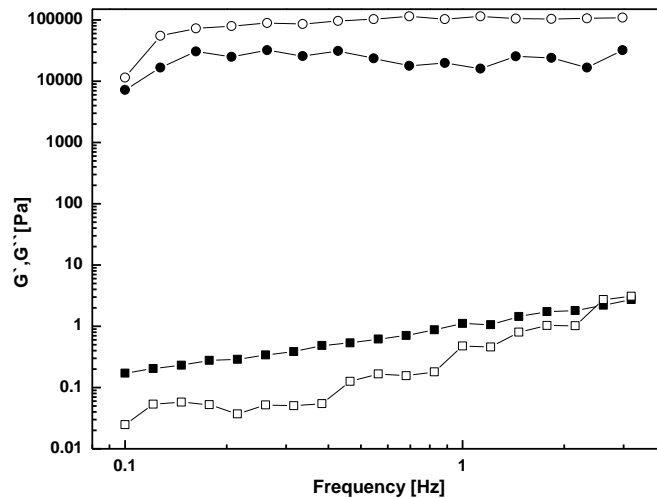


Fig. 27. Viscoelastic moduli  $G'$  and  $G''$  versus frequency for 5 wt. % suspension of 0.8 Cr mol %  $\text{TiO}_2$  nanorods acid treated.  $G'$  (open),  $G''$  (solid) at 0kV/mm (■) and 3 kV/mm (●).

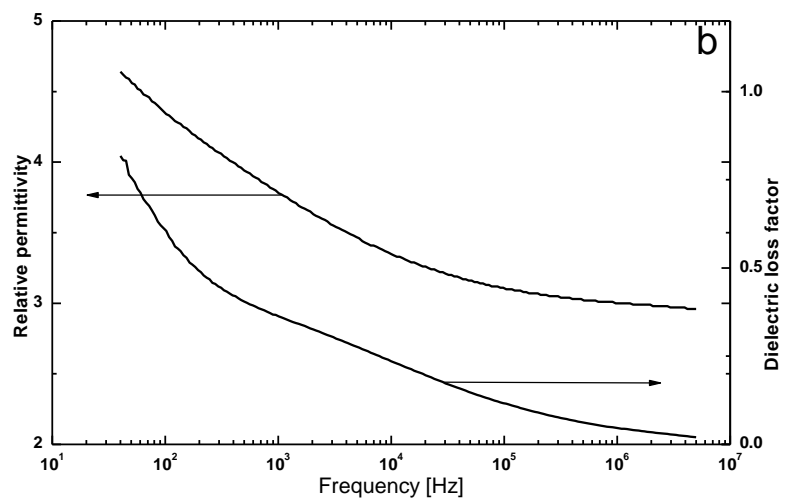
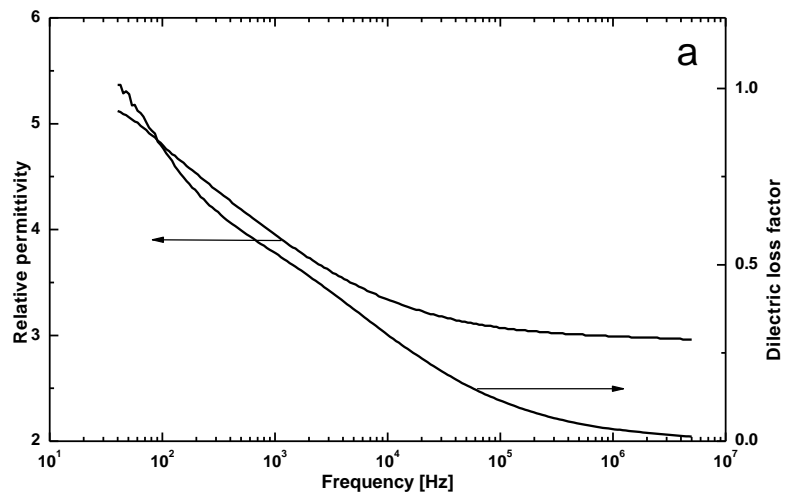


Fig. 28. Frequency dependencies of the relative permittivity  $\epsilon'$  and dielectric loss factor  $\epsilon''$  for 0.7 Cr mol %  $\text{TiO}_2$  nanorods water treated (a) and 0.8 Cr mol %  $\text{TiO}_2$  nanorods acid treated (b) with 5 wt. % suspensions.

It is generally accepted that interfacial polarization providing fluids with significant ER activity occurs at an optimum polarization rate corresponding to a frequency between about  $10^2$  and  $10^5$  Hz. Dielectric measurements of suspensions of 0.7 mol % Cr doped  $\text{TiO}_2$  nanorods water and acid treated are shown in figure 28. Figure 28 shows that the dielectric loss  $\varepsilon''$ , has a maximum at much lower frequencies. This corresponds to long relaxation times in the electric field and, consequently, to a low polarization rate.

The particle polarizability, proportional to the slope of the frequency spectra of relative permittivity, is not too high and has almost the same value for both samples as shown in figure 28. This suggests that, from the point of view of the ER phenomenon, the effect of treatment  $\text{TiO}_2$  nanorods with water and acid affect the shape and content of Cr in the samples. However, slight difference can be noted. As a result, the responses of the different sample in the electric field have slight difference in viscosity and shear stress measurements but following the same trend for both suspensions. The increase in dielectric constant value was accepted because some of titanium compound achieved a giant dielectric constant. Calcium copper titanium oxide shows a giant dielectric constant and it reaches 50000 at 50 Hz. The dielectric constant was found to be dependent on temperature sample treatment [96].

Taking the importance of yield stress which plays critical role in designing smart devices into account, the yield stress was analyzed as a function of electric field strength. Here, we estimated the dynamic yield stress from a controlled shear rate measurement (CSR) by extrapolating the shear stress to zero shear rates. We then plotted the dynamic yield stress as a function of various electric fields for 10 wt. % suspension of 1.4 Cr mol %  $\text{TiO}_2$  nanoparticles, Figure 29. It is well known that, the dynamic yield stress and electric field was presented as follows:

$$\tau_y \propto E^n \quad (9)$$

The dependency of the dynamic yield stress on the electric field strength differs from the  $E^2$  dependency suggested by the polarization model. The ER response is influenced by the conductivity of the particles and the interaction between the particles and medium. The increase in the yield stress with increase in the electric field strength is due to the increase in the electrostatic forces between the particles.

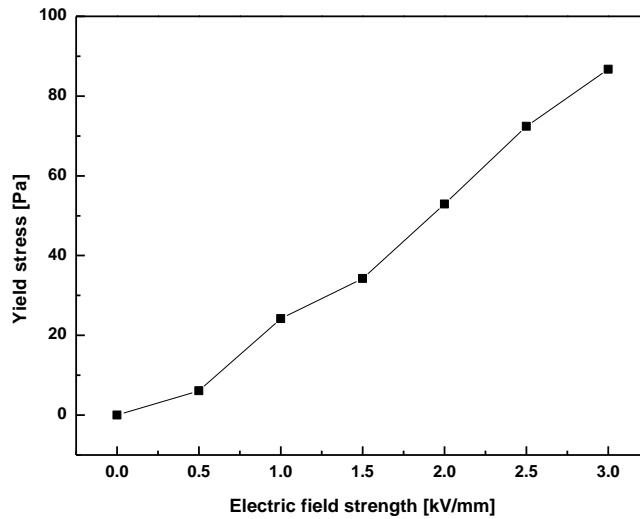


*Fig. 29. Yield stress versus electric field strength for 10 wt. % suspensions of 1.4 Cr mol % TiO<sub>2</sub> nanorods water treated sample in silicone oil suspensions.*

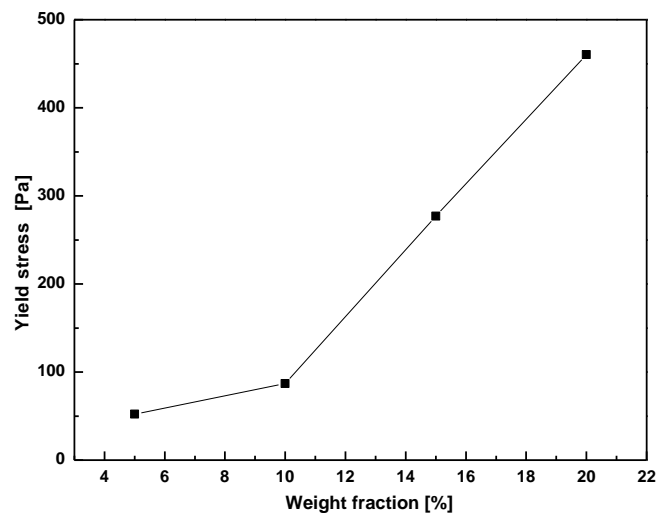


*Fig. 30. Yield stress versus weight fraction of 1.4 Cr mol % TiO<sub>2</sub> nanorods water treated sample in silicone oil suspensions.*

Figure 30 shows the yield stress of 1.4 Cr mol % TiO<sub>2</sub> nanoparticles suspension with different weight fraction. The behavior shows nearly linear behavior according to polarization model with this equation:



$$\tau_y \propto \dot{\gamma}^1 \quad (10)$$

From these results it was concluded that the ER effect of Cr doped TiO<sub>2</sub> nanorods with nanocavities suspensions progress by both, conduction and polarization model.

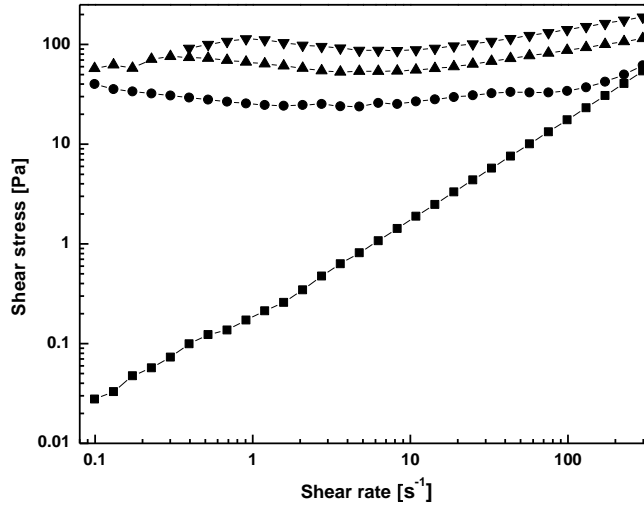


Fig. 31. Shear stress versus shear rate dependence for 10 wt. % suspensions of 1.4 mol % Cr-TiO<sub>2</sub> nanorods particles (water treated) in silicone oil at 0,(■),1,(●),2,(▲),3,(▼)kV/mm.

Figure 31 shows the dependence of shear stress on shear rate for 10 wt. % of 1.4 Cr mol % doped TiO<sub>2</sub> nanorods tested in a controlled shear rate mode. Without an electric field, the ER fluid acts as ideal viscous fluid where the shear stress grew linearly with the shear rate. When an electric field was applied, yield stresses appeared and increased step-wise with the electric field strengths. After the appearance of the yield stress, the shear stress decreased as a function of the shear rate to a minimum, called the critical shear rate, before increasing again. This phenomenon was considered the result of the changing particles microstructure. In the presence of an electric field, the particles were polarized and connected to each other to form chain-like structures. In the shear field, these structures were destroyed and reformed under the cooperation of the electrostatic and hydrodynamic forces. Moreover the time needed for the relaxation process lagged behind the action of the shear rate. Therefore, the shear stress decreased in the

electrostatic dominated region (low shear rate region) and increased in the hydrodynamic force dominated region (high shear rate region) thereafter.

Figure 32 shows the curves of shear stress versus shear rate for 20 wt. % of 1.4 Cr % TiO<sub>2</sub> particles. The results show that the suspension behaves as Newtonian behavior at low shear rate (till 1 s<sup>-1</sup>) due to high concentration of the particles. Above 1 s<sup>-1</sup> the suspension behaves as pseudoplastic (as in figure 31) with shear thinning which can be explained by the decrease in concentration because the particles climb on the inner rotating cylinder as in Weissenberg effect which we were able to see after the finishing the measurement with or without the electric field. This behavior explained in the literature for polymer rheological behavior at low shear rate and the stress increase followed by plateau then increase which imply that the flow is unstable and this behavior is concentration dependent [97]. This idea can be supported by the shear viscosity curves of 20 wt. % shown in figure 34.

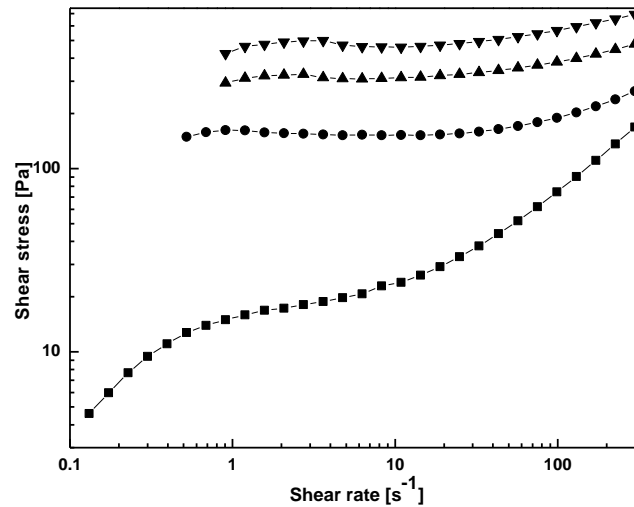
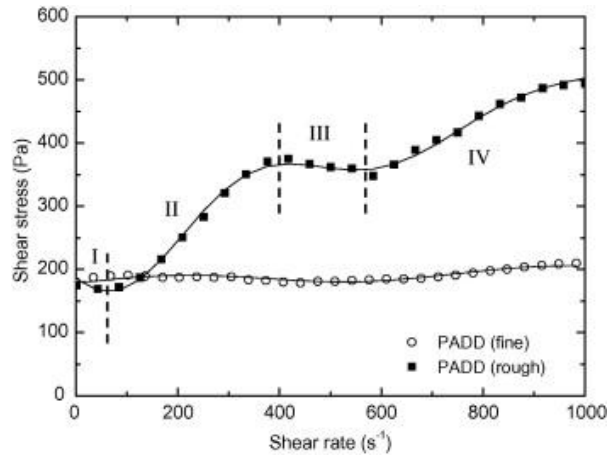


Fig. 32. Shear stress versus shear rate dependence for 20 wt. % suspensions of 1.4 mol % Cr-TiO<sub>2</sub> nanorods particles (water treated) in silicone oil at 0, (■), 1, (●), 2, (▲), 3, (▼) kV/mm.

Figure 33 shows the fit of the suggested model to flow curves for poly(acrylamidino diethylenediamine) fine and rough particles based ER fluids at electric field strength of 2 kV/mm. The rough particles suspension shows different flow behavior at different shear rate. The flow curve shows four different flow regions. Region I for the slow polarizations and fully-formed lamellar patterns,

while region II represents the increase of the shear stress with increase of the shear stress with increased with shear rate after fully-formed fibrillar and lamellar patterns. Region III shows an abrupt decrease of the shear stress due to the destruction of the chain and lamellar structures. Region IV shows the slow-destruction rate of the chain and lamellar structures due to competition of reformation and destruction between the particles [41].



*Fig. 33. Fit of the suggested model to flow curves for poly-PADD fine and rough particles based ER fluids at an electric field of 2 kV/mm [41].*

In figure 34, the Newtonian behavior was seen at low shear rate where the viscosity does not depend on the shear rate. Above  $1 \text{ s}^{-1}$  the material behaves as a non-Newtonian and the viscosity starts to decrease with shear rate increasing until the effect of electric field strengths show nearly no effect at high shear rate because of dominant dynamic forces resulted from the shearing.

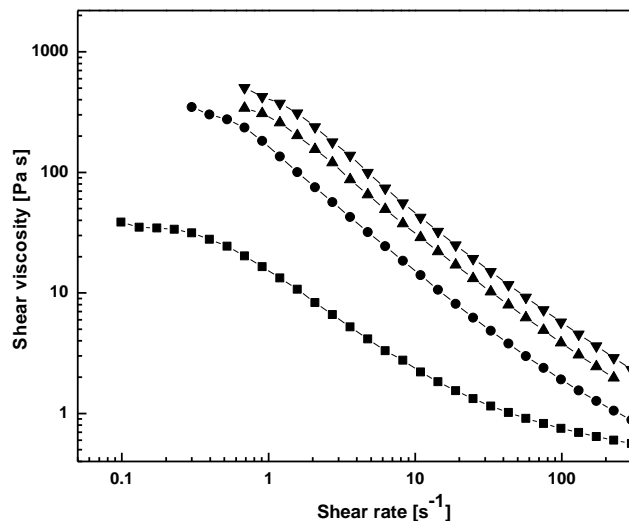


Fig. 34. Shear viscosity versus shear rate for 20 wt. % suspensions of 1.4 mol % Cr-TiO<sub>2</sub> nanorods particles (water treated) in silicone oil at 0, (■), 1, (●), 2, (▲), 3, (▼) kV/mm.

### 3.1.3 Conclusions

Different Cr mol percent doped-TiO<sub>2</sub> nanorods with nanocavities were synthesized using hydrothermal synthesis. These TiO<sub>2</sub> nanorods were treated with different washing method and in the final step, one was washed with distilled water and the other one washed with 0.1 M HCl solution. The particles were characterized by scanning electron microscopy (SEM), transmission electron microscopy (TEM) and electron dispersive energy (EDX). ER behavior (ER) was investigated for all samples and it showed that the ER effect for the samples washed with water was higher than that of the acid treated one. It was found that, the highest ER effect was for the sample doped with 0.7 mol percent of Cr. The yield stress was 126 Pa at 3 kV/mm for 5 wt. % suspension of 0.7 mol Cr-doped TiO<sub>2</sub> particles.

## 3.2 Polypyrrole results

Nanowire- and nanoribbon-like PPy can be synthesized in the presence of long chain cationic surfactants such as CTAB and anions of the oxidizing agent APS. The number of critical micelle plays important role in the formation of wire- or ribbon-like structure besides to the oxidizing agent.

### 3.2.1 Morphology and structure

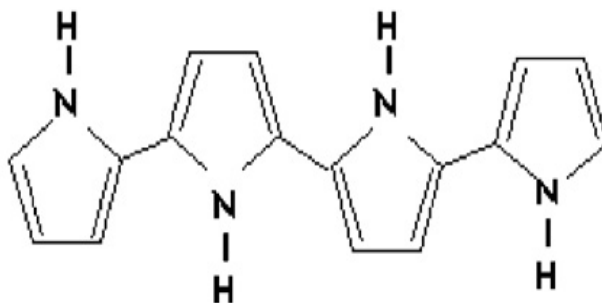


*Fig. 35. PPy chain structure.*

The morphology of PPy appeared to be ribbon-like nanostructures with width in the range of between 25 and 85 nm, heights in the range of several nanometers, and lengths up to several micrometers (figure 36) [91].

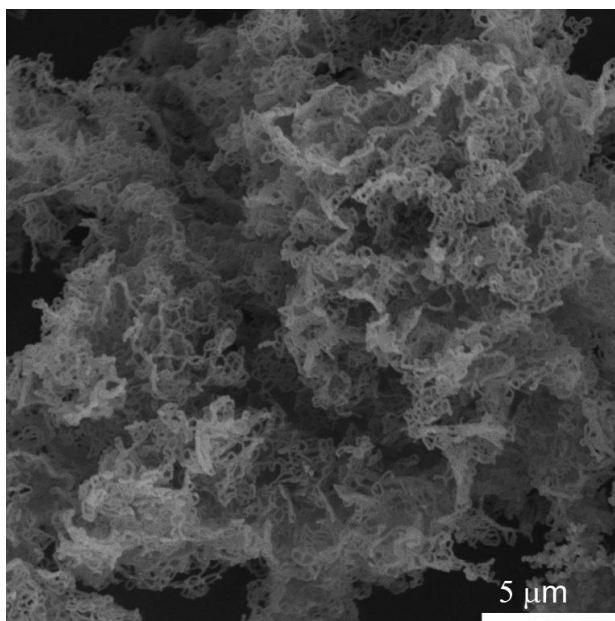


*Fig. 36. SEM picture of PPy particle structure.*

### 3.2.2 Rheological properties and conductivity

Figure 37 shows the flow curves of shear stress as a function of shear rate for PPy1 and PPy2 suspensions under different electric field strengths. In the absence of an electric field, both samples behave like dilute suspensions by showing a slight departure from the Newtonian fluid behavior. When an electric field is applied, the suspensions exhibit a strong increase in shear stress and their flow behavior become like Bingham fluid with notable yield stress. PPy2 shows higher shear stress upon the application field which means that the microstructure induced by the electrostatic force is stiffer between the particles of PPy2 than the microstructure formed between PPy1 particles. Furthermore, observation of fig. 36 indicates that the shear stress slightly decreases and then increases as the shear rate increases demonstrating the existence of critical shear rate [98]. Below the critical shear rate, the shear stresses decreased as a function of shear rate, and then above the critical shear rate the fluid exhibited pseudo-Newtonian behavior. In a low shear rate region, the electrostatic interactions among particles induced by external electric fields are dominant compared to hydrodynamic interactions induced by the external flow field. The aligned particular structures begin to break with shear deformation, and the broken structures tend to reform the chains by the applied electric field, depending on the magnitude of the applied shear and particle-particle interaction in the fibrils. The decrease in shear stress is observed when increase in the reformed structures with shear rate is not as complete as those before applying shear flow.

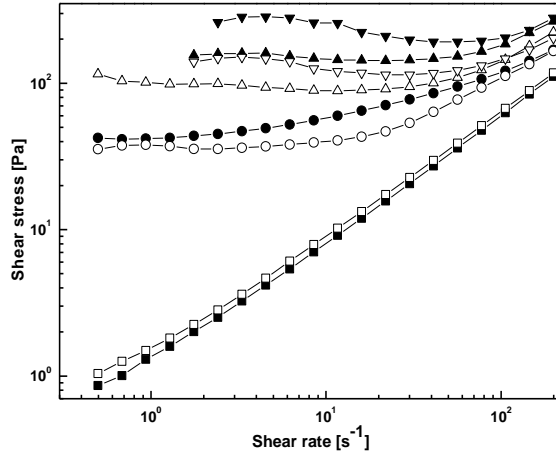


Fig. 37. Shear stress versus shear rate dependence for 3 wt. % PPy ribbon particles PPy1 (open) and PPy2 (solid) suspensions. Electric field strengths  $E$  (kV/mm): ( $\square, \blacksquare$ ) 0.0, ( $\circ, \bullet$ ) 1.0, ( $\triangle, \blacktriangle$ ) 2.0, ( $\nabla, \blacktriangledown$ ) 3.0.

Interfacial polarization is an important factor for an ER fluid, and can be described by the complex dielectric constant,  $\varepsilon = \varepsilon' - i\varepsilon''$ . It is known that a good ER effect requires two important factors, including a dielectric relaxation peak in  $\varepsilon''$  (expressed by  $\sigma/2\pi f$ , where  $\sigma$  is the conductivity and  $f$  is frequency) within the range of  $10^2$ - $10^5$  Hz and a large  $\Delta\varepsilon'$  ( $\Delta\varepsilon' = \varepsilon'_{100 \text{ Hz}} - \varepsilon'_{100 \text{ kHz}}$ ). The relaxation time  $\lambda$  and  $\Delta\varepsilon'$ , which are related to interfacial polarization and the yield stress enhancement for ER materials, can greatly affect the ER properties.

Figure 38 shows the dielectric properties of ER fluids (3 wt. %) based on PPy1 and PPy2 conductivity modified particles. It is clearly seen that the conductivity affects the dielectric constant and loss factor. PPy2 with lower conductivity ER fluid shows large  $\Delta\varepsilon'$  and dielectric loss peaks, indicating strong and fully interfacial polarization. Thus, the chain structure can be maintained when the deformation starts, so that the higher yield stress are expected to be achieved. In the other hand, PPy1 shows smaller  $\Delta\varepsilon'$  and the dielectric loss peak shifts to lower frequency which mean higher relaxation time, which indicates that its polarization is not as good as PPy2.

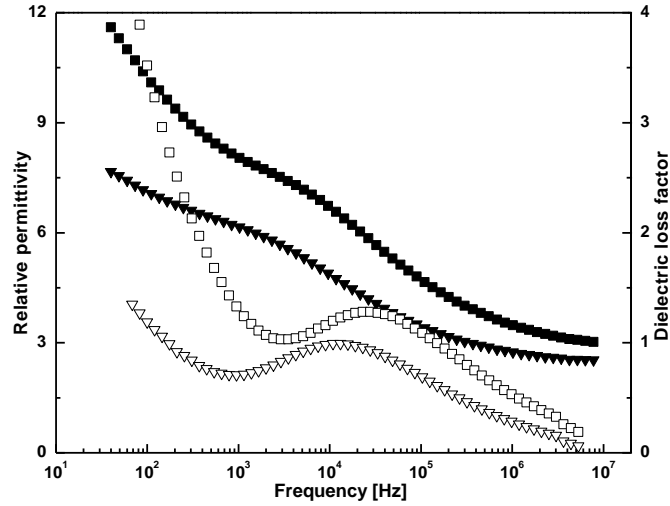


Fig. 38. Dependence of relative permittivity (solid) and dielectric loss factor (open) on frequency of PPy1 (▼, ▽) and PPy2 (■, □) suspensions.

The dependence of the dynamic yield stress on the electric field strength is presented in Fig. 39 for 3 wt. % of different conductivity PPy1 and PPy2. The symbols represent experimental data and the lines indicate the linear regression of the data. The yield stresses of PPy2 (lower conductivity) are greatly enhanced by more treatment with  $\text{NH}_4\text{OH}$  solution compared to PPy1 (higher conductivity) which treated less times. The dynamic yield stress is the plateau stress at very low shear rates and is related to polarization forces. The results show an agreement with the power law  $\tau_0 = q E^\alpha$ , where  $\alpha$  represents the response of particle polarizability to the electric field strength. Higher ( $\alpha = 1.73$ ) for PPy2 indicates the better polarization response than PPy1 ( $\alpha = 1.63$ ). Higher  $q$  value for suspension of PPy2 sample ( $q = 1.45$ ) corresponds to higher stiffness of generated ER structures in comparison to suspension of PPy1 sample ( $q = 1.13$ ) as shown in table 1.

sample	$\alpha$	$q$
PPy1	1.63	1.13
PPy2	1.73	1.45

Table 1. Values of parameters in power law model for PPy1 and PPy2.



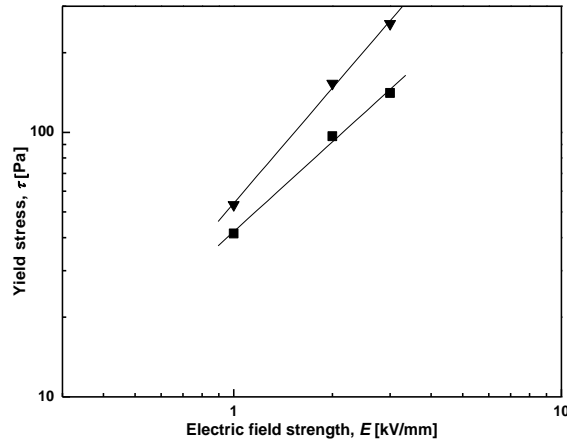


*Fig. 39. Dependence of the yield stress on electric field strength for 3 wt. % PPy ribbon particles PPy1 (■) and PPy2 (▼) suspensions.*

The dependence of the apparent shear viscosity on the shear rate is shown in figure 40. As can be seen, the viscosity increases rapidly in the low shear rate region (by 2 to 3 orders of magnitude) with electric field for both sample suspensions, which supports the fact that the fluid is strongly solidified under electric field due to electrostatic force. PPy2 shows stronger and stiffer structure compared to PPy1. On the other hand, at high shear rates, the shear viscosity tends to reach the same value as in zero-field and shear thinning behavior is also clearly observed. This is caused by dominant hydrodynamic interactions over electrostatic forces between the particles.

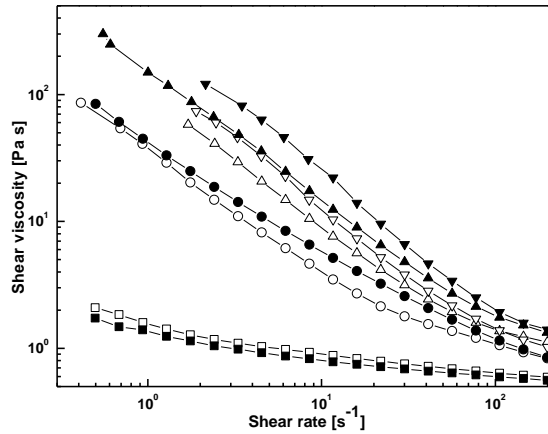


Fig. 40. Dependence of shear viscosity on shear rate for 3 wt. % PPy ribbon particles PPy1 (open) and PPy2 (solid) suspensions. Electric field strengths  $E$  (kV/mm): ( $\square$ ,  $\blacksquare$ ) 0, ( $\circ$ ,  $\bullet$ ) 1, ( $\triangle$ ,  $\blacktriangle$ ) 2, ( $\nabla$ ,  $\blacktriangledown$ ) 3.

On the other hand, since the ER fluids under electric fields often display a viscoelastic behavior, the dynamic rheological measurements are also used to examine the ER properties. Figure 41 shows the frequency dependence of storage modulus  $G'$  of PPy1 and PPy2 at 0.0 and 3.0 kV/mm. It is seen that the suspensions of each show a solid-like behavior, *i.e.* the storage modulus is larger than loss modulus and  $G'$  remains at a near plateau over a broad frequency range. The storage modulus of PPy2 is larger than that of PPy1 suspension at an equal electric field. It has been accepted for ER fluids that the plateau of the frequency-dependent curves of viscoelastic functions is a characteristic of aligned 3D microstructures under electric fields, which is sufficiently strong to transmit the elastic forces through particle-particle bonds. Therefore, the larger storage modulus of PPy2 suspension reflects its higher solidified level (rigidity) or ER effect, which is also in good accordance with its higher yield stress.

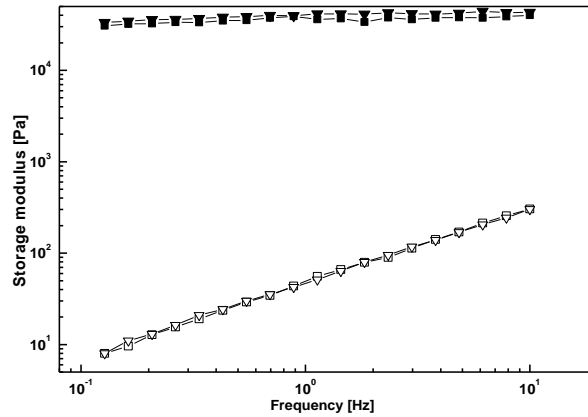


Fig.41. Dependence of storage modulus on the frequency for 3 wt. % PPy ribbon particles PPy1 ( $\square, \blacksquare$ ) and PPy2 ( $\nabla, \blacktriangledown$ ) suspension. Electric field strengths  $E$  (kV/mm): 0 (open), 3 (solid).

The neutral (undoped) PPy is a dielectric with the gap of 4 eV. Upon oxidation (doping), the  $\pi$ -electron are removed from the upper level of the valence zone with a simultaneous shift of the boundary  $\pi$ -levels (the highest occupied HOMO and lowest vacant LUMO) to lower energies. The gap reduces to  $\leq 2.5$  eV and the polymer becomes a semiconductor [99].

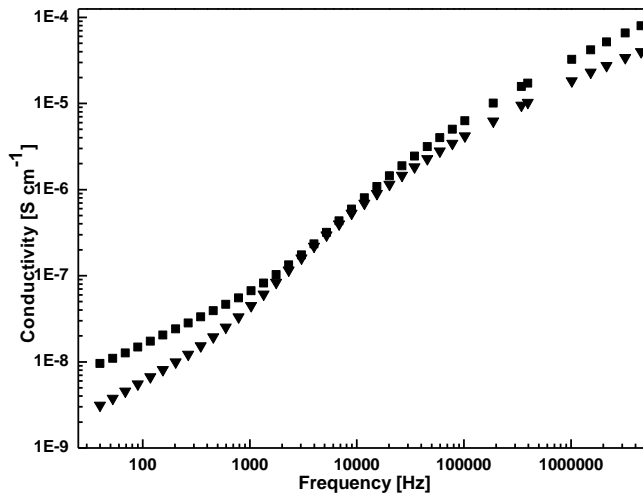


Fig.42. Dependence of conductivity on frequency of PPy1 ( $\blacksquare$ ) and PPy2 ( $\blacktriangledown$ ) suspensions.

The treatment of the prepared PPy ribbon-like structure with  $\text{NH}_4\text{OH}$  to decrease conductivity by dedoping of the ions resulted from the oxidation-reduction

reaction. The sample treated two times will lose more ions which make it less conductive (PPy2) compared to the one treated one time with  $\text{NH}_4\text{OH}$  which is higher conductive (PPy1). Figure 42 shows a plot of the conductivity of PPy1 and PPy2 particles versus frequency. As can be seen from the figure, the conductivity of both sample increased with increase in frequency. However, the conductivity of PPy1 particles is higher than that for PPy2 particles which support the idea of decreasing the conductivity by washing with  $\text{NH}_4\text{OH}$  by dedoping [100].

It is accepted that the conductivity enhance polarization. However, if the conductivity exceeds specific value for specific ER fluid, it will be a disadvantage because of the current passing through the suspension will be higher and less amount of energy stored between the particles by electrostatic forces. The current pass through the suspension flows through particles and between their gaps in the liquid phase which mean it is electrostatics, depends on conductivity ratio between the solid particles and liquid phase  $\sigma_s/\sigma_L$  [101, 102]. According to these mention facts we can predict that the electrostatic forces between PPy2 particles is higher than that for PPy1 due to suitable conductivity which enhance the polarization and decrease the current leakage simultaneously.

### **3.2.3 Conclusions**

PPy ribbon-like particles with different conductivity were synthesized by oxidative polymerization. The samples were treated with  $\text{NH}_4\text{OH}$  different times to decrease the conductivity due to dedoping process. The sample which was treated once was named PPy1 and the other sample which was treated twice was named PPy2. The ER behavior of both samples (PPy1 and PPy2) was investigated under different electric field strengths and it showed that the one with lower conductivity (PPy2) has higher ER effect. It was shown that, 3 wt. % suspensions in silicone oil indicated a very large ER effect for the lower conductivity one with 256 Pa at 3 kV/mm. The highest ER effect was reflected by the better suitability of dielectric properties of PPy2.

### 3.3 TiO<sub>2</sub> with different morphology and its ER effect

#### 3.3.1 Morphology characterization

As can be seen from figures (43-48) the structure morphology of TiO<sub>2</sub> has changed upon different treatment conditions like temperature, solvent used, time of heating and concentration of the starting material. At low concentration, the materials tend to form rod-like structure. However, with increase in concentration the materials tend to become more flat when heated at same temperature and for the same period of time. As can be seen in figure 44, the new structure morphology has higher diameter and nearly the same length as in the low concentration one. This difference in shape and size affects ER behavior of the material by enhancing polarization process with increased in size.

Weight of TiO <sub>2</sub> (g)	Temperature <sup>o</sup> (C)	Time of heating (hour)	Designation
0.3	200	24	Safa1
1.2	200	24	Safa2
1.2	200	48	Safa3

*Table 2. the experimental parameters and designation of different TiO<sub>2</sub> particles.*

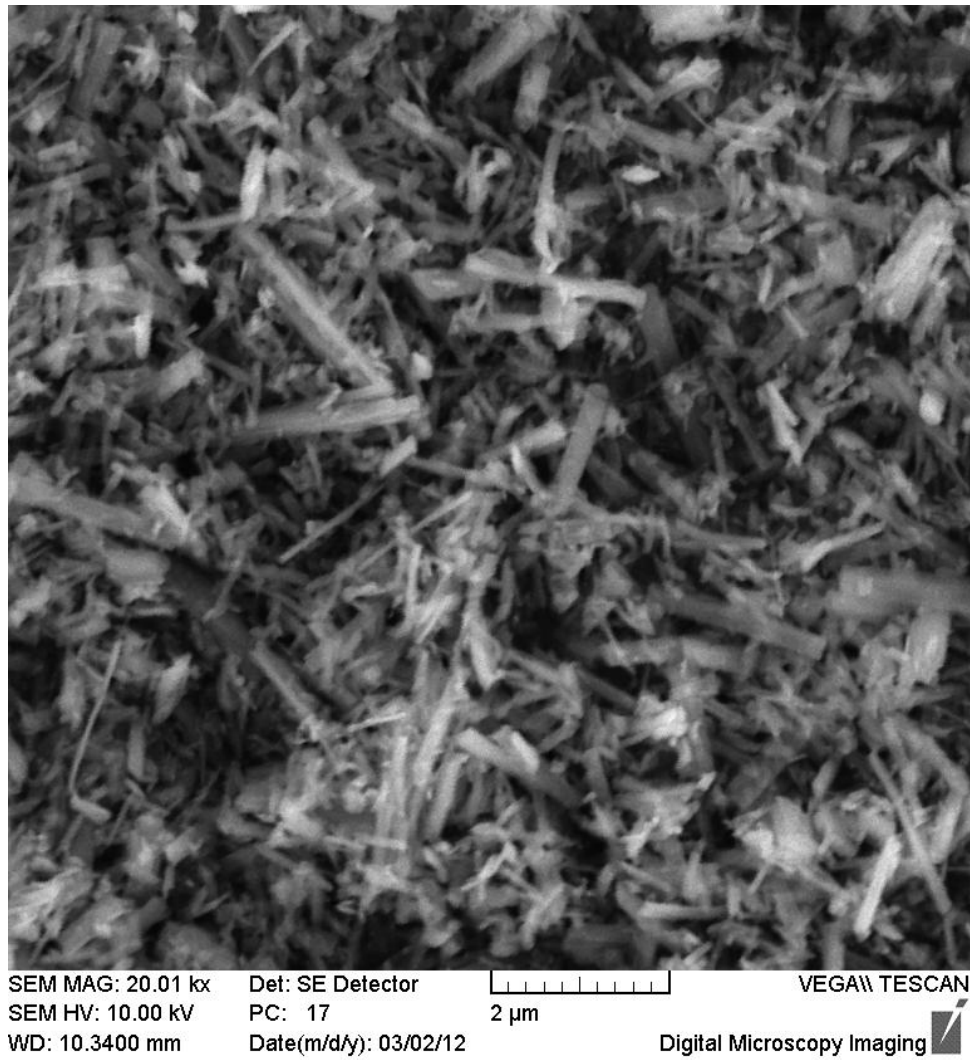


*Fig. 43. SEM image for Safal particles.*

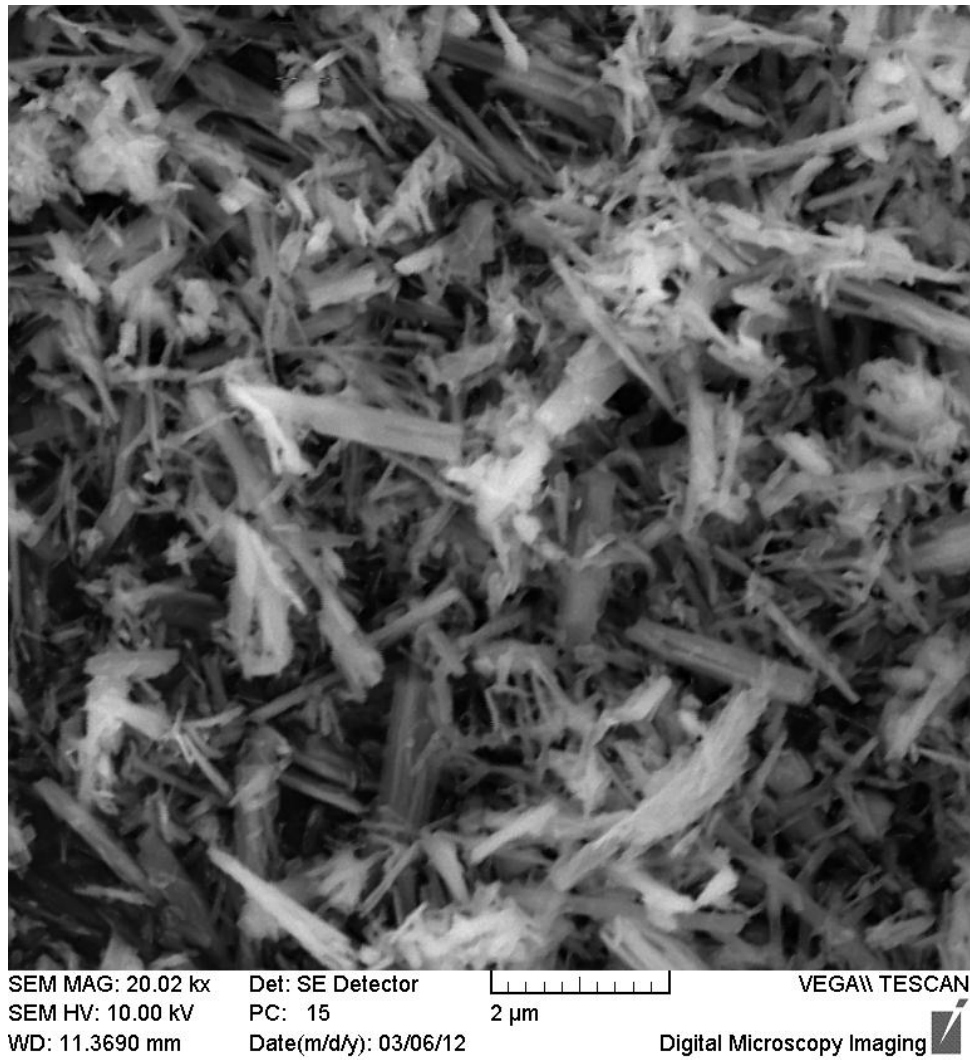


*Fig. 44. SEM image for Safa2 particles.*

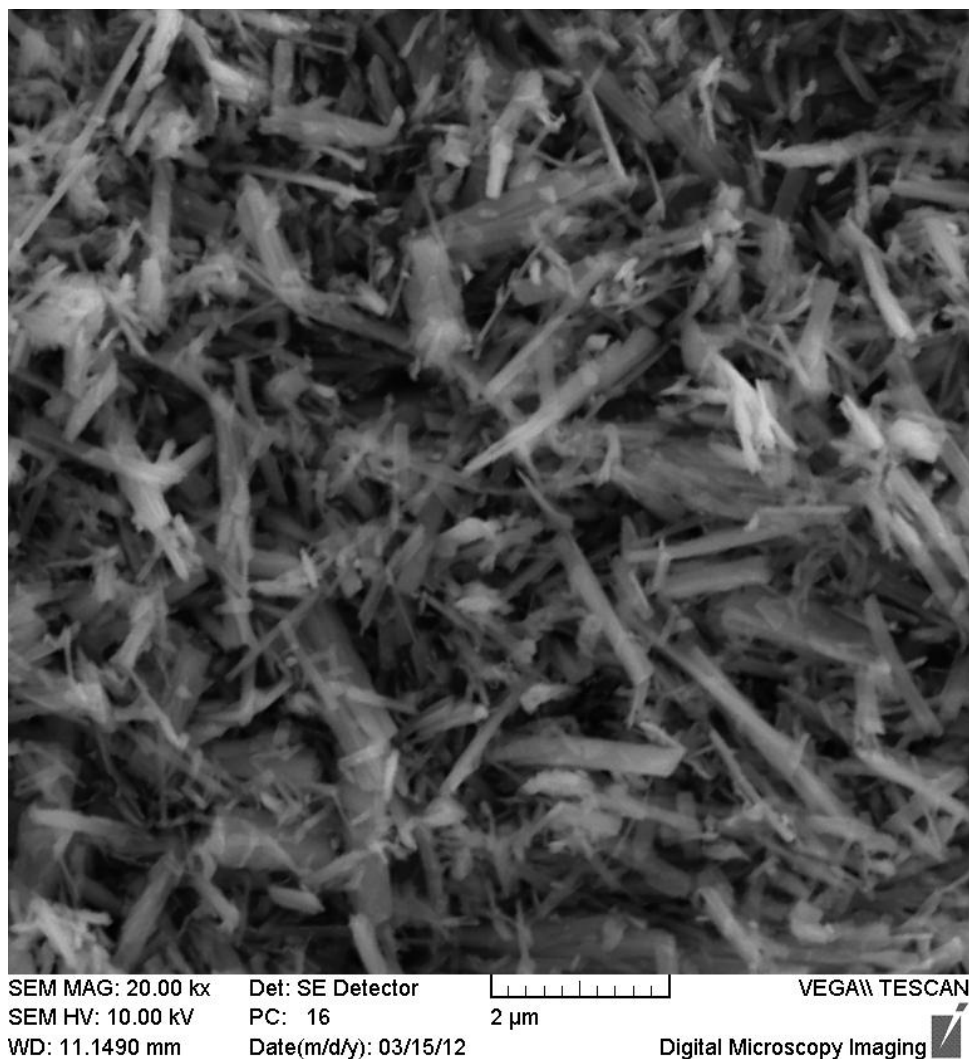


*Fig. 45. SEM image for Safa3 particles.*

The morphology was almost the same (rod-like structure) when we heated the solution at the same degree but for longer time. The particles becomes longer and wider than the other two TiO<sub>2</sub> nanorods.

When a solution with medium concentration with higher volume of 10 M NaOH solution was heated at 180<sup>0</sup>C for 48 the particles tend to become longer and wider than the materials prepared at the same time of heating but with concentration and volume of solvent used. The particles were more homogenous when we use a suitable one solvent instead of two miscible solvents. For immiscible solvents surfactant can be used to enhance the reaction process. Also, the used solvent affects mainly conductivity because it involves in the internal structure of TiO<sub>2</sub> particles.



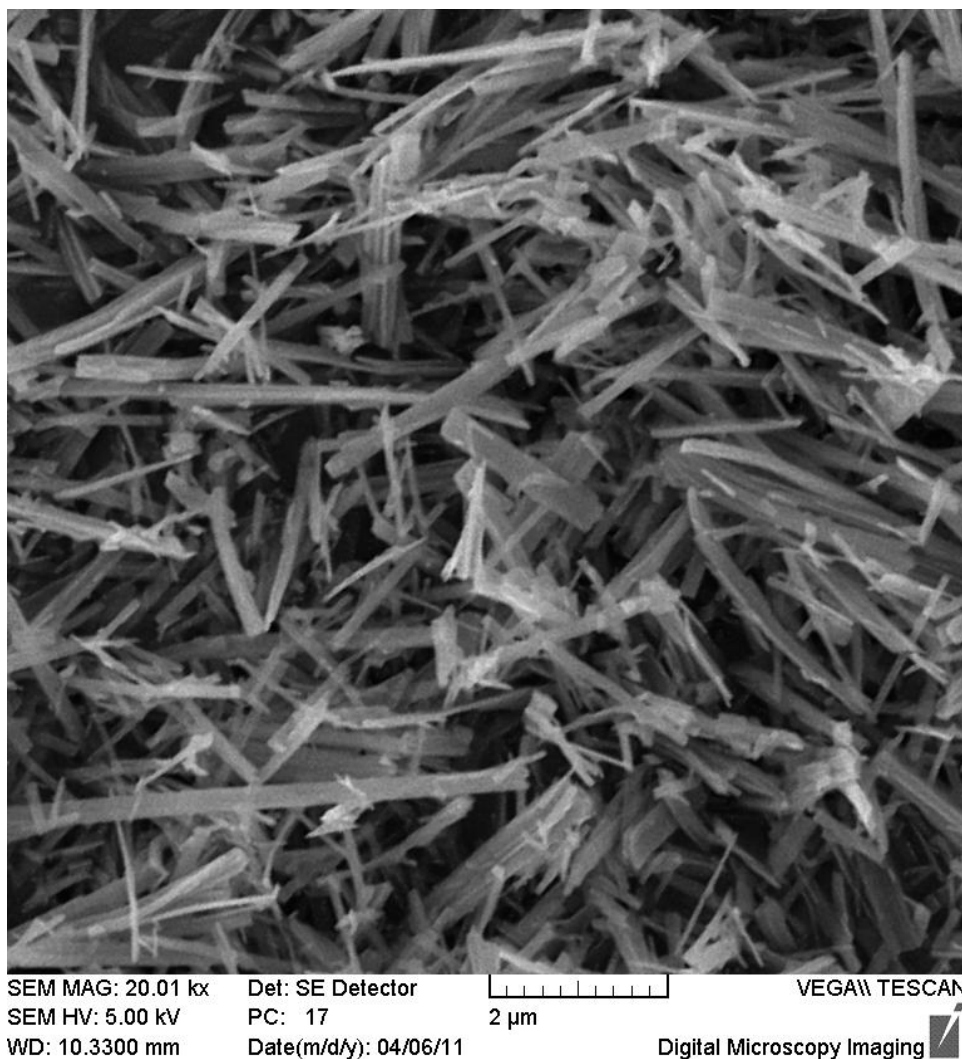
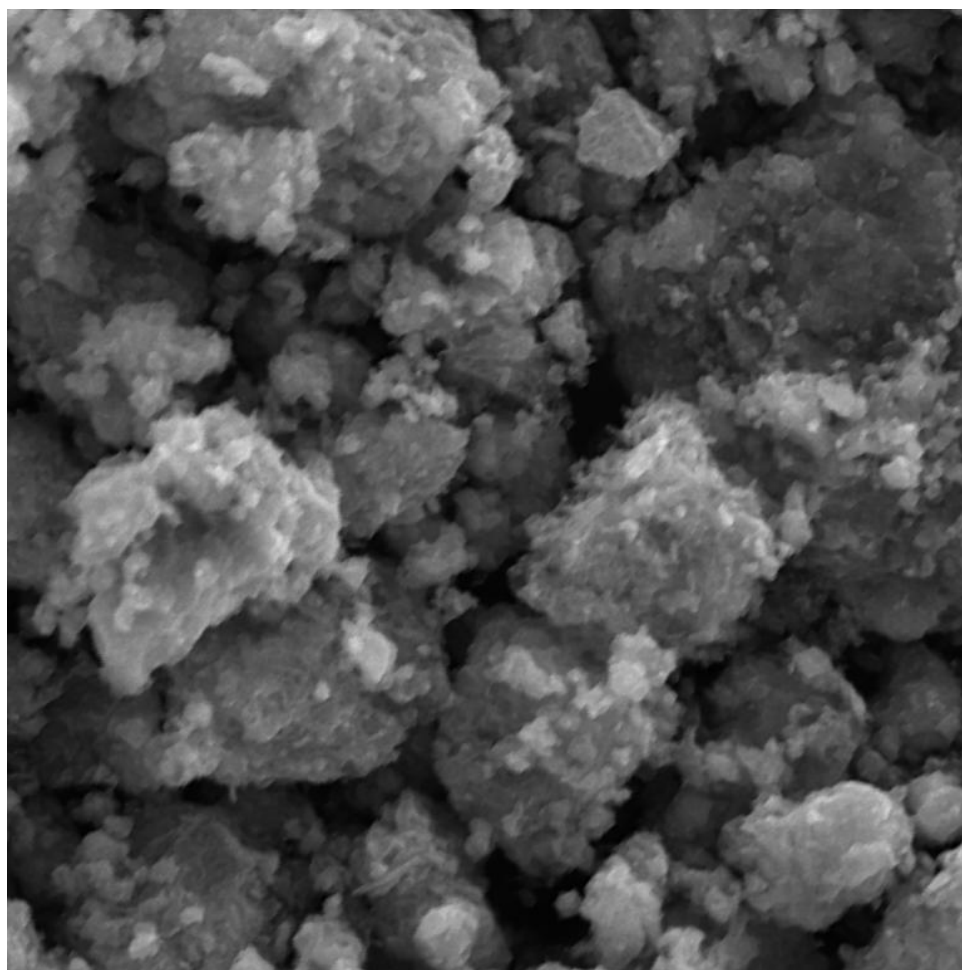


*Fig. 46. SEM image for medium  $\text{TiO}_2$  concentration solution heated at  $180^\circ\text{C}$  for 48 h.*

When another two solutions differ in  $\text{TiO}_2$  concentration in 10 M NaOH and absolute alcohol with ratio 1:1 were heated at the same temperature and for the same time there was no effect of concentration on the morphology of the product. The produced  $\text{TiO}_2$  particles tend to agglomerate and the morphology cannot be recognized by SEM images as shown in figures 47, 48.

Because of the big particles and indefinite morphology of these  $\text{TiO}_2$  samples, it was not used for ER measurements.



SEM MAG: 20.00 kx Det: SE Detector VEGA\\ TESCAN  
SEM HV: 10.00 kV PC: 16 2 μm  
WD: 10.0730 mm Date(m/d/y): 03/12/12 Digital Microscopy Imaging

*Fig. 47. SEM image for low concentration TiO<sub>2</sub> heated at 150<sup>0</sup>C for 24 h.*

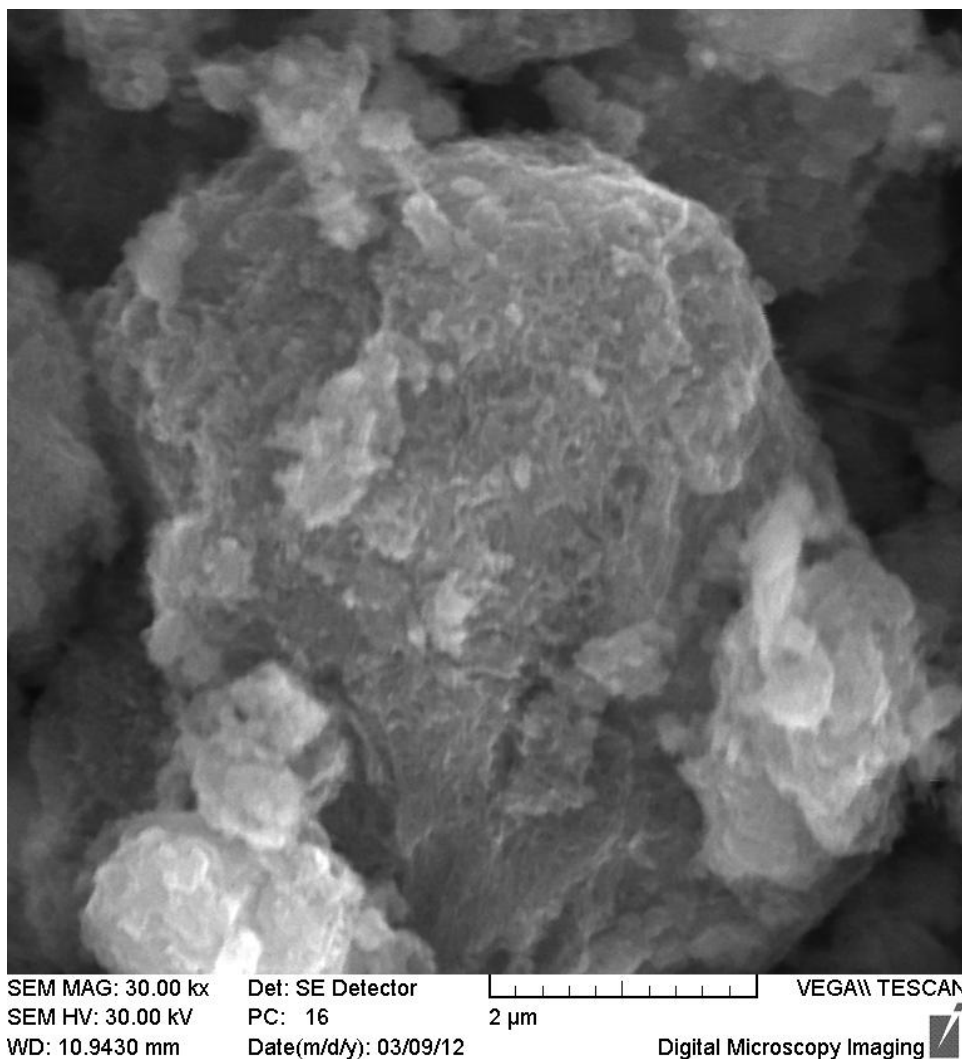


*Fig. 48. SEM image for high concentration TiO<sub>2</sub> heated at 150<sup>o</sup>C for 24 h.*

Figure 49 displays the XRD patterns of TiO<sub>2</sub> nanorods. The crystalline structure was almost the same for all prepared samples. After solvothermal treatment and washing with water, the TiO<sub>2</sub> precursor is transformed into sodium titanate (Na<sub>2</sub>Ti<sub>3</sub>O<sub>7</sub>), as indicated by the figure. The anatase crystalline phase, having diffraction lines of planes at 2θ values of 25.1°, 29.7°, 43.5°, and 47.7° which is in agreement with the value of New Jersey Zinc Co., Palmerton, PA, USA.

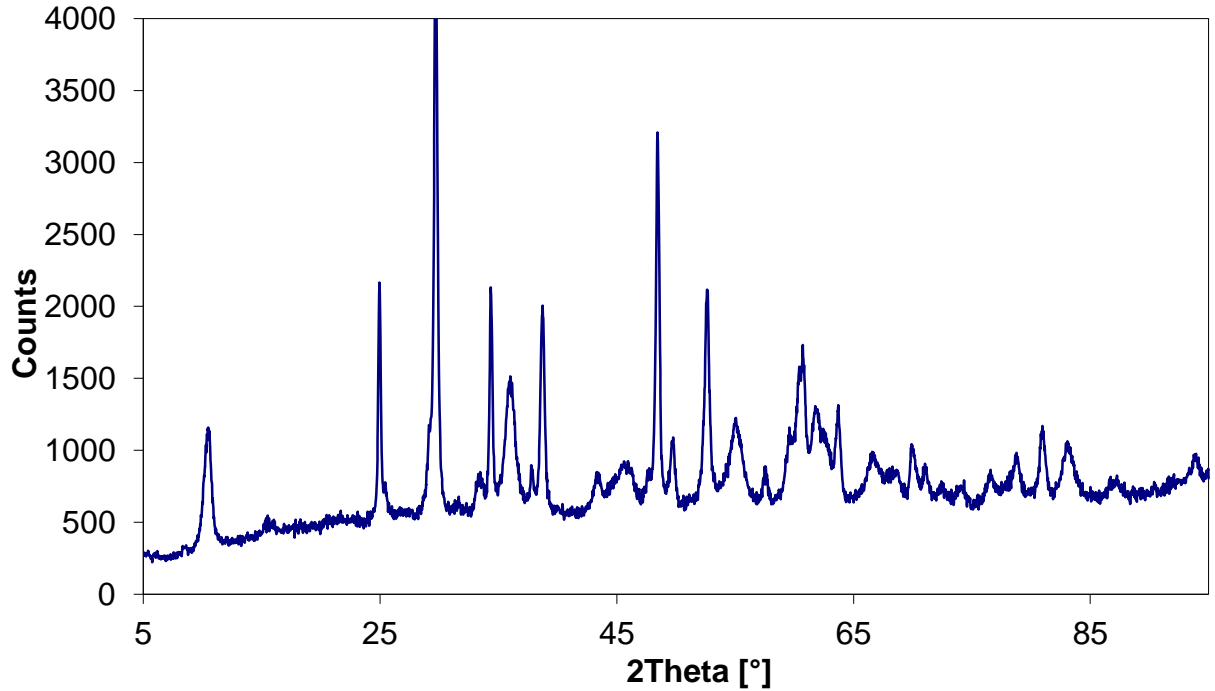


Fig. 49. XRD- spectra for  $\text{TiO}_2$  nanoparticles as sodium titanate.

### 3.3.2 ER properties

Figure 50 shows the dependence of the yield stress of the  $\text{TiO}_2$  particle-based ER suspensions with different morphology on the external electric field. As the shear rate close to zero, the shear stress approaches a limiting value. The value is the apparent yield stress. The viscosity of silicone oil used here was 200 mPas. According to figure 50 the bigger particle size  $\text{TiO}_2$  based ER fluids, the yield stress is rather low and the maximum yield stress is 48 Pa at  $E = 3.0$  kV/mm, while the other  $\text{TiO}_2$  particles with lower particle size show higher yield stress at the same electric field strength. The yield stress was higher for  $\text{TiO}_2$  particles with higher length and lower diameter width. The yield stress show linear increase with increase in electric field strength. The relation could be expressed as  $\tau = qE^\alpha$ , and we can predict from the graph that  $q$  is higher in case of small diameter  $\text{TiO}_2$  particles compared to the other two bigger size  $\text{TiO}_2$  particles. Higher  $q$  value means that the strongest and stiffer internal structure formed by this particles as a result of electric field effect.

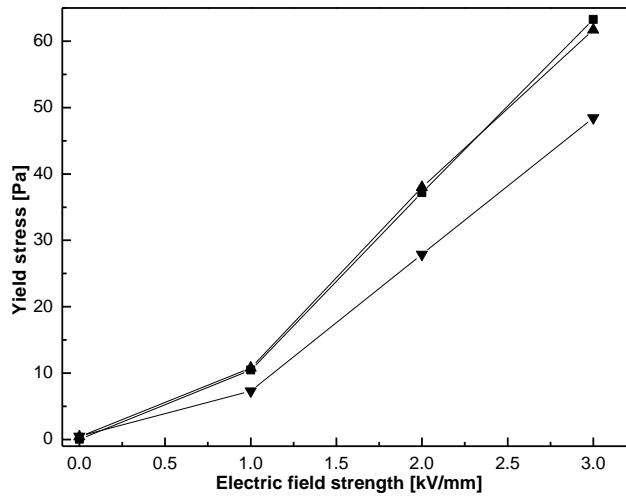


Fig. 50. Yield stresses versus electric field strengths for (Safa1, ■), (Safa2, ▲) and (Safa3, ▼).

The ER behavior under 0 and 3 kV/mm is presented in figure 51 for Safa1, Safa2 and Safa3 suspensions in silicone oil. Without an electric field all TiO<sub>2</sub> particle suspensions behave like a Newtonian fluid with the slope of the logarithm of the shear stress to the logarithm of the rate of 1.0. By applying an electric field to the suspensions, the shear stresses for the three ER suspensions dramatically increase and even the suspensions show a yield stress, showing shear-thinning behavior. The shear stresses and yield stresses with the increase in electric field (here at 3kV/mm was presented).

The steady-shear rheological response can be described as that of Bingham fluid, showing the prevalent features of the ER response – an apparent yielding phenomenon at low shear rates and shear thinning behavior approaching a constant viscosity at high shear rates. This yield stress appears as a result of the electrostatic forces interaction between the particles induced by the electric field.

At shear rates range (1 – 35) s<sup>-1</sup>, however, anomalous behavior where the shear stress decreases with shear rate is observed. The anomalous behavior might arise from a negative synergistic interaction between hydrodynamic and polarization forces.

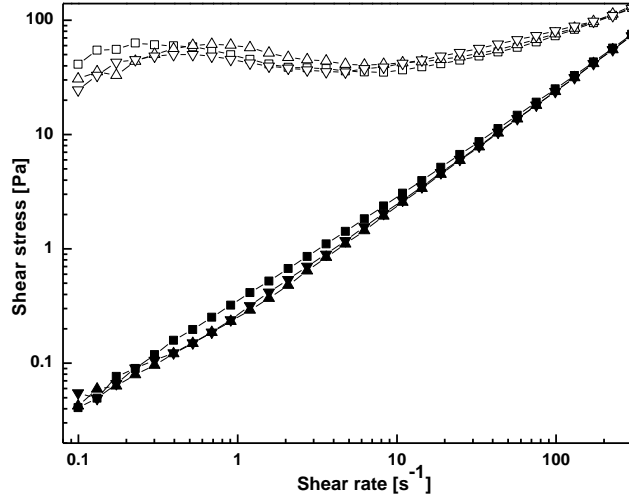


Fig. 51. Shear stress versus shear rate dependence for 5 wt. % suspensions in silicon oil of (Safa1, ■), (Safa2, ▲) and (Safa3, ▼) at  $E$  (kV/mm): (0.0, solid), (3.0, open).

Also, this competition between electrostatic and hydrodynamic forces can be explained depending on Mason dimensionless number which gives an idea of the suitability of the suspension properties. Mason number is defined as the ratio between hydrodynamic forces to electrostatic force as follows

$$M_n = \frac{F^H}{F^E} \quad (11)$$

where  $F^H$  is the hydrodynamic force and  $F^E$  is the electrostatic polarization force.

This dimensionless analysis can be used to describe the behavior of ER fluids for a wide variety of combination of  $\dot{\gamma}$  and  $E$  [103, 104].

Figure 52 shows the shear viscosity behavior as a function of shear rate for 5 wt. %  $\text{TiO}_2$  particle suspensions at 0 and 3 kV/mm electric field strengths. Without an electric field, the suspensions behaved like a Newtonian fluid with a constant viscosity. With an applied electric field to the suspensions, a marked increase in the shear viscosity appeared at low shear rates (fig. 52). It is known that the ER effect of suspensions depended on the relative influences of the polarization and hydrodynamic forces. At low shear rates, the polarization forces are dominant over hydrodynamic forces, and the viscosity is mainly determined by the polarization forces, increasing with increasing electric field strength. Therefore, the viscosity

increases with applying electric field. As the shear rate increases, the shear viscosity decreases because the relative dominance of the polarization force over the hydrodynamic force decreases: the destruction of the structure is becoming fast. At high shear rates, hydrodynamic force is dominant and the viscosity approaches to the viscosity in the absence of an applied electric field, due to structural changes in the suspensions: the destruction rate of the structure becomes faster than the reformation rate. The higher shear viscosity was for the suspension of Safa1 in low shear rate region. With increase in the shear rate, all suspensions almost have the same shear viscosity probably due to increase in the hydrodynamic force with weak polarization force between the particles in the suspensions. At higher shear rate region all suspensions have the same shear viscosity: the hydrodynamic force is dominant and the structure regeneration by polarization force is very slow compared to destructive rate by the hydrodynamic force.

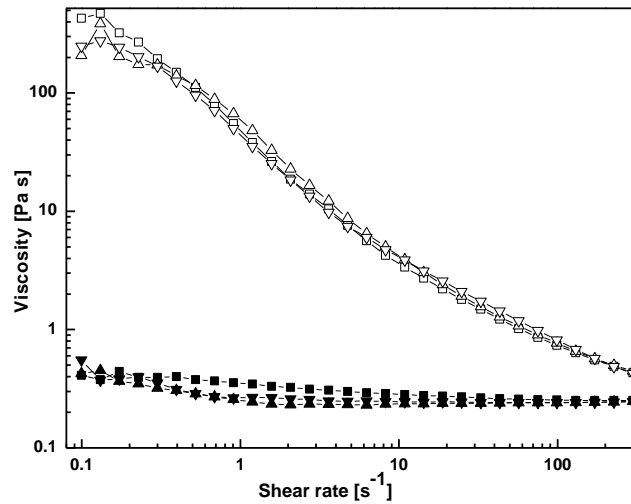


Fig. 52. Shear viscosity versus shear rate dependence for 5 wt. % suspensions in silicone oil of (Safa1,  $\blacksquare$ ), (Safa2,  $\blacktriangle$ ) and (Safa3,  $\blacktriangledown$ ) at  $E$  (kV/mm): (0.0, solid), (3.0, open).

The ER response depends on interfacial polarization and the dielectric properties of ER suspensions are very useful for probing the mechanism that controls the electric properties of the materials [105]. Figure 53 shows the suspension relative permittivity as a function of electric field frequency. The relative permittivity of the suspensions increased with decreasing frequency of the electric field. The increase in relative permittivity was higher in  $\text{TiO}_2$  particle suspensions of Safa1 and Safa3 than Safa2 suspension. At middle frequency region the increase in the relative permittivity was steeper for Safa1 suspension compared to the other two

suspensions. Safa1 suspension shows the highest difference in relative permittivity at 100 and  $10^5$  Hz compared to other two suspensions which was reflected by higher ER effect.

The difference in relative permittivity for Safa1, Safa2 and Safa3 was 0.38, 0.23 and 0.34 respectively as shown in table 3. The differences in relative permittivity are not large enough and the behavior of the relative permittivity differences is consistent with the ER behavior.

Sample	Safa1	Safa2	Safa3
Relative permittivity	0.38	0.23	0.34
Relaxation time [s]	0.0011	0.0006	0.0025

Table 3. Relative permittivity and relaxation time values of Safa1, Safa2 and Safa3 particle suspensions.

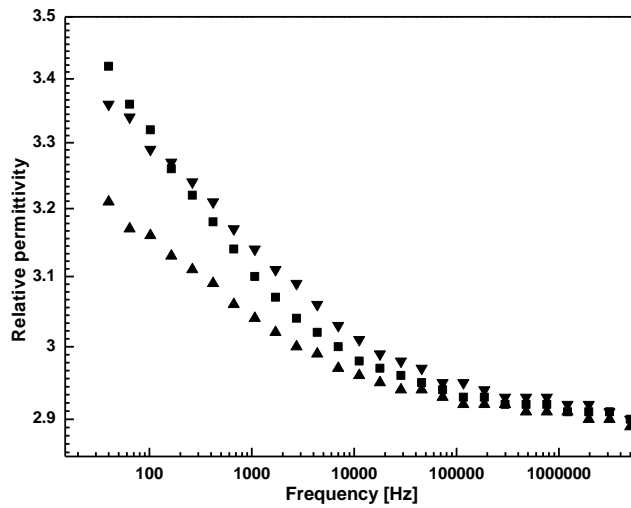


Fig. 53. Relative permittivity versus frequency for 5 wt. % of (Safa1, ■), (Safa2, ▲) and (Safa3, ▼) in silicone oil suspensions.

Figure 54 shows the dielectric loss factor dependence on the electric field frequency. It is proposed that for a large ER effect, ER fluids should have dielectric relaxation between 100 and  $10^5$  Hz [106]. The dielectric relaxation peaks for the suspensions shifted to the lower frequency region. The relaxation times for the suspensions increased as the relaxation peaks shifted to lower frequency region which is disadvantage for ER fluids behavior. The relaxation time can be calculated according to the relation



$$t_{rel} = 1/2\pi f \quad (12)$$

where  $t_{rel}$  is the relaxation time and  $f$  is the frequency of the electric field. The relaxation times of suspensions of Safa1, Safa2 and Safa3 were 0.0011, 0.0006 and 0.0025 s, respectively as shown in table 3. The higher relaxation times ER fluids exhibited a weak ER effect.

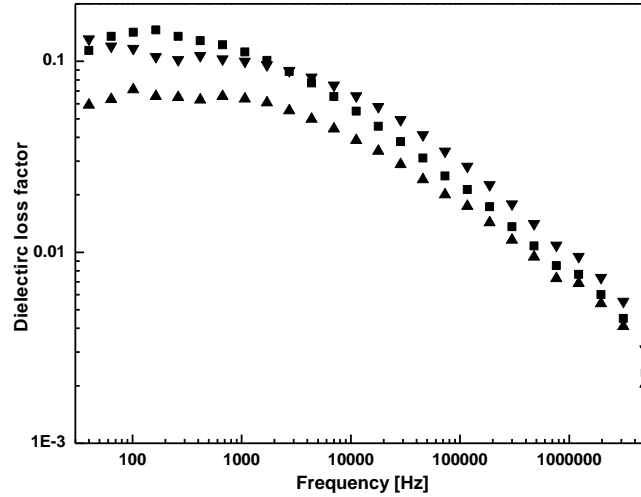


Fig. 54. Dielectric loss factor versus frequency for  $TiO_2$  nanoparticle (Safa1, ■), (Safa2, ▲), (Safa3, ▼)

In addition to relative permittivity and dielectric loss factor, the particles conductivity affects the ER behavior of the ER fluids. Figure 55 shows the conductivity of the three sample suspensions as a function of frequency. The conductivity of the particle suspensions increased with the increase in electric field frequency. According to universal dielectric response, the AC conductivity is frequency dependent at higher frequency values and the AC conductivity increases as the frequency of the electric field increases following power law behavior

$$\sigma(\omega) = k \omega^n \quad (13)$$

where  $\sigma$  is the conductivity,  $\omega$  is the angular frequency and  $(k, n)$  are constants [107,108].

From figure 55, it is seen that the conductivity of these suspensions followed the power law behavior. However, at low frequency, the conductivity was highest for

TiO<sub>2</sub> particle suspension Safa1 and the lowest was for Safa2 particle suspension. At higher frequency the conductivity has changed and the highest conductivity one was for Safa3 suspension possibly due to well aligned structure of the particles.

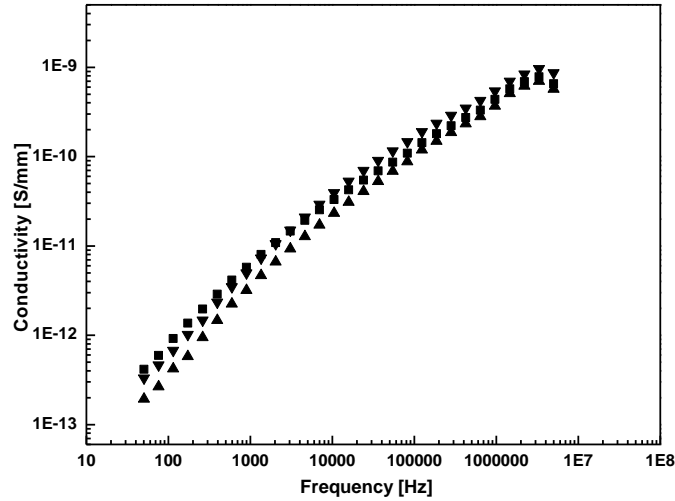


Fig. 55. Conductivity versus frequency for TiO<sub>2</sub> nanoparticle (Safa1, ■), (Safa2, ▲), (Safa3, ▼)

### 3.3.3 Conclusions

Different TiO<sub>2</sub> particles with different morphologies were synthesized by solvothermal synthesis route using anatase TiO<sub>2</sub>, 10 M NaOH solution and absolute ethanol as reactant. Different solutions were prepared by changing the concentration of TiO<sub>2</sub>, the volume of NaOH and absolute ethanol. These solutions were heated at different temperatures and for different heating times. The morphology of the particles was characterized using SEM and XRD spectroscopy. The TiO<sub>2</sub> particles morphology was always rod-like shape with differences in lengths and diameters. The ER effect for 5 wt. % suspensions was investigated at different electric field strengths. The ER behavior of Safa1 and Safa2 suspensions showed practically almost the same behavior and their yield stresses was higher than that of Safa3 suspension. The shape and size of the particle suspension play important role in ER behavior.

## CHAPTER 4

### CLOSING REMARKS

#### 4.1 General conclusions

This doctoral thesis demonstrates two different factors affecting ER behavior of ER fluids which include conductivity and morphology. The main conclusions from this research work are:

Cr-doped TiO<sub>2</sub> nanorods particles were synthesized using hydrothermal synthesis. In this method, NaOH solution was used to enhance recrystallization of TiO<sub>2</sub> (P25) particles by heating the solution in autoclave at moderate temperature for a specific time. The ER behavior of 5 wt. % of different Cr mol % doped TiO<sub>2</sub> particles in silicon oil suspensions were tested under different electric field strengths. The effect of Cr doping percent enhanced the ER effect until a maximum followed by a decrease. This behavior was related to the increase in conductivity of the particles with increasing the Cr doping percent. The effect of morphology was ignored because all sample particles have the almost the same morphology. The highest ER effect was for the sample treated with water compared to that treated with HCl, because of the increase in the chlorine ion (Cl<sup>-</sup>) reflected by increase in the conductivity. The ER measurement shown that, the highest ER effect was for the sample doped with 0.7 mol % of Cr. The yield stress was 126 Pa at 3 kV/mm for 5 wt. % silicone oil suspension.

PPy ribbon-like particle was synthesized by oxidative polymerization using the effect of micelle number on the produced PPy morphology. PPy ribbon-like structure was synthesized with different conductivities by washing with NH<sub>4</sub>OH solution. The effect of the washing process was in the dedoping of the produced PPy ribbon-like structure. The particle with lower conductivity was named PPy2 which was treated twice with NH<sub>4</sub>OH solution and the other sample with higher conductivity was named PPy1 since it was treated once with NH<sub>4</sub>OH solution. The ER behavior of 3 wt. % PPy1 and PPy2 silicone oil suspensions were tested under different electric field strengths. PPy2 suspension showed higher ER effect than PPy1 suspension. PPy2 showed a large ER effect; only 3 wt. % of PPy2 particles in silicone oil suspension showed higher yield stress and its yield stress reached 256 Pa at 3 kV/mm.

Solvothermal synthesis was used to synthesize different TiO<sub>2</sub> morphologies. The effect of solvent, heating time, temperature and concentration of the starting material (TiO<sub>2</sub>) on the morphology of the produced TiO<sub>2</sub> were investigated. In all experiments the starting anatase TiO<sub>2</sub> powder recrystallizes to a rod-like particle. The difference was in the length and diameter of these particles. The ER effect of 5 wt. % of different produced TiO<sub>2</sub> particle in silicone oil suspensions was measured.

It was shown that, the particles produced by only changing the concentration (Safa1 and Safa2) indicated practically almost the same ER behavior. The ER behavior of the particle produced by increasing the heating time (Safa3) was the weakest one. The ER effect depends on the morphology of the particles in the suspensions.

Finally, from the research study and literature review it can be concluded that to have a better ER effect for particles suspension we should compromise between the major factors affecting the ER behavior. The factors are suitable particle chemical composition, suitable conductivity and suitable morphology.

## **4.2 Contribution to science and practice**

In this work attention is given to the conductivity and morphology effect on ER behavior of the materials. Increasing the conductivity of the particles enhanced the ER behavior. The morphology of the solid particles affects the ER effect. The conductivity and morphology effects on ER behavior have been discussed in detail in this work. This study will throw light on the factors that causes a better ER behavior and will be a useful reference in future.

## **4.3 Future works**

- Synthesis of PPy ribbon-like structure as a composite with titanate nanorods.
- Synthesis of carbon nanotube and graphene composites with titanate coating layer.
- Solvothermal synthesis of new different morphologies of TiO<sub>2</sub> doped with different metals.

## REFERENCES

- [1] MEEPHO, M., WATTASIRIWECH, D., WATTANASIRIWECH, S., ANGWATTANA, P. Influence of reaction medium on formation of nanocrystalline YSZ prepared by conventional and modified solvothermal process. *Energy Procedia*. 2011, vol. 9, p. 545-552.
- [2] ZHAN, J. H., YANG, X. G., XIE, Y., LI, B. F., QAIN, Y. T., JIA, Y. B. A solvothermal route for the synthesis of ammonium tungsten bronze. *Solid State Ionics* 1999, vol. 126, p. 373-377.
- [3] DEMAZEAU, G., MILLET, J. M., CROS, C., LARGETEAU, A. Solvothermal synthesis of microcrystallites of transition metal oxides. *J. Alloy. Compd.* 1997, 262-263, p. 271-274.
- [4] CHANG, H-Y., LEE, H-D., WU, M-L., LIN, L-J. Highly efficient cathodoluminescence of nanophosphors by solvothermal route. *J. Lumin.* 2010, vol. 130, p. 969-975.
- [5] BYRAPPA, K., ADSCHIRI, T. Hydrothermal technology for nanotechnology. *Prog. Cryst. Growth Charact. Mater.* 2007, vol. 53, p. 117-166.
- [6] LEE, J-S., CHOI, S-CH. Solvent effect on synthesis of indium tin oxide nanopowders by a solvothermal process. *J. Eur. Ceram. Soc.* 2005, vol. 25, p. 3307-3314.
- [7] LU, CH-H., LEE, CH-H., WU, CH-H. Microemulsion-mediated solvothermal synthesis of copper indium diselenide powders. *Sol. Energy Mater. Sol. C* 2010, vol. 94, p. 1622-1626.
- [8] YIBING, Z., XINJIAN, F., LEI, J. Synthesize TiO<sub>2</sub> microspheres self-assembled from nanorods via hydrothermal treatment. *Sci. China Ser. B-Chem.* 2007, vol. 50, p. 175-178.
- [9] FUMIN, W., ZHANSHENG, S., FENG, G., JINTING, J., MOTONARI, A. Morphology control of anatase TiO<sub>2</sub> by surfactant-assisted hydrothermal method. *Chin. J. Chem. Eng.* 2007, vol. 15, p. 754-759.
- [10] LI, H., DUAN, X., LIU, G., JIA, X., LIU, X. Morphology controllable synthesis of TiO<sub>2</sub> by a facile hydrothermal process. *Mater. Lett.* 2008, vol. 62, p. 4035-4037.
- [11] IZUMI, F. The polymorphic crystallization of titanium(IV) oxide under hydrothermal conditions. II. The roles of inorganic anions in the nucleation of rutile and anatase from acid solution. *Bull. Chem. Soc. Jpn.* 1978, vol. 51, p. 1771-1776.

- [12] CHEN, W., SUN, X., WENG, D. Morphology control of titanium oxides by tetramethylammonium cations in hydrothermal conditions. *Mater. Lett.* 2006, vol. 60, p. 3477-3480.
- [13] WEN, B-M., LIU, C-Y., LIU, Y. Solvothermal synthesis of ultralong single-crystalline TiO<sub>2</sub> nanowires. *New. J. Chem.* 2005, vol. 29, p. 969-971.
- [14] XIE, R-C., SHANG, J. K. Morphology control in solvothermal synthesis of titanium oxide. *J. Mater. Sci.* 2007, vol. 42, p. 6583-6589.
- [15] KASUGA, T. Formation of titanium oxide nanotubes using chemical treatment and their characteristic properties. *Thin Solid Films* 2006, vol. 496, p. 141-145.
- [16] ZHOU, Y., YOU, Y., ZHANG, S-Y., WAN, L., XU, D-F., KUANG, J-C. Forming mechanism of TiO<sub>2</sub> nanofibres prepared by hydrothermal method. *J. Inorg. Mater.* 2008, vol. 23, p. 1075-1079.
- [17] YIN, J., ZHAO, X. Titanate nano-whisker electrorheological fluid with high suspended stability and ER activity. *Nanotechnology* 2006, vol. 17, p. 192-196.
- [18] YANALI, S., SHUZHEN, M., JURAN, L., MINGXIU, L., JUAN, W., SHAOHUO, Z. Effect of microstructure on electrorheological property of pure TiO<sub>2</sub> particle material. *J. Mater. Sci. Technology* 2006, vol. 22, p. 572-576.
- [19] WINSLOW, W. M. 1947 US Patent 2,417, 850.
- [20] BETTIS, E. S., MANN, E. R. A servo employing the magnetic fluid clutch. *Rev. sci. Instrum.* 1949, vol. 20, p. 97-101.
- [21] ALMAJDALAWI, SH., PAVLINEK, V., CHENG, Q., SAHA, P., MRLIK, M., STENICKA, M. Electrorheological properties of suspensions of polypyrrole ribbon particles in silicone oil. *AIP-Conference Proceeding* 2011. Vol. 1375, p. 275-283.
- [22] RANKIN, P. J., GINDER, J. M., KLINGENBERG, D. J. Electro- and magneto-rheology. *Curr. Opin. Colloid Interface Sci.* 1998, vol. 3, p. 373-381.
- [23] CHENG, Q., PAVLINEK, V., LENGALOVA, A., LI, C., HE, Y., SAHA, P. Conducting polypyrrole confined in ordered mesoporous silica SBA-15 channels: preparation and its electrorheology. *Microporous Mesoporous Mater.* 2009, vol. 93, p. 263-269.
- [24] FILISKO, FE. RADZILOWSKI, LH. An intrinsic mechanism for the activity of aluminosilicate based electrorheological materials. *J. Rheol.* 1990, vol. 34, p. 539-552.

- [25] DEKEE, D., TURCOTTE, G. Viscosity of biomaterials. *Chemical Eng. Commun.* 1980, vol. 6, p. 273- 282.
- [26] CHO, M. S., CHOI, H. J., JHON, M. S. Shear stress analysis of a semiconducting polymer based electrorheological fluid system. *Polymer* 2005, vol. 46, p. 11484- 11488.
- [27] KIM, S. G., KIM, J. W., CHOI, H. J., SUH, M. S., SHIN, M. J., JHON, M. S. Synthesis and electrorheological characterization of emulsion polymerized dodecylbenzenesulfonic acid doped polyaniline-based suspensions. *Colloid Polym. Sci.* 2000, vol. 278, p. 894-898.
- [28] KIM, S. G., LIM, J. Y., SUNG, J. H., CHOI, H. J., SEO, Y. Emulsion polymerized polyaniline synthesized with dodecylbenzenesulfonic acid and its electrorheological characteristics: temperature effect. *Polymer* 2007, vol. 48, p. 6622- 6631.
- [29] MEZGER, T. G. *The Rheology Handbook. 1<sup>st</sup> ed. William Andrew Publishing* 2002. 252 p. ISBN 0815515294.
- [30] WU, C. W., CONRAD, H. Multi-coated spheres: recommended electrorheological particles. *J. Phys. D-Appl. Phys.* 1998, vol. 31, p. 3312-3315.
- [31] DAVIS, L. C. Polarization forces and conductivity effect in electrorheological fluids. *J. Appl. Phys.* 1992, vol. 72, p. 1334- 1340.
- [32] CHOI, U. S., AHN, B. G. Electrorheology of cellulose phosphate ester suspension as a new anhydrous ER fluid. *Colloid Surf. A: Physicochem. Eng. Asp.* 2000, vol. 168, p. 71-76.
- [33] McNEISH, D. JUNG, K., BALIK, C. M., CONRAD, H. Effect of preparation procedure and electric field frequency on the dielectric constant and electrorheology of a ziolite/silicone oil suspension. *Int. J. Mod. Phys.* 2005. Vol. 19, p. 1191-1197.
- [34] KIM, J. W., LIU, F., CHOI, H. J. Polypyrrole/clay nanocomposite and its electrorheological characteristics. *J. Ind. Eng. Chem.* 2002, vol. 8, p. 399-403.
- [35] YOON, D. J., KIM, Y. D. Synthesis and electrorheological behavior of sterically stabilized polypyrrole-silica-methylcellulose nanocomposite suspension. *J. Colloid Interface Sci.* 2006, vol. 303, p. 573-578.
- [36] SARI, B., YAVAS, N., MAKULOGULLARI, M., EROL, O., UANL, H. I. Synthesis, electrorheology and creep behavior of polyindole/polyethylene composites. *Reac. Funct. Polym.* 2009, vol. 69, p. 808-815.
- [37] BELZA, T., PAVLINEK, V., SAHA, P., QUADRAT, O. Electrorheological properties of suspensions of silica nanoparticles modified by urea and N,N-

- dimethylformamide. *Colloid Surf. A: Physicochem. Eng. Asp.* 2007, vol. 297, p. 142-146.
- [38] LENGALOVA, A., PAVLINEK, V., SAHA, P., QUADRAT, O., STEJSKAL, J. The effect of dispersed particle size and shape on the electrorheological behavior of suspensions. *Colloids Surf. A: Physicochem. Eng. Asp.* 2003, vol. 227, p. 1-8.
- [39] LENGALOVA, A., PAVLINEK, V., SAHA, P., STEJSKAL, J., KITANO, T., QUADRAT, O. The effect of dielectric properties on the electrorheology of suspensions of silica particles coated with polyaniline. *Physica A* 2003, vol. 321, p. 411-424.
- [40] LENGALOVA, A., PAVLINEK, V., SAHA, P., STEJSKAL, J., QUADRAT, O. Electrorheology of polyaniline-coated inorganic particles in silicone oil. *J. Colloid Interface Sci.* 2003, vol. 258, p. 174-178.
- [41] KO, G. Y., CHOI, U. S., CHUN, Y. J. Influence of particle size on shear behavior of amine-group-immobilized polyacrylonitrile dispersed suspension under electric field. *J. Colloid Interface Sci.* 2009, vol. 335, p. 183- 188.
- [42] KIM, Y. D., JUNG, J. C. Preparation of polymethacrylate-based side-chain liquid crystalline polymers with various lengths of aliphatic spacer and their electrorheology. *Korean J. Chem. Eng.* 2010, vol. 27, p. 32- 36.
- [43] PAVLINEK, V., SAHA, P., KITANO, T., STEJSKAL, J., QUADRAT, O. The effect of polyaniline layer deposited on silica particles on electrorheological and dielectric properties of their silicone-oil suspensions. *Physica A* 2005, vol. 353, p. 21- 28.
- [44] KIM, Y. D., PARK, D. Y. The electrorheological responses of suspensions of polypyrrole-coated polyethylene particles. *Colloid Polym.* 2002, vol. 280, p. 828- 834.
- [45] STENICKA, M., PAVLINEK, V., SAHA, P., BLINOVA, N. V., STEJSKAL, J., QUADRAT O. Effect of hydrophilicity of polyaniline particles on their electrorheology: Steady flow and dynamic behavior. *J. Colloid Interface Sci.* 2010, vol. 346, p. 236- 240.
- [46] YIN, J., XIA, X., XIANG, L., ZHAO, X. Conductivity and polarization of carbonaceous nanotubes derived from polyaniline nanotubes and their electrorheology when dispersed in silicone oil. *Carbon* 2010, vol. 48, p. 2958- 2967.
- [47] YIN, J., ZHAO, X. Electrorheological properties of titanate nanotube suspensions. *Colloid Surf. A: Physicochem. Eng. Asp.* 2008, vol. 329, p. 153- 160.



- [48] CONRAD, H., LI, Y., CHEN, Y. The temperature-dependence of the electrorheology and related electrical-properties of corn starch/ corn oil suspensions. *J. Rheol.* 1995, vol. 39, p. 1041-1057.
- [49] KIM, Y. D., SONG, I. C. Electrorheology and dielectric of polypyrrole dispersions. *J. Mater. Sci.* 2002, vol. 37, p. 5051-5055.
- [50] HONG, C. H., CHOI, H. J. Shear stress and dielectric analysis of H<sub>3</sub>PO<sub>4</sub> doped polyaniline based electrorheological fluid. *J. Macromol. Sci. B* 2007, vol. 46, p. 683-692.
- [51] STINCKA, M., PAVLINEK, V., SAHA, P., BLINOVA, N. V., STEJSKAL, J., QUADRAT, O. Conductivity of flowing polyaniline suspensions in electric field. *Colloid Polym. Sci.* 2008, vol. 286, p. 1403-1409.
- [52] YIN, J., XIA, X., XIANG, L., ZHAO, X. Temperature effect of electrorheological fluids based on polyaniline carbonaceous nanotubes. *Smart Mater. Struct.* 2011, vol. 20, p. 015002-1 to 8.
- [53] TRLICA, J., SAHA, P., QUADRAT, O., STEJESKAL, J. Electrorheological activity of polyphenylenediamine suspension in silicone oil. *Physica A* 2000, vol. 283, p. 337-348.
- [54] BELZA, T., PAVLINEK, V., SAHA, P., BENES, M. J., HORAK, D., QUADRAT, O. Electrorheology of silicone oil suspensions of urea-modified poly [(glycidyl methacrylate)-co (ethylene dimethacrylate)] particles. *Physica A* 2007, vol. 385, p. 1-8.
- [55] CHO, C. H., CHOI, H. J., KIM, J. W., JHON, M. S. Synthesis and electrorheology of aniline/pyrrole copolymer. *J. Mater. Sci.* 2004, vol. 39, p. 1883-1885.
- [56] KIM, Y. D., KIM, J. H. Synthesis of polypyrrole-polycaprolactone composites by emulsion polymerization and the electrorheological behavior of their suspensions. *Colloid Polym. Sci.* 2008, vol. 286, p. 631-637.
- [57] LEE, I. S., CHO, M. S., CHOI, H. J. Preparation of polyaniline coated (methyl methacrylate) microsphere by graft polymerization and its electrorheology. *Polymer* 2005, vol. 46, p. 1317-1321.
- [58] HIROSE, Y., OTSUBO, Y. Electrorheology of suspensions of poly(ethylene glycol)/poly(vinyl alcohol) blend particles. *Colloid Surf. A-Physicochem. Eng. Asp.* 2008, vol. 317, p. 438-442.
- [59] RAMOS-TEJDA, M. M., ESPIN, M. J., PEREA, R., DELGADO, A. V. Electrorheology of suspensions of elongated goethite particles. *J. Non-Newton. Fluid Mech.* 2009, vol. 159, p. 34-40.

- [60] ESPIN, J. M., DELGADO, A. V., PLOCHARSKI, J. Z. Effect of additives and measurement procedure on the electrorheology of hematite/silicone oil suspensions. *Rheologica Acta* 2006, vol. 45, p. 865-876.
- [61] AHMARI, H., ETEMAD, S. GH. Electrorheological response of SnO<sub>2</sub> and Y<sub>2</sub>O<sub>3</sub> nanoparticles in silicone oil. *Rheologica Acta* 2009, vol.48, p. 217-220.
- [62] KAWAI, A., UCHIDA, K., KAMIYA, K., GOTOH, A., HAYASHI, S., IKAZAKI, F. The effect of surface characteristics of silica nanoparticles on electrorheology. *Adv. Powder Technol.* 1996, vol. 7, p. 153-160.
- [63] FENG, P., WAN, Q., WANG, T. H. Anomalous electrorheological behavior of ZnO nanowires. *Appl. Phys. Lett.* 2005, vol. 87, p. 033114-1 to 033114-3.
- [64] YOON, D. J., KIM, Y. D. Electrorheological properties of polypyrrole-SnO<sub>2</sub>-methylcellulose nanocomposite suspensions. *J. Mater. Sci.* 2007, vol. 42, p. 5534-5538.
- [65] KIM, B. S., KIM, B., SUH, K. D. Electrorheological properties of carbon nanotube/polyelectrolyte self-assembled polystyrene particles by layer-by-layer assembly. *J. Polym. Sci. Pol. Chem.* 2008, vol. 46, p. 1058-1065.
- [66] SLOBODIAN, P., PAVLINEK, V., LENGALOVA, A., SAHA, P. Polystyrene/multi-wall carbon nanotube composites prepared by suspension polymerization and their electrorheological behavior. *Curr. Appl. Phys.* 2009, vol. 9, p. 184-188.
- [67] FANG, F. F., CHO, M. S., CHOI, H. J., YOON, S. S., AHN, W. S. Electrorheological characteristics of conducting polypyrrole/swollen MCM-41 nanocomposite. *J. Ind. Eng. Chem.* 2008, vol. 14, p. 18- 21.
- [68] CHENG, Q., HE, Y., PAVLINEK, V., LENGALOVA, A., LI, C., SAHA, P. Preparation and electrorheology of new mesoporous polypyrrole/MCM-41 suspensions. *J. Mater. Sci.* 2006, vol. 41, p. 5047-5049.
- [69] FANG, F. F., CHOI, H. J., AHN, W. S. Electrorheology of a mesoporous silica having conducting polypyrrole inside expanded pores. *Microporous Mesoporous Mat.* 2010, vol. 130, p. 338-343.
- [70] LIU, Y. D., FANG, F. F., CHOI, H. J. Silica nanoparticle decorated conducting polyaniline fibers and their electrorheology. *Mater. Lett.* 2010, vol. 64, p. 154- 156.
- [71] QIAO, Y., YIN, J., ZHAO, X. Oleophilicity and the strong electrorheological effect of surface-modified titanium oxide nanoparticles. *Smart Mater. Struct.* 2007, vol. 16, p. 332-339.

- [72] CHENG, Q., PAVLINEK, V., HE, Y., YAN, Y., LI, C., SAHA, P. Synthesis and electrorheological characteristics of sea urchin-like TiO<sub>2</sub> hollow spheres. *Colloid Polym. Sci.* 2011, vol. 289, p. 799-805.
- [73] YIN, J., ZHAO, X., XIANG, L., XIA, X., ZHANG, Z. Enhanced electrorheology of suspensions containing sea-urchin-like hierarchical Cr-doped titania particles. *Soft Matter* 2009, vol. 5, p. 4687-4697.
- [74] ZHAO, X. P., YIN, J. B. Preparation and electrorheological characteristics of rare-earth-doped TiO<sub>2</sub> suspensions. *Chem. Mater.* 2002, vol. 14, p. 2258-2263.
- [75] TANG, H., HE, J., PERSELLO, J. Giant electrorheological effect of aluminum-doped TiO<sub>2</sub> nanoparticles. *Particuology* 2010, vol. 8, p. 442-446.
- [76] SEDLACIK, M., MRLIK, M., PAVLINEK, V., SAHA, P., QUADRAT, O. Electrorheological properties of suspensions of hollow globular titanium oxide/polypyrrole particles. *Colloid Polym. Sci.* 2011, vol. 290, p. 41-48.
- [77] CHUAN, W., YIHUA, Z., YI, J., XIAOLING, Y., CHUNZHONG, L. Fabrication and characterization of mesoporous TiO<sub>2</sub>/polypyrrole-based nanocomposite for electrorheological fluid. *Mater. Res. Bull.* 2008, vol. 43, p. 3263-3269.
- [78] LEE, I. S., LEE, J. Y., SUNG, J. H., CHOI, H. J. Synthesis and electrorheological characteristics of polyaniline-titanium dioxide hybrid suspension. *Synthetic Met.* 2005, vol. 152, p. 173-176.
- [79] BOKIAS, G., DURAND, A., HOURDET, D. Molar mass control of poly(N-isopropylacrylamide) and poly(acrylic acid) in aqueous polymerizations initiated by redox initiators based on persulfates. *Macromol. Chem. Phys.* 1998, vol. 199, p. 1387-1392.
- [80] BREZOI, D. V. Polypyrrole films prepared by chemical oxidation in aqueous FeCl<sub>3</sub> solution. *J. Sci. arts* 2010, vol. 1, p. 53-58.
- [81] CHEN, J. H., HUANG, Z. P., WANG, D. Z., YANG, S. X., LI, W. Z., WEN, J. G., REN, Z. F. Electrochemical synthesis of polypyrrole films over each of well-aligned carbon nanotubes. *Synthetic Met.* 2002, vol. 125, p. 289-294
- [82] DUBAL, D. P., LEE, S. H., KIM, J. G., KIM, W. B., LOKHANDE, C. D. Porous polypyrrole clusters prepared by electropolymerization for a high performance supercapacitor. *J. Mater. Chem.* 2012, vol. 22, p. 3044-3052.
- [83] WEI, J., ZHAO, L., PENG, S., SHI, J., LIU, Z. Wettability of urea-doped TiO<sub>2</sub> nanoparticles and their high electrorheological effects. *J. Sol-Gel Sci. Technol.* 2008, vol. 47, p. 311-315.

- [84] MCINTYRE, E. C., OH, H. J., GREEN, P. F. Electrorheological phenomena in polyhedral silsesquioxane cage structure/PDMS system. *Appl. Mater. Interface* 2010, vol. 2, p. 965-968.
- [85] KLINGENBERG, D. J., ZUKOSKI, C. F., HILL, J. C. Kinetics of structure formation in electrorheological suspensions. *J. Appl. Phys.* 1993, vol. 73, p. 4644-4648.
- [86] SHING, P. Mechanism of the giant electrorheological effect. *Int. J. Mod. Phys. B* 2005, vol. 19, p. 1157-1162.
- [87] PARK, D. P., LIM, S. T., CHOI, H. J., CHOI, S. B. Electrorheological characteristics of solvent-cast polypyrrole/clay nanocomposite. *J. Appl. Polym. Sci.* 2009, vol. 112, p 1365-1371.
- [88] GUAN, J. G., WEI, J. H., ZHAO, S. L., RUAN, R. Z. BaTiO<sub>3</sub>-coated polyaniline core-shell nanocomposite particles for electrorheological fluids. In WILSON, A.R., VARADAN, W. *Smart Materials II*. 1<sup>st</sup> ed. Bellingham: PIE-International Society for optical Engineering, 2002, vol. 4934, p. 86-95.
- [89] HAO, T., XU, Z., XU, Y. Correlation of the dielectric properties of dispersed particles with the electrorheological effect. *J. Colloid Interface Sci.* 1997, vol. 190, p. 334-340.
- [90] HAO, T. Electrorheological suspensions. *Adv. Colloid Interface Sci.* 2002, vol. 97, p. 1-35.
- [91] ZHU, H., TAO, J., DONG, X. Preparation and photoelectrochemical activity of Cr-doped TiO<sub>2</sub> nanorods with nanocavities. *J. Phys. Chem. C* 2010, vol. 114, p. 2873-2879.
- [92] ZHANG, X., ZHANG, J., SONG, W., LIU, Z. Controllable synthesis of conducting polypyrrole nanostructures. *J. Phys. Chem. B* 2006, vol. 110, p. 1158-1165.
- [93] WEN, W., HUANG, X., YANG, S., LU, K., SHENG, P. The giant electrorheological effect in suspensions of nanoparticles. *Nat. Mater.* 2003, vol. 2, p. 727-730.
- [94] DAVIS, L., S. Time-dependent and non-linear effects in electrorheological fluids. *J. Appl. Phys.* 1997, vol. 81, p. 1985-1991.
- [95] YOON, H., LEE, J., PARK, D. W., HONG, C. K., SHIM, S. E. Preparation and electrorheological characteristic of CdS/polystyrene composite particles. *Colloid Polym. Sci.* 2010, vol. 288, p. 613-619.
- [96] JESURANI, S., KANAGESAN, S., VELMURUGAN, R., THIRUPHATI, C., SIVAKUMAR, M., KALAIVANI, T. Nanoparticles of the giant dielectric material, calcium copper titanate from a sol-gel technique. *Mater. Lett.* 2011, vol. 65, p. 3305-3308.

- [97] JARY, D., SIKORAV, J. L., LAIREZ, D. Nonlinear viscoelasticity of entangled DNA molecules. *Europhys. Lett.* 1999, vol. 46, p. 251-255.
- [98] KIM, J. W., NOH, M. H., CHOI, H. J., LEE, D. C., JHON, M. S. Synthesis and electrorheological characteristics of SAN-clay composite suspensions. *Polymer* 2000, vol. 41, p. 1229-1231.
- [99] VERNITSKAYA, T. V., EFIMOV, O. N. Polypyrrole: a conducting polymer; its synthesis, properties and applications. *Russ. Chem. Rev.* 1997, vol. 66, p. 443-457.
- [100] GONON, P., FOULC, J. N., ATTEN, P., BOISSY, C. Particle-particle interactions in electrorheological fluids based on surface conducting particles. *J. Appl. Phys.* 1999, vol. 86, p. 7160-7169.
- [101] PARTHASARATHY, M., KLINGENBERG, D. J. Electrorheology: mechanism and models. *Mater. Sci. Eng. R-Rep.* 1996, vol. R17, p. 57-103.
- [102] FELICI, N. J. Interfacial effects and electrorheological forces: Criticism of the conduction model. *J. Electrostat.* 1997, vol. 40 & 41, p. 567-572.
- [103] KLINGENBERG, D. J., ULICNY, J. C., GOLDEN, M. A. Mason numbers for magnetorheology. *J. Rheol.* 2007, vol. 51, p. 883-893.
- [104] MARSHALL, L., ZUKOSKI, C. F., GOODWIN, J. W. Effects of electric fields on the rheology of non-aqueous concentrated suspensions. *J. chem. Soc., Faraday Transactions I* 1989, vol. 85, p. 2785-2795.
- [105] KLINGENBERG, D. J., DIERKING, D., ZUKOSKI, C. F. Stress-transfer mechanisms in electrorheological suspensions. *J. chem. Soc., Faraday Transactions* 1991, vol. 87, p. 425-430.
- [106] IKAZAKI, F., KAWAI, A., UCHIDA, K., KAWAKAMI, T., EDAMURA, K., SAKURAI, K., ANZAI, H., ASAKO, Y. Mechanism of the electrorheology: the effect of the dielectric property. *J. Phys. D: Appl. Phys.* 1998, vol. 31, p. 336-347.
- [107] PANTENY, S., STEVENS, R., BOWEN, C. R. The frequency dependent permittivity and AC conductivity of random electrical networks. *Ferroelectrics* 2005, vol. 319, p. 199-208.
- [108] JONSCHER, A. K., Physical basis of dielectric loss. *Nature* 1975, vol. 253, p. 717-719.

## LIST OF FIGURES AND TABLES

<b>Fig. 1.</b>	Images of autoclaves used for solvothermal synthesis.
<b>Fig. 2</b>	Scanning electron microscopy (SEM) and Transmission electron microscopy (TEM) images for TiO <sub>2</sub> nanoparticles.
<b>Fig.3</b>	Growth mechanism of TiO <sub>2</sub> nanoparticles crystal.
<b>Fig. 4</b>	Shear stress versus shear rate curves for 10 wt. % PPy/MCM-41 particles in silicone oil at different electric field strengths.
<b>Fig. 5</b>	Static yield stress versus electric field strength for PPy–SBA-15 based ER fluids.
<b>Fig. 6</b>	The reaction mechanism of electropolymerization of pyrrole.
<b>Fig. 7</b>	The reaction mechanism of electropolymerization of pyrrole.
<b>Fig. 8</b>	Frequency dependencies of the relative permittivity and dielectric loss factor on the left and right respectively.
<b>Fig. 9</b>	Comparison of the predicted shear stresses with that measured for cellulose phosphate ester suspension ( $\phi = 0.3$ volume fraction, $\dot{\gamma} 10 \text{ s}^{-1}$ ).
<b>Fig. 10</b>	Schematic illustration of the ER particles (a) and the non-ER particles (b) behavior before and after an external electric field is applied.
<b>Scheme .1</b>	Synthesis method of TiO <sub>2</sub> nanoparticles.
<b>Fig. 11</b>	Images of TNR particle suspension under microscope before (a) and (b) after electric field application.
<b>Fig. 12</b>	SEM image for 0.0 Cr mol % TiO <sub>2</sub> nanorods.
<b>Fig. 13</b>	SEM image for 0.7 Cr mol % TiO <sub>2</sub> nanorods.
<b>Fig. 14</b>	SEM image for 3.8 Cr mol % TiO <sub>2</sub> nanorods.
<b>Fig. 15</b>	SEM image for 4.9 Cr mol % TiO <sub>2</sub> nanorods.
<b>Fig. 16</b>	TEM image for 0.0 Cr mol % TiO <sub>2</sub> nanorods before heating.
<b>Fig. 17</b>	TEM image for 0.0 Cr mol % TiO <sub>2</sub> nanorods after heating.
<b>Fig. 18</b>	TEM image for 0.7 Cr mol % TiO <sub>2</sub> nanorods after heating.
<b>Fig. 19</b>	EDX for 0.7 Cr mol % TiO <sub>2</sub> nanorods water treated.
<b>Fig. 20</b>	EDX for 4.3 Cr mol% TiO <sub>2</sub> nanorods hydrochloric acid treated.
<b>Fig. 21</b>	Shear stress versus shear rate of 5 wt. % suspensions of 0.7 mol % Cr-TiO <sub>2</sub> nanorods

	particles (solid-water treated) and 0.8 % Cr-TiO <sub>2</sub> nanorods particles (open-HCl treated) in silicone oil suspensions at 0, (■), 1,(●), 2,(▲), 3, (▼) kV/mm.
<b>Fig. 22.</b>	Shear viscosity versus shear rate of 0.7 mol % Cr-TiO <sub>2</sub> nanorods suspension in silicone oil at different electric field strengths. (water-treated)
<b>Fig. 23</b>	Shear viscosity versus shear rate of 0.8 mol % Cr-TiO <sub>2</sub> nanorods suspension at different Electric field strengths. (Acid treated)
<b>Fig. 24</b>	Yield stresses versus Cr mol % doping for 5 wt. % of TiO <sub>2</sub> nanorods suspensions (water treated) at 3kV/mm.
<b>Fig. 25</b>	Yield stresses values versus electric field strengths for 0.7 Cr mol % TiO <sub>2</sub> nanorods-water treated (■) and 0.8 Cr mol % TiO <sub>2</sub> nanorods-acid treated (●).
<b>Fig. 26</b>	Viscoelastic modulus versus frequency for 5 wt. % suspension of 0.7 Cr mol % TiO <sub>2</sub> nanorods water treated. Elastic (open), viscous (solid) at 0, (■), 3, (●) kV/mm.
<b>Fig. 27</b>	Viscoelastic modulus versus frequency for 5wt. % suspension of 0.8Cr mol % TiO <sub>2</sub> nanorods acid treated. Elastic (open), viscous (solid) at 0, (■), 3, (●) kV/mm.
<b>Fig. 28</b>	Frequency dependencies of the relative permittivity $\epsilon'$ and dielectric loss factor $\epsilon''$ for 0.7 Cr mol % TiO <sub>2</sub> nanorods water treated (a) and 0.8 Cr mol % TiO <sub>2</sub> nanorods acid treated (b) with 5 wt. % suspensions.
<b>Fig. 29</b>	Yield stress versus electric field strength for 10 wt. % suspensions of 1.4 Cr mol % TiO <sub>2</sub> nanorods water treated sample in silicone oil suspensions.
<b>Fig. 30</b>	Yield stress versus weight fraction of 1.4 Cr mol % TiO <sub>2</sub> nanorods water treated sample in silicone oil suspensions
<b>Fig. 31</b>	Shear stress versus shear rate for 10 wt. % suspensions of 1.4 mol % Cr-TiO <sub>2</sub> nanorods particles (water treated) in silicone oil at 0, (■), 1,(●), 2, (▲), 3, (▼)kV/mm.
<b>Fig. 32</b>	Shear stress versus shear rate for 20 wt. % suspensions of 1.4 mol % Cr-TiO <sub>2</sub> nanorods particles (water treated) in silicone oil at 0, (■), 1,(●), 2, (▲), 3, (▼)kV/mm.
<b>Fig. 33</b>	Fit of the suggested model to flow curves for poly(acryloamidino diethylenediamine) PADD rough particles based ER fluids at an electric field of 2 kV/mm.
<b>Fig. 34</b>	Shear viscosity versus shear rate for 20 wt. % suspensions of 1.4 mol % Cr-TiO <sub>2</sub> nanorods particles (water treated) in silicone oil at 0, (■), 1,(●), 2, (▲), 3, (▼)kV/mm.

<b>Fig. 35</b>	PPy chain structure
<b>Fig. 36</b>	SEM picture of PPy particle structure.
<b>Fig.37</b>	. Shear stress versus shear rate dependence for 3 wt. % PPy ribbon particles PPy1 (open) and PPy2 (solid) suspensions. Electric field strengths E (kV/mm): (□,■) 0.0, (○, ●) 1.0, (△, ▲) 2.0, (▽, ▼) 3.0.
<b>Fig. 38</b>	Dependence of relative permittivity (solid) and dielectric loss factor (open) on frequency of PPy1 (▼,▽) and PPy2 (■, □) suspensions.
<b>Table 1</b>	Values of quantities in power law model for PPy1 and PPy2.
<b>Fig. 39</b>	Dependence of the yield stress on electric field strength for 3 wt. % PPy ribbon particles PPy1 (■) and PPy2 (▼) suspensions.
<b>Fig. 40</b>	Dependence of viscosity on shear rate for 3 wt. % PPy ribbon particles PPy1 (open) and PPy2 (solid) suspensions. Electric field strengths E (kV/mm): (□,■) 0, (○, ●) 1, (△, ▲) 2, (▽, ▼) 3.
<b>Fig. 41</b>	The dependence of storage modulus on the frequency for 3 wt. % PPy ribbon particles PPy1 (□,■) and PPy2 (▽,▼) suspension. Electric field strengths E (kV/mm): 0 (open), 3 (solid).
<b>Fig. 42</b>	Dependence of conductivity on frequency of PPy1 (■) and PPy2 (▼) suspensions.
<b>Table 2</b>	The experimental parameters and designation of different TiO <sub>2</sub> particles.
<b>Fig. 43</b>	SEM image for Safa1 particles.
<b>Fig. 44</b>	SEM image for Safa2 particles.
<b>Fig. 45</b>	SEM image for Safa3 particles.
<b>Fig. 46</b>	SEM image for medium concentration TiO <sub>2</sub> heated at 180 <sup>0</sup> C for 48 h.
<b>Fig. 47</b>	SEM image for low concentration TiO <sub>2</sub> heated at 150 <sup>0</sup> C for 24 h.
<b>Fig. 48</b>	SEM image for high concentration TiO <sub>2</sub> heated at 150 <sup>0</sup> C for 24 h.
<b>Fig. 49</b>	XRD- spectra for TiO <sub>2</sub> nanoparticles as sodium titanate.
<b>Fig. 50</b>	Yield stresses versus electric field strengths for (Safa1,■), (Safa2,▲), (Safa3,▼)
<b>Fig. 51</b>	Shear stress versus shear rate for (Safa1,■), (Safa2,▲), (Safa3,▼)
<b>Fig. 52</b>	Shear stress versus shear rate for (Safa1,■), (Safa2,▲), (Safa3,▼)



<b>Table 3</b>	Relative permittivity and relaxation time of Safa1, Safa2 and Safa3 particle suspensions.
<b>Fig. 53</b>	Relative permittivity versus frequency for TiO <sub>2</sub> nanoparticle (Safa1,■), (Safa2,▲), (Safa3,▼)
<b>Fig. 54</b>	Dielectric loss factor versus frequency for TiO <sub>2</sub> nanoparticle (Safa1,■), (Safa2,▲), (Safa3,▼)
<b>Fig. 55</b>	Conductivity versus frequency for TiO <sub>2</sub> nanoparticle (Safa1,■), (Safa2,▲), (Safa3,▼)

## NOMENCLATURE AND SYMBOLS

<i>Symbol</i>	<i>Meaning</i>	<i>Units</i>
$\tau_0$	<i>Yield stress</i>	<i>Pa</i>
$\tau$	<i>Shear stress</i>	<i>Pa</i>
$\eta_{pl}$	<i>Plastic viscosity</i>	<i>Pa s</i>
$\dot{\gamma}$	<i>Shear rate</i>	<i>s<sup>-1</sup></i>
$E$	<i>Electric field</i>	<i>V</i>
$H$	<i>Magnetic field</i>	<i>T, H/mm</i>
$t_1, t_2, t_3$	<i>Time</i>	<i>s</i>
$\tau_y$	<i>Yield stress</i>	<i>Pa</i>
$\eta_\infty$	<i>Final viscosity</i>	<i>Pa s</i>
$\eta_1$	<i>Initial viscosity</i>	<i>Pa s</i>
$E_c$	<i>Critical electric field strength</i>	<i>V</i>
<i>AC</i>	<i>Alternating current</i>	<i>A</i>
<i>DC</i>	<i>Direct current</i>	<i>A</i>
<i>CSS</i>	<i>Control shear stress</i>	<i>-</i>
<i>CSR</i>	<i>Control shear rate</i>	<i>-</i>
$q$	<i>Constant in power law</i>	<i>-</i>
$f$	<i>Frequency</i>	<i>Hz</i>

$\omega$	<i>Angular frequency</i>	$\text{Hz}^{-1}$
$\eta^*$	<i>Complex viscosity</i>	$\text{Pa s}$
$\gamma$	<i>Deformation ( shear strain)</i>	$m$
<i>LVR</i>	<i>Linear viscoelastic region</i>	-
$n$	<i>Constant in power law model</i>	-
$\epsilon'$	<i>Relative permittivity</i>	-
$\epsilon''$	<i>Dielectric loss factor</i>	-
$\alpha, \beta, \gamma$	<i>Related to crystal type of the materials</i>	-
$\xi$	<i>Zeta-electrokinetic potential</i>	$V$
<i>ER</i>	<i>Electro-rheological</i>	-
<i>MR</i>	<i>Magneto-rheological</i>	-
$P$	<i>Polarization density</i>	<i>Polarized particle/volume</i>
$A_s$	<i>A structure factor pertaining to the alignment of the particles</i>	-
$K_f$	<i>Dielectric constant</i>	-
$\phi$	<i>Volume fraction</i>	-
$F_\gamma$	<i>Force at specific shear</i>	$N$

	<i>strain</i>	
<i>pH</i>	<i>Acidity value of a solution</i>	-
<i>M</i>	<i>Molar concentration</i>	<i>Mol/l</i>
<i>eV</i>	<i>Electron volt</i>	-
<i>HOMO</i>	<i>Highest occupied molecular orbital</i>	-
<i>LUMO</i>	<i>Lowest unoccupied molecular orbital</i>	-
$\sigma_s$	<i>Conductivity of a solid phase</i>	<i>S/m</i>
$\sigma_L$	<i>Conductivity of a liquid phase</i>	<i>S/m</i>
$\sigma$	<i>Conductivity</i>	<i>S/m</i>
<i>k</i>	<i>Constant</i>	-
$F^H$	<i>Hydrodynamic force</i>	<i>N</i>
$F^E$	<i>Electrostatic force</i>	<i>N</i>
<i>Mn</i>	<i>Mason number</i>	-
$G'$	<i>Storage or elastic modulus</i>	<i>Pa</i>
$G''$	<i>Loss or viscous modulus</i>	<i>Pa</i>
<i>T</i>	<i>Temperature</i>	<i>K, C</i>

## CURRICULUM VITAE

Shawqi Almajdalawi

- 1992 B.Sc. – Yarmouk University in Jordan
- 1998 M.Sc. - Yarmouk University in Jordan
- 1999 diploma in pedagogy, Jordanian University in Jordan
- 1992-2009 various employments: Teaching Assistant , lecturer, School Teachers Supervisor, local consultant for different projects with Jordanian Ministry of Education and SJE company funded by the Canadian agency (CIDA), Pharmacy, and Authoring.
- 2009 Ph.D. studies at Polymer Centre, Faculty of Technology, Tomas Bata University in Zlin, Czech Republic

- [1] TASHTOUSH, H., ABU-ORABI, S., T., ALMAJDALAWI, SH., AL-TALIB, M. Synthesis and spectroscopic properties of 4, 5-bis-[5-aryl-1, 3, 4-oxadiazol-2-yl]-1-substituted benzyl-1, 2, 3-triazoles. *Indian J. Heterocycl. Chem.* 1999, vol.8, p. 183-189.
- [2] ALMAJDALAWI, SH., PAVLINEK, V., CHENG, Q., SAHA, P., MRLIK, M., STENICKA, M. Electrorheological properties of suspensions of polypyrrole ribbon particles in silicone oil. *AIP-Conference Proceeding.* vol. 1375, 2011, p. 275-283.
- [3] ALMAJDALAWI, SH., PAVLINEK, V., SEDLACIK, M., MRLIK, M., QUADRAT, Q. Preparation and electrorheology of titanium oxide/polypyrrole hollow globular clusters suspensions. In: *Conducting polymers: Formation, structure, properties and applications, meeting on macromolecules*, Prague, Czech Republic, 2011. ISBN 978-80-85009-69-9.
- [4] ALMAJDALAWI, SH., PAVLINEK, V., MRLIK, M., CHENG, Q., SEDLACIK, M. Synthesis of electrorheological behavior of Cr-doped TiO<sub>2</sub> nanorods with nanocavities suspensions in silicone oil. *13<sup>th</sup> International Conference on Electrorheological Fluids and Magnetorheological Suspensions.* Turkey, 2012 (accepted).
- [5] ALMAJDALAWI, SH., PAVLINEK, V., MRLIK, M., CHENG, Q., PIYAMANOCHA, P., PASTOREK, M. Solvothermal synthesis of different TiO<sub>2</sub> morphology and their electrorheological characteristics. *13<sup>th</sup>*

- International Conference on Electrorheological Fluids and Magnetorheological Suspensions*. Turkey, 2012 (accepted).
- [6] SEDLACIK, M., ALMAJDALAWI, S., MRLIK, M., PAVLINEK, V., SAHA, P., STEJSKAL, J., QUADRAT, O. Viscoelastic properties of electrorheological suspensions of core-shell (carbon/polyaniline) particles in silicone oil. *13<sup>th</sup> International Conference on Electrorheological Fluids and Magnetorheological Suspensions*. Turkey 2012 (accepted).
- [7] MRLIK, M., PAVLINEK, V., ALMAJDALAWI, S., SAHA, P., STEJSKAL, J. Behavior of aniline oligomer silicone oil suspensions under oscillatory shear. *13<sup>th</sup> International Conference on Electrorheological Fluids and Magnetorheological Suspensions*. Turkey 2012 (accepted).